AD

TECHNICAL REPORT

75-84-FEL

FREEZE-DEHYDRATION BY MICROWAVE ENERGY

Philippe Rene F. Peltre

Worcester Polytechnic Institute

Worcester, Massachusetts 01609

Project reference: 1T161101A91A07

FEL-16

Approved for public release;
distribution unlimited.

December, 1974

UNITED STATES ARMY
NATICK DEVELOPMENT CENTER
NATICK, MASSACHUSETTS 01760

Food Engineering Laboratory

Approved for public release; distribution unlimited.

Citation of trade names in this report does not constitute an official indorsement or approval of the use of such items.

Destroy this report when no longer needed. Do not return it to the originator.

SECURITY CLASSIFICATION OF THIS PAGE (When Data Entered)

REPORT DOCUMENTATION PAGE

READ INSTRUCTIONS BEFORE COMPLETING FORM

1. REPORT NUMBER TR 75-84 FEL	2. GOVT ACCESSION NO.
3. RECIPIENT'S CATALOG NUMBER	
4. TITLE (and Subtitle) FREEZE-DEHYDRATION BY MICROWAVE ENERGY	5. TYPE OF REPORT & PERIOD COVERED Final
	6. PERFORMING ORG. REPORT NUMBER FEL-16
7. AUTHOR(s) Philippe Rene F. Peltre	8. CONTRACT OR GRANT NUMBER(s) DAAG17-71-G-0001
9. PERFORMING ORGANIZATION NAME AND ADDRESS Worcester Polytechnic Institute Worcester, Massachusetts 01609	10. PROGRAM ELEMENT, PROJECT TASK AREA & WORK UNIT NUMBERS 1T161101A91A07 6.1
11. CONTROLLING OFFICE NAME AND ADDRESS Food Engineering Laboratory U.S. Army Natick Laboratories Natick, Massachusetts 01760	12. REPORT DATE December 1974
	13. NUMBER OF PAGES 159
14. MONITORING AGENCY NAME & ADDRESS(if different from Controlling Office)	15. SECURITY CLASS. (of this report) UNCLASSIFIED
	15a. DECLASSIFICATION/DOWNGRADING SCHEDULE

16. DISTRIBUTION STATEMENT (of this Report)

Approved for public release; distribution unlimited

17. DISTRIBUTION STATEMENT (of the abstract entered in Block 20, if different from Report)

18. SUPPLEMENTARY NOTES

19. KEY WORDS (Continue on reverse side if necessary and identify by block number)

DEHYDRATION	MICROWAVE ENERGY	HEAT TRANSFER	MATHEMATICAL MODEL
DEHYDRATED FOODS	ENERGY	BEEF	EQUATIONS
FREEZE DRIED FOODS	HEATING	ANALYSIS	MELTING
FREEZE DRYING	MICROWAVES	MICROWAVE DIELECTRIC PROPERTIES	

20. ABSTRACT (Continue on reverse side if necessary and identify by block number)

A general unsteady state analysis is used to derive a mathematical model of the freeze-drying process using microwave heating. The system of partial differential equations is solved numerically by Crank-Nicolson method. The temperature and water vapor concentration profiles inside the material being dried are calculated.

DD FORM 1 JAN 73 1473 EDITION OF 1 NOV 65 IS OBSOLETE

SECURITY CLASSIFICATION OF THIS PAGE (When Data Entered)

20. Abstract (continued)

The model is applied to simulate the freeze-dehydration of beef meat by microwave dielectric heating at 2450 MHz. The results of the calculations show that the microwave freeze-drying process is mainly controlled by heat transfer. The study of the effects of the process constraints and variables upon the drying time and/or the freeze-dryer output indicates that an optimal operation (highest product yield) would be for an operation near corona and overheating (or melting) conditions. Drying times as short as $1\frac{1}{2}$ hours should be possible, if corona is to occur beyond a peak strength of 255 V/cm.

Experimental drying curves have been obtained for the freeze-drying of beef meat with microwave heating at 2450 MHz. The experimental drying curves are in good agreement with those simulated by the model. The small differences may be attributed to an uncertainty on the numerical values used for the physical properties in the model or non-ideal experimental conditions. An experimental value of the heat transfer coefficient of 1.9×10^{-4} cal/sec/cm^2/$^\circ$C (at the surface of the sample exposed to the vacuum) is also obtained.

FOREWORD

Dehydration has been used for millenia to extend storage life of food products. If properly done and followed by appropriate packaging, a wide variety of food products can be maintained without significant change at ambient temperatures for very long periods. Weight savings may be as high as 90%. Accordingly, dehydration has always played an important role in the preparation of military rations.

Efforts to improve the process have culminated in freeze-drying or dehydration by sublimation. The results have been dramatic and with many products consumer acceptance approaches that for fresh or frozen counterparts. The cost of freeze-drying is high due to the equipment required and low through-put rate. Present procedures are slow because as the product dries from the surface inward the energy for sublimation must pass by conduction through dry product which is an effective thermal insulator. Transfer of microwave energy is nearly unaffected by the dry layer. Thus, theoretically, microwave freeze-drying should permit drying much more rapidly.

Investigations of microwave freeze-drying have indicated many problems. This study covers theoretical and experimental approaches toward their solution. Included is a mathematical simulation of the drying process which it is hoped will constitute a valuable tool for future process design, optimization and control.

This study was undertaken under a grant from US Army Natick Laboratories No. DAAG17-71-G-0001, Project Number 1T161101A91A07, In-House Laboratory Independent Research. This manuscript was previously submitted to Worcester Polytechnic Institute in partial fulfillment of requirements for the PhD degree in Chemical Engineering. The project Officer for this grant was Dr. Clarence K. Wadsworth.

TABLE OF CONTENTS

		Page No.
List of Tables		vii
List of Figures		viii
Abstract		xi
Chapter		
I.	Introduction	1
II.	Literature Survey	4
	1. The Microwave Freeze-Drying Process	4
	2. Modeling the Freeze-Drying Process	5
	3. Physical Properties of Beef Meat with Reference to Microwave Freeze-Drying	7
	3.1 Thermal Conductivities	7
	3.2 Diffusivities	8
	3.3 Dielectric Properties	8
	3.4 Specific Heat of Frozen and Dried Beef	9
Part I:	Mathematical Simulation of a Freeze-Drying Process Using Microwave Energy	10
III.	The Freeze-Drying Process	11
	1. General Description	11
	2. Sharpness of the Sublimation Zone	12
	3. Heat Transfer	13
	4. The Microwave Power Conversion	14
	5. Mass Transfer	16
	6. Moisture Sorption in the Dry Layer	17

TABLE OF CONTENTS (Cont'd)

Chapter		Page No.
IV.	The Mathematical Model	19
	1. The Transport Equations	19
	2. The Boundary Conditions	22
	3. Initial Values	23
	4. Fix-Boundary Transformation and Normalization	23
V.	The Numerical Method	27
	1. The Finite Differences Method of Approximation	28
	2. Method of Solution	30
	3. The General Numerical Scheme of Solution .	33
	4. Stability, Accuracy of the Solution and Simulation Speed	33
Part II:	Application to the Freeze-Drying of Beef Meat at 2450 MHz	37
VI.	Numerical Data Used in the Calculations	38
	1. The Constants	38
	2. Effective Thermal Conductivity of Frozen Beef	40
	3. Effective Thermal Conductivity of Dried Beef	41
	4. Effective Diffusivity	45
	5. Dissipation Factor of Frozen and Dried Beef	47
	6. Ice-Water Vapor Equilibrium Relationship .	47

TABLE OF CONTENTS (Cont'd)

Chapter		Page No.
VII.	Theoretical Results	52
	1. Typical Simulation Outcome	52
	2. Process Variables	59
	3. Feasible Operation Domain	60
	4. Effect of the Process Variables on the Drying Time	72
Part III	Correlation with Experimental Drying Curves	81
VIII.	Experimental Set-Up and Procedure	82
	1. Experimental Set-Up	82
	1.1 The Microwave Freeze-Dryer	82
	1.2 The Data Acquisition System	85
	2. General Experimental Procedure	87
	2.1 Tuning of Cavity	87
	2.2 Sample Preparation	87
	2.3 Experimental Procedure for a Run	88
IX.	Experimental Results and Correlation with Mathematical Model	90
	1. Experimental Results	90
	2. Comparison with Simulated Drying Curves	98
X.	Conclusions	111
XI.	Recommendations	114
	Appendix	116
	A.1 Finite Difference Equations	116
	A.2 Energy Balance at the Interface	120

TABLE OF CONTENTS (Cont'd)

Chapter		Page No.
	Appendix (continued)	
	A.3 Boundary Condition at the Outer Surface	123
	B.1 Solution of the System of Finite Difference Equations	125
	B.2 Forcing and Accelerating the Convergence of an Iteration Scheme	127
	C. Sample Calculations (Run No. 15)	130
	C.1 Calculation of h	130
	C.2 Calculation of E	131
	D. Computer Output	133
	E. Experimental Results	134
	F. Computer Programs Listings	144
	Nomenclature	153
	References	156

LIST OF TABLES

Table	Title	Page No.
2.1	Sources of Thermal Conductivity Data for Frozen Beef	7
3.1	Variations of Knudsen Number as a Function of Pressure	17
5.1	Stability of the Numerical Solution	35
6.1	Numerical Values of the Constants Used in the Simulation	39
6.2	Reported Diffusivity Data and Computed Values	46
7.1	Assumed Operating Conditions	55
9.1	Experimental Conditions	92

LIST OF FIGURES

Figure	Title	Page No.
4.1	Model with Expected Forms of the Concentration and Temperature Profiles for the Microwave Freeze-Drying Process.....	20
5.1	Numerical Grid in the Fixed Boundary Domain	28
5.2	General Algorithm Flow Chart - Subroutine MWFD	34
6.1	Thermal Conductivity of Frozen Beef vs $\sqrt{T_f - T}$, for Various Moisture and Fat Contents	42.1
6.2	Variations of Parameter a in Eq. (6.2) vs Fat Content of Frozen Beef	43
6.3	Variations of Parameter b in Eq. (6.3) vs Moisture Content of Frozen Beef	43
6.4	Thermal Conductivity of Dried Beef vs Pressure	44
6.5	Variations of K_F (cal/sec/cm^2/(V/cm)^2) with Temperature	48
6.6	Variation of K_D (cal/sec/cm^2/(V/cm)^2) with Temperature	49
6.7	Ice-vapor Equilibrium Relationship	50
7.1	Typical Concentration and Temperature Profiles for the Microwave Freeze-Drying Process	54
7.2	Variations of the Temperatures and of the Interface Position as a Function of Time	56
7.3	Variations of the Powers Absorbed in the Sample and of the Interface Position as a Function of Time	57

LIST OF FIGURES (Cont'd)

Figure	Title	Page No.
7.4	Limiting Surface for the Feasible Operation Domain Corresponding to the No Melting Constraint (L = 1.27 cm)	63
7.5	Maximum Allowable Electric Field (for no melting) as a Function of the Total Pressure in the Vacuum, at Various Partial Pressures of Water Vapor L = 1.27 cm	64
7.6	Maximum Allowable Electric Field (for no melting) as a Function of the Partial Pressure of Water Vapor in the Vacuum, at Various Total Pressures L = 1.27 cm	65
7.7	Variations of the Maximum Temperature in the Frozen Region (at any time) with the Electric Field, at Various Total Pressures L = 1.27 cm; P_R^W = .075 mmHg	67
7.8	Variations of the Maximum Temperature in the Dried Layer (at any time) with the Electric Field, at Various Total Pressures L = 1.27 cm; P_R^W = .075 mmHg	68
7.9	Effects of the Sample Half Thickness L on the Maximum Temperature in the Frozen Region (at any time). $P_R = P_R^W$ = .075 mmHg	70
7.10	Effects of the Sample Half Thickness L on the Maximum Temperature in the Dried Layer (at any time). $P_R = P_R^W$ = .075 mmHg	71
7.11	Variations of the Total Drying Time as a Function of the Electric Field, at Various Pressures of the Vacuum Chamber. L = 1.27 cm; P_R^W = .075 mmHg	73
7.12	Effects of the Total Pressures in the Vacuum on the Drying Time and the Maximum Temperature Reached by the Frozen Core. E = 90 V/cm, P_R^W = .075 mmHg, L = 1.27 cm	75

LIST OF FIGURES (Cont'd)

Figure	Title	Page No.
7.13	Effects of the Sample Thickness on the Total Drying time for Various Field Strengths. $P_R = P_R^W = .075$ mmHg	77
7.14	Effects of the Sample Size on the Output of the Microwave Freeze-Dryer for Various Electric Field Strengths. $P_R = P_R^W = .075$ mmHg.	79
8.1	Schematic of the Experimental Set-Up	83
9.1	Experimental Drying Curves (power runs) $P_R = .3$ mmHg	95
9.2	Experimental Drying Curves (pressure runs)	96
9.3	Drying Rate vs Time, Run No. 15	98
9.4	Drying Rate vs Time, Run No. 12	102
9.5	Drying Rate vs Time, Run No. 17	103
9.6	Drying Rate vs Time, Run No. 13	104
9.7	Experimental (Run No. 12) and Simulated Drying Curves. $P_R = .3$ mmHg	105
9.8	Experimental (Run No. 17) and Simulated Drying Curves. $P_R = .3$ mmHg	106
9.9	Experimental (Run No. 13) and Simulated Drying Curves. $P_R = .3$ mmHg	107
9.10	Experimental (Run No. 25) and Simulated Drying Curves. $P_R = 1$ mmHg	108
9.11	Experimental (Run No. 27) and Simulated Drying Curves. $P_R = .2$ mmHg	109
B.2.1	Geometrical Representation of the Iteration Scheme	128

ACKNOWLEDGMENTS

The author is indebted to Professor Y.H. Ma for his guidance and encouragement throughout this investigation. He wishes to acknowledge the financial support of the United States Army Natick Laboratories through Grant No. DAAG17-71-C-0001.

Sincere appreciation is expressed to Dr. C.K. Wadsworth and Mr. John Swift, and others of the United States Army Natick Laboratories for their invaluable help and assistance in the experimental part of this work.

The author wishes to especially thank Mrs. O'Brien, Mssrs. T.Y. Lee and D. Cortelek for their assistance in the preparation of this thesis.

The excellent typing of the manuscript by Ms. M. Pietal is also gratefully acknowledged.

- Chapter I -

INTRODUCTION

For many years, dehydrated food products have received a lot of attention as they greatly simplify storage and conservation problems. In effect, dehydrated food products can be kept at room temperature over long periods of time if properly packaged. On the other hand, the loss of the moisture content represents a saving in weight of approximately 75%.

Various means of dehydration have been developed to suit the needs of the industry. Among these, the freeze-drying process is of special interest as it is most suited for heat sensitive materials such as biologicals and food products.

In this technique, which was developed in the early 1950's the material to be dried is first deep frozen and then dehydrated by sublimation of its frozen moisture content. As the dehydration proceeds an outer dried layer forms while the frozen core retreats. It has been observed experimentally that a sharp sublimation zone separates distinctly the nearly completely dried layer, and the fully hydrated and frozen core. The sublimation is maintained by keeping the sublimation zone temperature below the melting point of the frozen material. A low partial pressure of water vapor in the surrounding atmosphere provides the driving force necessary for the dehydration to take place. Water vapor partial pressures of the order of .1 mmHg are usually maintained by means of a low temperature condenser (-40 to -50°C). The dehydration is generally conducted under vacuum (.1 to 1 mmHg) in order to decrease the resistance to the water vapor flow through

the porous dried layer, although, a sublimation under atmospheric conditions is physically possible (Hohner (1970)).

Although it has proven very successful and is widely used, conventional freeze-drying processes use an external, surface heating (i.e., hot plates, infra red lamps) to supply the necessary enthalpy of sublimation to the product. The poor thermal conductivity of food products results in long drying times due to upper-limits on the temperature gradients allowable in the product in order to avoid melting and/or thermal degradation of the dried material. Overheating of the dried product is particularly undesirable with respect to the reversibility of the freeze-drying process as poor rehydration characteristics may develop (Kuprianoff (1961)).

Microwave dielectric heating has shown a great potential in accelerating freeze-drying (Hoover et al. (1966)). Its feasibility was demonstrated on an experimental scale in the late 1950's by Jackson et al. (1957) and Copson (1958). Hoover et al. (1966) have shown that use of microwave energy to replace conventional (external) heating may reduce drying times by factors of 3 - 13 which would allow the use of a continuous or at least semi-continuous process. The shorter drying times are due to the fact that microwave energy is dissipated throughout the bulk of the material being dried, particularly in the frozen core. Thus, the problem of supplying the enthalpy of sublimation by conduction from the surface can be overcome.

However, the microwave freeze-drying process has remained in the experimental stage. The lack of a systematic theoretical study of the process as well as problems with the relatively new microwave heating technology seem to have hampered the development of this new technique. Among the problems involved in the design of a microwave freeze-dryer, the most critical ones are the corona discharge occuring at low pressures, the difficulty of obtaining a uniform heating of the frozen product, and the difficulty of coupling efficiently microwave energy with the material being dried.

The question of corona discharge in the microwave applicator is

of prime importance as its formation drastically decreases the power efficiency and may result in severe burns of the product. Thus, the electric field in the microwave applicator must be kept below its break-down value. This constitutes an additional constraint imposed on the process. Previous studies have shown that the electric field strength at which breakdown (corona discharge) occurs is a function of the pressure in the vacuum, the design of the microwave generator and the geometry of the microwave applicator (MacDonald (1966), Gould & Kenyon (1971)). Experimental results by Gould & Kenyon on the phenomenon of gaseous breakdown with reference to freeze-drying indicate breakdown field strengths of 200 to 300 V/cm RMS in the pressure range 2 to .1 mmHg. In this pressure range, the highest strengths are reached for the lowest pressure values.

Research has been undertaken at the U.S. Army, Natick Laboratories, in an effort to develop the microwave freeze-drying technique. As part of this work, the present investigation is intended to provide a mathematical simulation of the freeze-drying process using microwave dielectric heating. It will constitute a useful tool in the future for process design, optimization and control.

The objectives of this work can be stated as follows:

1. Develop a mathematical model to describe the process.
2. Study the response of the mathematical model to various freeze-drying conditions in order to test its validity and provide design guidelines. Of prime concern will be the effects of the process constraints and variables on the drying time.
3. Obtain experimental drying curves of beef samples and compare them with predicted drying curves as a verification of the simulation.

- Chapter II -

LITERATURE SURVEY

During the last twenty-five years, there have been numerous publications on the various aspects of conventional freeze drying. However, very little information could be found on microwave freeze-drying. It should be pointed out that there still is a need for a systematic theoretical study of the conventional freeze-drying process.

1. The microwave freeze-drying process

Most of the work done on this subject falls in a few isolated experimental studies which were directed toward the development of this new technique. Jackson et al. (1957), Copson (1962) successfully accelerated freeze-drying with microwave energy on an experimental scale. They found that microwave heating should allow drastic reductions of the drying time, although engineering problems, particularly glow discharge may complicate its application. Harper (1961), Kan & Yeaton (1961) obtained experimental data on the dielectric properties of various food products between microwave frequencies of 500 and 3000 MHz. Hoover et al. (1966) obtained comparative drying curves for radiant and microwave (at 632 and 915 MHz) freeze-drying of various food products. They demonstrated that use of microwave freeze-drying may reduce drying times by factors of 3 to 13 as compared to radiant (surface) heating. They found that with

microwave heating the drying times were essentially independent of the thickness of the sample. It should be noted that the microwave power input level was increased in their experiments, in the same ratio as that of the thickness. They reported variations of the glow power vs pressure for the microwave applicator which they used. In a succeeding paper, they used engineering data derived from their experimental results to discuss the feasibility of the microwave freeze-drying process.

General analyses about the microwave freeze-drying process have been reported in the recent years. Copson (1962) published a book in which he described in detail the theoretical and engineering problems arising in the application of microwave heating to freeze-drying. Parker (1968) made an extensive use of the data of Hoover et al., to illustrate the possibilities of microwave freeze-drying, as one of the multiple applications of microwaves in Power Engineering. Other reviews have been done by Decareau (1962), Meryman (1964), and Harper et al. (1962).

Based on Hoover's experimental data for microwave freeze-drying at 915 MHz, Hammond (1967) made an economic evaluation of microwave vs radiant heating and concluded that both methods were economically competitive. However, he also pointed out that his analysis was very sensitive to the assumptions which he made.

More recently, Gould and Kenyon (1971) studied experimentally the problem of corona breakdown in microwave freeze-drying at 2450 MHz. They also derived an equation which shows the effect of a dielectric load on the gas discharge in a microwave cavity.

2. Modeling the freeze-drying process

There has not been, yet, any comprehensive analysis of the freeze-drying process using microwave heating. Previous analyses have been limited to simplified approaches using a quasi-state assumption and were aimed at preliminary design applications (Copson (1962)).

On the other hand, there have been many publications concerned

with a theoretical description of the conventional freeze-drying process using external heating. The reader is referred for more information to the excellent review of King (1971), and an extensive collection of articles on Lyophilisation edited by Rey (1964).

Although theoretical studies of conventional freeze-drying are not applicable to microwave freeze-drying (this point will be discussed below), it is of interest to review some of the most recent and complete studies as they emphasize the need for a general, transient analysis of the freeze-drying process.

These studies have generally employed the simplifying assumption of a pseudo-steady state. This assumption is not applicable to microwave freeze-drying because of the fast temperature transients occuring in the sample. However, this assumption is generally quite good in the radiant heating case as shown by Sandall et al. (1967). Hill and Sunderland (1971) have presented a theoretical analysis considering the simultaneous energy and mass transfer during dehydration. Although they considered the time variation of the interface temperature, they have neglected the transient behavior of temperature and concentration both in the ice-core and in the dried layer. Fox and Thompson (1972) considered the transient transport equations in the dried layer for two limiting cases: quasi-steady state with heat leakage in the ice-core and transient solutions with a uniform ice-core temperature. Hohner (1970) considered the transient behavior of both mass and energy transport equation with a numerical technique.

Thus, there is seemingly a need for a general analysis of the freeze-drying process which would account for all transient effects in both the frozen and the dried regions. Such a study would permit the simulation of the radiant freeze-drying process and thus, allow a systematic theoretical study.

The objective of this work is to develop a general study using microwave dielectric heating. Microwave freeze-drying is indeed a more general case. In effect, it includes a heat generation term in the energy equation, whereas, conventional freeze-drying, using

surface heating does not. A model of the microwave freeze-drying process would be readily applicable to the conventional one by setting the volumetric heat generation term to zero and adjusting the boundary conditions of the equations governing the process to account for the surface heating.

3. Physical properties of beef meat with reference to microwave freeze-drying

3.1 Thermal conductivities

The thermal conductivity of dried beef meat has been measured by Harper (1961, 1962) at various pressures in the range 10^{-3} - 10^{3} mmHg. The measurements were made using heat flow transducers, located on both sides of the sample. He also derived an equation to predict the thermal conductivity of the porous material which showed very good agreement with his experimental data. Other thermal conductivity values have been reported for dried beef. However, they are generally the results of calculations from the drying rate data and may lack accuracy as they depend on the assumptions employed in the calculations (Massey and Sunderland (1967)).

Quite a few data (see Chapter 6, Sec. 2) have been reported on the thermal conductivity of frozen beef meat as it is of prime importance in refrigeration applications. The various literature sources have been listed in Table 2.1 with the composition of the beef samples used in the measurements.

Table 2.1 - Sources of thermal conductivity data for frozen beef

Source	% moisture	% fat
Lentz (1961)	75	.9
Miller & Sunderland (1963)	69.5	--
Hill et al. (1967)	76.5	2.35
Hill et al. (1967)	78.7	1.4

These data have generally been obtained by measuring the heat flux through a slab of the sample placed between a cold and a hot plate. Accuracies better than 3% are quoted by the authors.

3.2 Diffusivities

The experimental data on the effective diffusivity of beef meat are very sparse. They are practically limited to measurements by Harper (1962) and Dyer & Sunderland (1966). Harper (1962) has measured the diffusivity of water vapor in dried beef at 38°C under 1 atm. He mentioned that the measurements were not easy to reproduce and that there was an uncertainty of 10 to 15% on the results. The measurements consisted of recording the gain in weight of sodium perchlorate placed above the sample through which water vapor was allowed to diffuse under atmospheric pressure.

Dyer & Sunderland (1966) have obtained diffusivity data in the range 1.44 to 2.28 mmHg, at an unspecified temperature. These data were compared to the results of a theory which they derived, to predict effective diffusivities in the transition flow regime. The agreement is of the order of 15 - 20%. They measured the water vapor flow by means of humidity transducers located on both sides of the sample within an evacuated chamber.

3.3 Dielectric properties

There has been data reported in the literature on the dielectric properties of beef meat, and other food products. A review of these data has been published by Nelson (1971). However, most of these data have been obtained for microwave heating applications and are usually limited to the fresh product at temperatures above freezing. Indeed, no data could be found for frozen and dried beef meat at 2450 MHz. The most readily applicable data were those reported by Kan & Yeaton (1961) at 3000 MHz. These data cover the range -59.4°C to 4.4°C for frozen beef (in 5.6°C increments) and -51.1°C to 82.2°C (in 11.2°C increments). The measurements were made using the shorted line method with coaxial standing wave detectors.

Results of measurements at 1000 MHz and 150 MHz are also reported.

Additional data points have been obtained by Harper et al. (1962) for frozen beef at -4° and -10°C for a frequency of 2000 MHz. Bengtsson & Risman (1971) also reported measurements for frozen raw beef at 2.8 MHz, by the cavity perturbation technique, at two temperatures: -20°C and -10°C.

3.4 Specific heat of frozen and dried beef

Experimental data for frozen and dried beef have been reported by Awbery & Griffith (1933) and Rey (1964).

- PART I -

MATHEMATICAL SIMULATION OF A FREEZE-DRYING PROCESS USING MICROWAVE ENERGY

Chapter III: The Freeze-Drying Process

Chapter IV: The Mathematical Model

Chapter V: The Method of Solution

- Chapter III -

THE FREEZE-DRYING PROCESS

Although this investigation has been conducted with reference to the freeze-dehydration of beef meat. it can easily be extended to the freeze-drying of other products, The simulation can also be applied to separation processes involving sublimation. Dielectric heating is considered in this investigation but, it should be noted that it does not limit the applicability of the analysis to the specific area of dielectric heating. On the contrary, it deals with a more general case than the conventional freeze-dehydration process using external heating. In effect, the present analysis includes a volumetric heat generation term in the governing energy balance equations. The present analysis can be used to simulate the conventional (surface heating) freeze-drying process by choosing the appropriate boundary conditions.

However, in extreme cases where the process parameters are drastically different from those assumed here, a revision of some of the assumptions may be necessary. For example, for much greater pore sizes and/or higher operating pressures, the description of the water vapor flow through the dried layer by Fick's equation may not be adequate as hydrodynamic flow predominates.

1. General description

In the freeze-drying technique, the material to be dried is

first deep frozen (around -35°C) and then dehydrated by direct sublimation of the frozen moisture absorbed in its pore structure. As the dehydration proceeds, the frozen core retreats inward while a porous, dried outer layer forms. A sublimation zone separates distinctly the frozen core and the dried layer, as observed experimentally by this investigator and other previous studies (Clark (1968), Hatcher (1964), Hardin (1965)).

For the sublimation to take place, the temperatures in the sublimation zone must be kept below the triple point of the absorbed moisture (around -1.5°C for beef meat). The water vapor from the phase change at the frozen front flows through the porous dried layer to the surrounding atmosphere where it is condensed by a vapor trap (moisture sink). Low operating pressures are usually used (.05 to 1mmHg) in order to insure a small resistance to mass transfer. In the case under investigation, the heat necessary for sublimation is supplied to the material by means of dielectric heating at a microwave frequency of 2450 MHz.

2. Sharpness of the sublimation zone

The assumption of a uniformly retreating ice front with a sharp boundary (URIF Model), has been commonly used by previous investigators, and is generally in good agreement with experiments. However, some questions have been raised regarding the degree of sharpness of the front. Bralsford (1967), while using the URIF Model, suggests that liquid diffusion is likely to broaden the sublimation zone, particularly as the temperature approaches the melting point of the frozen material. Moisture measurements by Brajnikov et al. (1969), and Hatcher (1964), indicate the possibility for a diffuse sublimation zone as thick as 1 to 2 mm. But, as suggested by King (1971), it could reflect the limit of resolution of the moisture measurement method which they used. Other evidences for a diffuse front have been reported and are discussed by King (1971).

On the other hand, visual examination of partially dried meat

samples (Hardin (1965)) and measurement of temperature histories during the drying process by Hatcher (1964) have shown a sharp transition zone. It should be noted that Hatcher's results seem to show some broadening of the transition zone in the latter stage of drying, although they could be interpreted by a non-planar but still-sharp front. An additional fact in support of the sharp frozen front is that, as already mentioned, models of conventional freeze-drying which have used the URIF Model of an infinitely sharp front have been in good agreement with experimental results (Bralsford (1967), Sandall et al. (1967)).

Thus the hypothesis of a sharp sublimation front seems to be a reasonable assumption for the description of the freeze-drying mechanism, despite the fact that some broadening of the front may occur as the temperature approaches the melting point.

3. Heat transfer

An important characterization of the freeze-drying process is its high energy needs. As compared to other processes, such as drying by vaporization, freeze-drying requires a greater amount of energy. In effect, the heat of sublimation corresponds to the sum of the heat of vaporization (595cal/g at 0°C) and the heat of fusion (80cal/g) and is 675 cal/g for ice.

Thus, one may expect that the rate of heat transfer to the sublimation front will be a determining factor for the total drying time. Indeed, vacuum freeze-drying processes are heat transfer limited as shown by studies with conventional, surface heating and, microwave dielectric heating (Ma & Peltre (1973)). This is due to the fact that the maximum temperature is to be kept below 60°C to avoid thermal degradation in the dried layer, and below -1.5°C in the frozen region to eliminate melting or vaporization. This results in an upper limit for allowable temperature gradients.

The sublimation front acts as a heat sink toward which the heat flows from both the frozen and dried regions. The heat transfer in both regions is essentially due to conduction. The use of

effective thermal conductivities and effective specific heats enables one to treat the porous medium as a continuum. A small but appreciable amount of heat is lost to the sublimation in the dried layer due to convection as shown by Dyer & Sunderland (1968).

Regarding the very low thermal conductivity of the solid matrix, the gas filling the pores, in the dried layer, is expected to have a significant contribution to the overall thermal conductivity of the dried layer. Indeed, experimental results (Harper (1962), Sandall et al. (1967)) show the effective thermal conductivity in the dried layer to be a function of pressure. On the other hand, the effective thermal conductivity in the frozen region varies significantly with the temperature (Lentz (1961)). These effects have been taken into account in the derivation of the model.

4. The microwave power conversion

With the microwave dielectric heating, energy is generated throughout the volume of the material due to the interaction of the electric field with the free and bound charges of the dielectric. The magnetic component of the electromagnetic field does not generate any energy because its direction is normal to the velocity of the charges. From these considerations, and assuming a linear and conductive dielectric, a formula can be derived to relate the time-averaged power generated in a unit volume of dielectric to the electric field peak strength in the dielectric, E_d,

$$\omega = \frac{\sigma_e}{2} E_d^2 \qquad (3.1)$$

It can be further transformed by expressing the electric conductivity σ_e in terms of the loss factor of the dielectric ϵ'' (also known as the imaginary part of the complex dielectric constant).

$$\omega = \pi f \epsilon_o \epsilon'' E_d^2 \qquad (3.2)$$

where f is the frequency of the wave.

If a polarization of the electric field normal to the surface

of the dielectric material exists, then the peak strength in the dielectric near the outer surface can be related to that in the surrounding vacuum by,

$$E_d = E/ (\epsilon'^2 + \epsilon''^2)^{\frac{1}{2}} \tag{3.3}$$

On the other hand, if the field is tangent to the surface, it is continuous. Then, one has,

$$E_d = E \tag{3.4}$$

Equation (3.3) is used as a dominant polarization of the field normal to the sample surface is expected in the experiments (see Chapter VIII, Sec. 2.3). However, it should be noted that the true situation must lie between these two extreme cases, depending on the amount and the direction of polarization of the electric field.

If one neglects the attenuation effect, the strength of the electric field is constant throughout the sample and equal to the value at the surface (for a uniform field distribution in the applicator). Penetration depths (E decreased to 1/e of its value at the surface) at 2450 MHz, for the operating conditions encountered, are greater than 3.5 cm, as opposed to the maximum half sample thickness used of 1.27 cm.

With these assumptions, the power conversion formula reduces to,

$$\omega = K E^2 \tag{3.5}$$

where the <u>dissipation coefficient</u> K is defined as,

$$K = \pi f \epsilon_o \epsilon''/(\epsilon'^2 + \epsilon''^2) \tag{3.6}$$

The effect of the temperature on the dissipation coefficient for both the frozen and the dried regions is of special importance. According to data by Kan & Yeaton (1961) as the temperature increases, K can increase by a factor of 4 for the frozen meat

between -40°C and 0°C, and by a factor of 2 for the dried meat between 0°C and 50°C. The increase in K value with increasing temperature has an acceleration effect on the power absorption by the dielectric. This may lead to a situation known as a "runaway" condition.

Finally, it is desired to avoid any melting of the frozen region in the course of the dehydration because of the very high loss factor of the wet meat which may trigger the runaway situation previously mentioned. Therefore, the constraint on the temperature in the frozen core will be that no melting occurs at any time.

5. Mass transfer

Although operation under atmospheric pressure is possible (Hohner (1970)), freeze-drying is generally conducted under vacuum (.05 to 1 mmHg) in order to decrease the resistance to the flow of water vapor through the dried layer. This type of operation is referred to as vacuum freeze-drying. The higher mass transfer rate reached under vacuum yields lower temperatures of the frozen core. This permits a higher heat input to the sample and leads to shorter drying times. The vacuum operation is practically necessary for microwave freeze-drying as short drying times are normally required for the effective use of microwave energy.

At the operating pressure range mentioned above, the mean free path of the molecules inside the pores of the dried layer is of the order of magnitude of the mean pore diameter (100 μ as observed by Harper (1962) for beef meat). Thus the flow regime corresponds to the transition region between molecular flow and slip flow. Table 3.1 shows the values of the Knudsen number at various pressures for dried beef meat.

The variations of the thermal conductivity of the dried layer with pressure (cf. Fig. 6.4) supports the fact that the flow is in the transition regime. Fig. 6.4 shows that the effective thermal conductivity is constant at pressures below .01 mmHg and corresponds to that of the solid matrix. As the pressure

increases the effective thermal conductivity increases. When the pressure reaches about 10 mmHg, the effective thermal conductivity starts to level off and becomes independent of the pressure again. This latter stage corresponds to the beginning of the continuous flow regime for which the kinetic theory of gases predicts that the thermal conductivity does not depend on the pressure.

Table 3.1 - Variations of Knudsen Number as a function of pressure (Temperature: 38°C)

Pressure	Mean free path	Knudsen Number[a]
mmHg	μ	-
760	.065	-
10	5	.05
1	50	.5
.1	500	5
.05	1000	10

a - calculated assuming a pore diameter of 100 μ and that the mean free path varies inversely with the pressure

Rather complex equations have been proposed to describe the gas flow in the transition region (Wakao et al. (1965)). However, previous studies particularly by Sandall et al. (1967) and Dyer & Sunderland (1966) show that it is possible to describe the flow by Fick's Equation using an effective diffusivity. Values of the effective diffusivity have been determined experimentally (Harper (1962), Dyer & Sunderland (1966), see Chapter VI, Sec. 4). Thus, Fick's Equation is used in this study.

6. Moisture sorption in the dried layer

As the water vapor from the sublimation flows through the

dried layer a finite amount of moisture is expected to be adsorbed by the dried meat. Sorption isotherms have been obtained for beef meat by Saravacos & Stinchfield (1965). However, calculations by Sandall (1966) for typical conditions of freeze-drying of turkey breast have shown that the average sorbed moisture content is approximately 3% of the initial moisture content or 1.5% moisture by weight. These calculations were based on adsorption data of King et al. (1968) and assumed an external heating through the dried layer. This surprisingly low number has been attributed to the fact that rather high temperatures and low pressures exist in the pores of the dried layer. A larger amount of adsorption may be expected for microwave freeze-drying as the temperature through the dried layer is somewhat lower. However, our own experimental observations show that the total moisture remaining in the dried layer once the ice core has been removed is less than 5% of the initial total weight of the sample.

On the basis of these observations and in order to simplify the model it seems reasonable to neglect the adsorption effect as the drying is generally limited to the removal of the ice.

- Chapter IV -

THE MATHEMATICAL MODEL

A one-dimensional model of the freeze-drying process using microwave dielectric heating is derived with the following assumptions which were discussed in detail in Chapter III:

i - The sublimation zone has a zero thickness and retreats uniformly.

ii - An effective diffusivity can be used to describe the vapor flow through the dried layer by Fick's Equation.

iii - The power generated by the microwaves in a unit volume can be calculated by Eqs. (3.5) and (3.6) from the field strength in the dielectric (if one assumes a polarization of the electric field normal to the slab surface).

iv - The moisture sorption effect in the dried layer can be neglected.

The material to be freeze-dried is assumed to have the geometry of an infinite slab as shown in Fig. 4.1. The left edge of the slab is insulated (or center line of a symmetric slab) while the right edge is exposed to a vacuum at temperature T_R and water vapor concentration C_R.

1. The transport equations

Application of the principles of conservation of mass and energy in the dried layer gives

$$\frac{\partial W}{\partial x} = - \sigma \frac{\partial C}{\partial t} \tag{4.1}$$

$$\frac{\partial Q_D}{\partial x} = - \rho_D C_D \frac{\partial T_D}{\partial t} + \omega_D \tag{4.2}$$

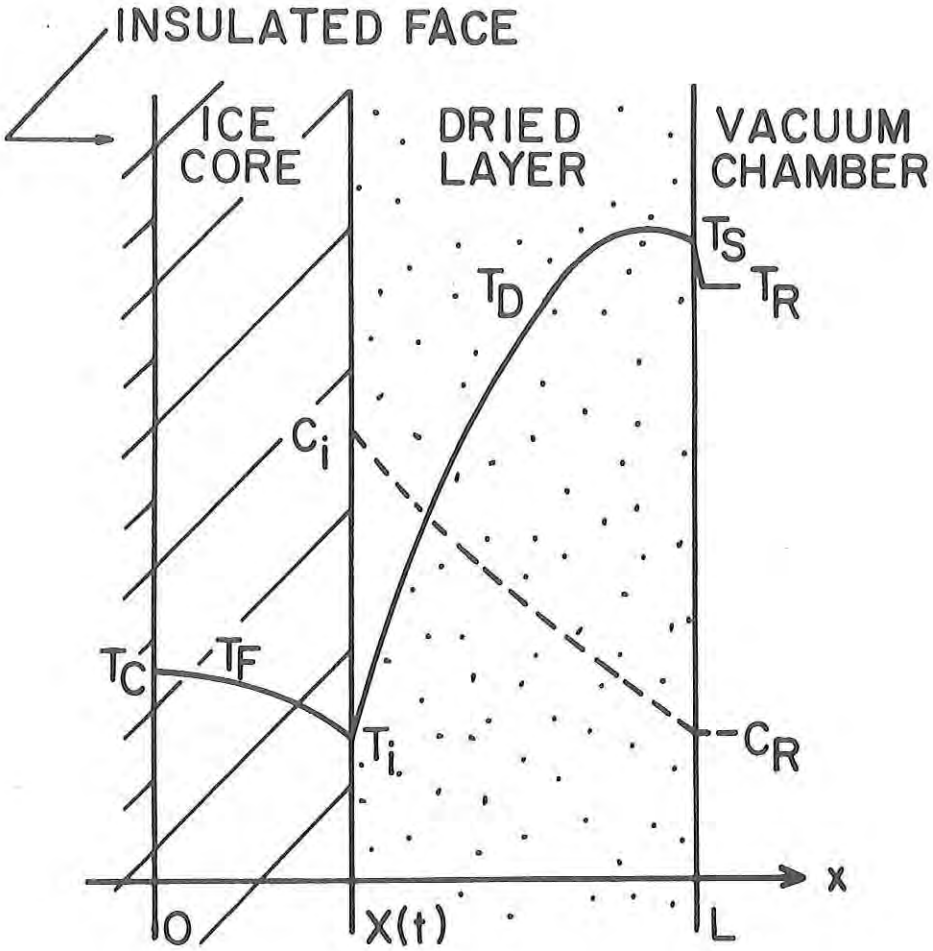

Figure 4.1 - Model with expected forms of the concentration and temperature profiles for the microwave freeze-drying process.

where the concentration C is that of the water vapor in the gas phase inside the pores. All other values are effective quantities. In the frozen region, one has

$$\frac{\partial Q_F}{\partial x} = - \rho_F C_F \frac{\partial T_F}{\partial t} + \omega_F \tag{4.3}$$

Assume that Fick's Equation can be used to describe the mass transfer in the dried layer. Then

$$W = - D \frac{\partial C}{\partial x} \tag{4.4}$$

Assume that the heat transfer in the dried layer is governed by conduction and convection. Then

$$Q_D = - k_D \frac{\partial T_D}{\partial x} + C_{pw} W (T_D - T_{ref}) \tag{4.5}$$

where T_{ref} is the reference temperature for enthalpy. Assume that heat transfer in the frozen region is due to conduction. Then

$$Q_F = - k_F \frac{\partial T_F}{\partial x} \tag{4.6}$$

Substitution of Equations (4.4), (4.5), and (4.6) into Equations (4.1), (4.2), and (4.3) gives

$$\frac{\partial^2 C}{\partial x^2} + \frac{1}{D} \frac{\partial D}{\partial x} \frac{\partial C}{\partial x} - \frac{\sigma}{D} \frac{\partial C}{\partial t} = 0 \tag{4.7}$$

$$\frac{\partial^2 T_D}{\partial x^2} + \left(\frac{1}{k_D} \frac{\partial k_D}{\partial x} - \frac{C_{pw} W_i}{k_D} \right) \frac{\partial T_D}{\partial x} - \frac{1}{\alpha_D} \frac{\partial T_D}{\partial t} = - \frac{\omega_D}{k_D} \tag{4.8}$$

$$\frac{\partial^2 T_F}{\partial x^2} + \frac{1}{k_F} \frac{\partial k_F}{\partial x} \frac{\partial T_F}{\partial x} - \frac{1}{\alpha_F} \frac{\partial T_F}{\partial t} = - \frac{\omega_F}{k_F} \tag{4.9}$$

The variation of the mass flux W with location has been neglected in the convection term of the heat transfer equation (4.8). It has been shown that the convective term is small compared to the other terms in the energy equation (Dyer & Sunderland (1968)). It also has been shown that the mass flux does not vary significantly

through the dried layer (Ma & Peltre (1973)).

2. <u>The boundary conditions</u>

At the insulated surface (or center line) we have

$$x = 0 \qquad \frac{\partial T_F}{\partial x} = 0 \qquad \text{for } t \geq 0 \tag{4.10}$$

At the outer surface of the dried layer, we have

$$x = L \qquad h(T_R - T_S) = k_D\left(\frac{\partial T_D}{\partial x}\right)_S \qquad \text{for } t \geq 0 \tag{4.11}$$

Due to the low ambient pressure, the resistance to the mass transfer at the outer surface can be neglected. Thus

$$x = L \qquad C(L,t) = C_R \qquad \text{for } t \geq 0 \tag{4.12}$$

At the interface (ice-front) a thermodynamic equilibrium between ice and vapor is assumed. Thus, the concentration of the water vapor can be related to the ice temperature by the equilibrium relationship, or mathematically by

$$x = X(t) \qquad C_i = f_E(T_i) \qquad \text{for } t \geq 0 \tag{4.13}$$

From Fick's Equation, we have

$$x = X(t) \qquad \left(\frac{\partial C}{\partial x}\right)_i = -\frac{1}{D} W_i \qquad \text{for } t \geq 0 \tag{4.14}$$

An energy balance at the interface also gives

$$x = X(t) \qquad k_F\left(\frac{\partial T_F}{\partial x}\right)_i - k_D\left(\frac{\partial T_D}{\partial x}\right)_i = -W_i \Delta H_s \qquad \text{for } t \geq 0 \tag{4.15}$$

There should not be any discontinuity in temperature at the interface. Thus

$$x = X(t) \qquad T_F = T_D = T_i \qquad \text{for } t \geq 0 \tag{4.16}$$

Finally, the rate of movement of the interface position can be related to the rate of sublimation by

$$-\rho\,\sigma\,\frac{dX}{dt} = W_i \tag{4.17}$$

3. Initial values

As the thickness of the dried layer is initially zero, it is not possible to define the initial temperature and concentration profiles in the dried layer. In order to facilitate the solution, an arbitrary, but small initial thickness δ_o of the dried layer is chosen. An initial thickness of .1% of the total slab thickness L is used in the numerical solution. Thus, in the frozen region, we have

$$t = 0^+ \qquad T_F = T_o \qquad \text{for } 0 \leq x \leq L-\delta_o \tag{4.18}$$

In the dried layer, the initial temperature profile is assumed linear and is given by

$$t = 0^+ \qquad \frac{T_S - T_D}{T_S - T_o} = \frac{L - x}{\delta_o} \qquad \text{for } L-\delta_o \leq x \leq L \tag{4.19}$$

where the surface temperature is given by the boundary condition at the outer surface, Eq. (4.11).

The initial concentration profile, which is also assumed to be linear, is determined from the initial rate of sublimation as no equilibrium is established yet between the water vapor and ice at the interface.

$$t = 0^+ \qquad C(x,0^+) = C_R + \frac{W_{i,o}}{D}(L - x) \qquad \text{for } L-\delta_o \leq x \leq L \tag{4.20}$$

The initial rate of sublimation $W_{i,o}$ is given by the energy balance at the interface, Eq. (4.15).

4. Fixed boundary transformation and normalization

Equations (4.7), (4.8), and (4.9) are a set of partial differential equations which are to be solved with a moving boundary. In order to facilitate the solution of these equations, Landau's transformation (Bankoff (1964)) is used to convert the problem of a moving boundary to that of a fixed boundary. The following transformations

$$z = \frac{L - x}{L - X(t)} \tag{4.21}$$

$$y = \frac{x}{X(t)} \tag{4.22}$$

are used in conjunction with the following normalized variables

$$\tau = \frac{\alpha_F^o \, t}{L} \tag{4.23}$$

$$S = \frac{X(t)}{L} \tag{4.24}$$

$$\Gamma = \frac{C - C_R}{C_{TP} - C_R} \tag{4.25}$$

$$\Theta = \frac{T - T_o}{T_R - T_o} \tag{4.26}$$

and

$$D^* = \frac{D}{\alpha_F^o} \tag{4.27}$$

$$\alpha^* = \frac{\alpha}{\alpha_F^o} \tag{4.28}$$

$$\omega^* = \frac{\omega}{\omega_F^o} \tag{4.29}$$

Substitution of the transformation and normalization equations into Equations (4.7), (4.8), and (4.9) gives

$$\frac{\partial^2 \Gamma}{\partial z^2} + \left[\frac{1}{D^*}\frac{\partial D}{\partial z} - \frac{1}{D^*} z(1-S)\frac{dS}{d\tau}\right]\frac{\partial \Gamma}{\partial z} - \frac{\sigma}{D^*}(1-S)^2 \frac{\partial \Gamma}{\partial \tau} = 0 \tag{4.30}$$

$$\frac{\partial^2 \Theta_D}{\partial z^2} + \left[\frac{1}{\alpha_D^*}\frac{\partial \alpha_D^*}{\partial z} - \left(\frac{C_{pw}\rho\,\sigma}{\rho_D C_D \alpha_D^*} + \frac{1}{\alpha_D^*} z\right)(1-S)\frac{dS}{d\tau}\right]\frac{\partial \Theta_D}{\partial z} - \frac{1}{\alpha_D^*}(1-S)^2 \frac{\partial \Theta_D}{\partial \tau} =$$

$$- \frac{\omega_D^*}{\alpha_D^*}\frac{\rho_F C_F}{\rho_D C_D}\frac{\omega_F^o L^2 (1-S)^2}{k_F^o (T_R - T_o)} \tag{4.31}$$

$$\frac{\partial^2\Theta_F}{\partial y^2} + \left[\frac{1}{\alpha_F^*}\frac{\partial\alpha_F^*}{\partial y} + \frac{1}{\alpha_F^*}\, y\, S\, \frac{dS}{d\tau}\right]\frac{\partial\Theta_F}{\partial y} - \frac{1}{\alpha_F^*}\, S^2\, \frac{\partial\Theta_F}{\partial\tau} = -\frac{\omega_F^*}{\alpha_F^*}\,\frac{\omega_F^o\, L^2\, S^2}{k_F^o(T_R - T_o)} \qquad (4.32)$$

The boundary and initial conditions become

$$y = 0 \qquad \frac{\partial\Theta_F}{\partial y} = 0 \qquad \text{for } \tau \geq 0 \qquad (4.33)$$

$$z = 0 \qquad \Theta_D - \frac{\rho_D C_D \alpha_D^* \alpha_F^o}{h\, L\, (1-S)}\,\frac{\partial\Theta_D}{\partial z} = 1 \qquad \text{for } \tau \geq 0 \qquad (4.34)$$

$$\Gamma = 0 \qquad \text{for } \tau \geq 0 \qquad (4.35)$$

At the interface where $y = z = 1$, one has

$$\Gamma_i = f_1(\Theta_i) \qquad \text{for } \tau > 0 \qquad (4.36)$$

$$\frac{\alpha_F^*}{S}\,\frac{\partial\Theta_F}{\partial y} + \frac{\rho_D C_D}{\rho_F C_F}\,\frac{\alpha_D^*}{1-S}\,\frac{\partial\Theta_D}{\partial z} = -\frac{L\ \Delta H_s\ W_i}{k_F^o\ (T_R - T_o)} \qquad \text{for } \tau \geq 0 \qquad (4.37)$$

$$\Theta_D = \Theta_F = \Theta_i \qquad \text{for } \tau \geq 0 \qquad (4.38)$$

and the movement of the interface is given by

$$\frac{dS}{d\tau} = -\frac{W_i\ L}{\rho\,\sigma\,\alpha_F^o} \qquad (4.39)$$

where the rate of sublimation can be represented by

$$W_i = \frac{D(C_{TP} - C_R)}{L(1-S)}\left(\frac{\partial\Gamma}{\partial z}\right)_{z=1} \qquad (4.40)$$

The initial conditions become

$$\Theta_F = 0 \qquad \text{for } 0 \leq y \leq 1 \qquad (4.41)$$

$$\Theta_D = (1 - z)\ \Theta_{S,o} \qquad \text{for } 0 \leq z \leq 1 \qquad (4.42)$$

where $\Theta_{S,o}$ is given by the boundary condition at the outer surface,

$$\Theta_{S,o} = \frac{h\ L\ (1-S)}{hL(1-S) + k_D^o} \qquad \text{for } z = 0 \qquad (4.43)$$

Finally, one has

$$\Gamma = z\left(\frac{\partial\Gamma}{\partial z}\right)_{z=1} = z\,\frac{L(1-S)W_{i,o}}{D_o(C_{TP}-C_R)} \qquad \text{for } 0 \leq z \leq 1 \quad (4.44)$$

- Chapter V -

THE NUMERICAL METHOD

Under the assumptions made earlier, the set of partial differential Equations (4.30), (4.31), and (4.32) with the initial and boundary conditions, Equations (4.33) through (4.44), constitutes a one-dimensional mathematical model of the microwave freeze-drying process. Solutions of these equations will provide one with a means to predict the time variations of the dependent variables such as temperature and concentration whithin the sample in the course of the dehydration and obtain some information on drying rate and drying time, necessary for design purposes.

The partial differential equations to be solved form a set of three parabolic equations with phase change at a moving boundary. Even in the simpler case of one equation, it is known mathematically as a very cumbersome problem and a general solution has been found only in special instances (Bankoff (1964)), such as that of a semi-infinite slab, often referred to as the Von Neumann problem. No general solution has been found yet for the finite slab with different properties on both sides of the moving boundary. In the case under consideration, there are three equations which are coupled through their boundary conditions at the moving boundary (interface). Moreover, all physical properties of the sample are considered as a function of the dependent variables (temperature and water vapor concentration). Thus, they are considered to

vary with both time and location. Consequently, an analytical or even a semi-analytical solution are discarded as most unlikely, and a numerical technique is used to obtain the solutions.

1. The finite-difference method of approximation

The fixed boundary domain of Chapter IV, Sec. 4, is divided into intervals as shown in Fig. 5.1. The space-axis is divided into M intervals of equal length Δy in the frozen region and K intervals of length Δz in the dried layer. The time axis is divided in intervals of duration $\Delta\tau$.

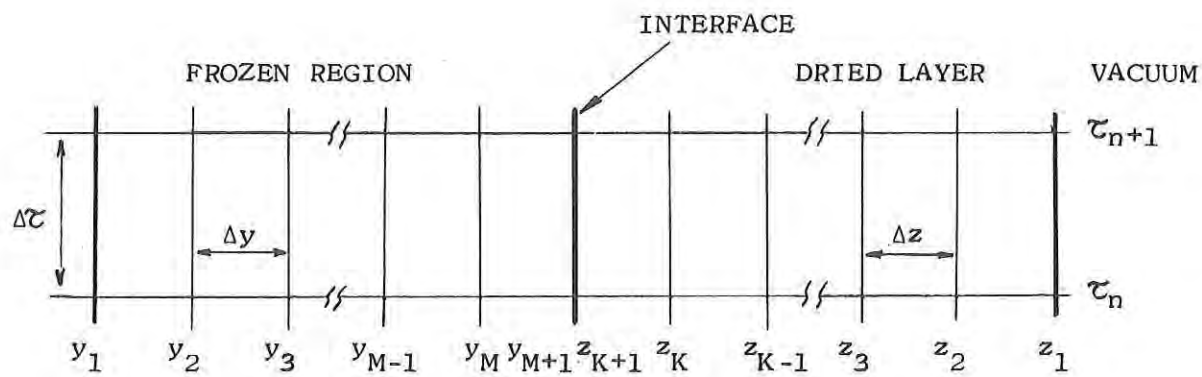

Figure 5.1 - Numerical grid in the fixed boundary domain

The size of $\Delta\tau$ is chosen so that the numerical solution is stable and accurate with reasonable computation time (see discussion, Sec. 4). The numerical grid thus obtained is used to derive finite-difference equations from the partial differential equations.

For this purpose the partial differential equations are approximated by the Crank-Nicolson method which offers the best approximation for the time-derivatives and thus the smallest truncation error (Smith (1965)).

The general technique used in the derivation of the finite-difference equations is described here and the reader is referred to Appendix A for the complete equations which are rather voluminous

due to the complexity of the mathematical system.

If one uses U as a dummy variable, then according to the Crank-Nicolson method, the following approximations are made: with

$$U_{k,n} = U(x_k, \tau_n) \tag{5.1}$$

one has

$$U_{k,n+\frac{1}{2}} = \tfrac{1}{2}\,(U_{k,n+1} + U_{k,n}) \tag{5.2}$$

$$\left(\frac{\partial U}{\partial x}\right)_{k,n+\frac{1}{2}} = \tfrac{1}{2}\left(\frac{U_{k+1,n+1} - U_{k-1,n+1}}{2\Delta x} + \frac{U_{k+1,n} - U_{k-1,n}}{2\Delta x}\right) \tag{5.3}$$

$$\left(\frac{\partial^2 U}{\partial x^2}\right)_{k,n+\frac{1}{2}} = \tfrac{1}{2}\left(\frac{U_{k+1,n+1} - 2U_{k,n+1} + U_{k-1,n+1}}{\Delta x^2} + \frac{U_{k+1,n} - 2U_{k,n} + U_{k-1,n}}{\Delta x^2}\right) \tag{5.4}$$

$$\left(\frac{\partial U}{\partial \tau}\right)_{k,n+\frac{1}{2}} = \frac{U_{k,n+1} - U_{k,n}}{\Delta \tau} \tag{5.5}$$

where x_k stands for z_k or y_k. This procedure is used to derive all the finite-difference equations. Typically, an equation such as

$$\frac{\partial^2 U}{\partial x^2} + a(x,\tau)\,\frac{\partial U}{\partial x} + b(x,\tau)\,\frac{\partial U}{\partial \tau} = c(x,\tau) \tag{5.6}$$

is approximated by

$$\frac{U_{k+1,n+1} - 2U_{k,n+1} + U_{k-1,n+1}}{\Delta x^2} + a_{k,n+1}\frac{U_{k+1,n+1} - U_{k-1,n+1}}{2\Delta x} + b_{k,n+1}\frac{U_{k,n+1} - U_{k,n}}{\Delta \tau}$$

$$+\frac{U_{k+1,n} - 2U_{k,n} + U_{k-1,n}}{\Delta x^2} + a_{k,n}\frac{U_{k+1,n} - U_{k-1,n}}{2\Delta x} + b_{k,n}\frac{U_{k,n+1} - U_{k,n}}{\Delta \tau} = c_{k,n+1} + c_{k,n} \tag{5.7}$$

It should be noted that the means of the products are evaluated as

$$(u.v)_{n+\frac{1}{2}} = \tfrac{1}{2}\,(u_{n+1}v_{n+1} + u_n v_n) \qquad (5.8)$$

2. Method of solution

Although it is clear that the coefficients in Equation (5.6) are time dependent and therefore unknown at time τ_{n+1}, let us suppose for simplicity that they are indeed known. Their determination will be discussed in the next section. Equation (5.7) can then be rearranged by grouping all known terms on the right hand side of the equal sign, to give the general form

$$U_{k-1} + \alpha_k U_k + \beta_k U_{k+1} = \gamma_k \qquad k = 2,\ldots,K \qquad (5.9)$$

Eq. (5.9) actually represents a set of K-1 linear equations at K-1 grid points between the boundaries: $x_2, x_3, \ldots, x_K$. Two more relations are obtained from the boundary conditions which are written in a general manner:

at the outer edge (center-line or external surface)

$$U_1 + \delta_1 U_2 = \lambda_1 \qquad \text{at } x = x_1 \qquad (5.10)$$

and at the interface

$$p\,U_K + U_{K+1} = q \qquad \text{at } x = x_{K+1} \qquad (5.11)$$

Details on the derivation of these relations as well as their actual complete form are given in Appendix A.

Equations (5.9), (5.10), and (5.11) form a set of K+1 linear equations which are to be solved with K+1 unknowns U_k, with $k = 1,\ldots,K+1$. The set is solved in a sequential manner by elimination (Gauss's elimination technique - Smith (1965)). A forward elimination reduces Equation (5.9) to the form

$$U_k + \delta_k U_{k+1} = \lambda_k \qquad k = 1,\ldots,K \qquad (5.12)$$

where the δ's and λ's are known. Equations (5.11) and (5.13) are solved simultaneously for U_{K+1}. The U_k's are then determined by Equation (5.12) through back subsitution.

$$U_K + \delta_K U_{K+1} = \lambda_K \tag{5.13}$$

$$U_K + p\, U_{K+1} = q \tag{5.11}$$

Details of the algorithm are given in Appendix B.

3. The general numerical scheme of solution

Before the equations can be solved to obtain the temperature and concentration profiles at τ_{n+1} by the method outlined in the previous section, the current position of the interface and values of the properties, (i.e., thermal diffusivity, diffusivity and dissipation coefficient) must be evaluated. As they are functions of the dependent variables (temperature and concentration), their values have to be assumed on the basis of their previous history and iterated if necessary.

The interface motion is related theoretically to the rate of sublimation, or the rate at which energy is consumed at the interface, by Equation (4.39)

$$\frac{dS}{d\tau} = - \frac{L\, W_i}{\rho\, \sigma\, \alpha_F^o}$$

This equation is used to calculate the position of the interface at τ_{n+1},

$$S_{n+1} = S_n - \Delta\tau \frac{L}{\rho\, \sigma\, \alpha_F^o} W_{i,n+\frac{1}{2}} \tag{5.14}$$

The rate of sublimation at τ_{n+1} is not known. One only knows the rate at τ_n and earlier. Thus, $W_{i,n+\frac{1}{2}}$ is approximated by

$$W_{i,n+\frac{1}{2}} = W_{i,n-\frac{1}{2}} + (W_{i,n} - W_{i,n-1}) = W_{i,n-\frac{1}{2}} + (\Delta W_i)_{n-\frac{1}{2}} \tag{5.15}$$

From the profiles calculated at τ_{n+1}, a value of $W_{i,n+\frac{1}{2}}$ is obtained by an energy balance at the interface (see Appendix A for details of the calculations) and used to recalculate the interface position

S_{n+1}. This process is repeated until the variation of S_{n+1} is only on the 7th digit. A fixed number of two iterations was found to be sufficient in most cases.

The properties, i.e., diffusivity, thermal diffusivity and dissipation coefficient, vary with both time and location. They are functions of the dependent variables (temperature and concentration). They are calculated from their current value through functional relationships derived from literature data (see Chapter VI). Consequently, as their exact value cannot be known unless the dependent variables are estimated, their value at τ_{n+1} is approximated by that at τ_n and iterated if need be. In fact, the physical properties are not strong functions of the temperature and concentration. Thus, they are not expected to vary significantly over one time-increment, considering the small size of the time-increment used ($\Delta t \leq 7.2$ sec as compared to a total drying time of 2 to 10 hours (7,200 to 36,000 sec)). This approximation proved to be satisfactory for the thermal diffusivity and the dissipation coefficient.

However, the approximation is not sufficient for the diffusivity, as small fluctuations on D^* are magnified in the term $\frac{\partial D^*}{\partial z}$ in Equation (4.30), which results in high fluctuations on the concentration. It is necessary to obtain a better accuracy of D^* to eliminate the concentration fluctuations. This was done by inserting the calculation of the diffusivity inside the iteration loop for the interface position, so that the value of D^* is updated once the temperature and concentration profiles have been calculated at τ_{n+1}.

This problem does not occur with the thermal diffusivity for the time-increment used, although the energy equations comprise a similar term $\frac{\partial \alpha_D^*}{\partial z}$ or $\frac{\partial \alpha_F^*}{\partial y}$. This can be explained by the fact that α_D^* and α_F^*. have a much smaller value than that of D^*. Fig. 5.2 gives the flow chart of the general numerical scheme.

The boundary conditions at the interface are such that, once the interface position and the properties have been estimated,

a second iteration loop is needed to calculate the profiles. In effect, as the heat and mass transfer equations are coupled at the interface, no explicit form of the boundary condition - such as Eq. (5.11) - can be obtained for these equations ((4.30), (4.31), and (4.32)). Thus, the temperature at the interface is assumed on the basis of its previous history,

$$T_{i,n+1} = T_{i,n} + (T_{i,n} - T_{i,n-1}) = T_{i,n} + (\Delta T_i)_{n-\frac{1}{2}} \qquad (5.16)$$

and then iterated. From the assumed interface temperature, the concentration at the interface can also be calculated through the equilibrium relationship. Thus, the temperature and concentration profiles at τ_{n+1} can be calculated. A theoretical value is then computed from a full energy balance at the interface and compared to the assumed value. Unless an agreement on the 6th digit is reached, a new value is assumed for the interface temperature T_i according to

$$T_i^{*j+1} = \xi T_i^j + (1 - \xi)\, T_i^{*j} \qquad (5.17)$$

and the iteration proceeds. The coefficient ξ in Equation (5.17) is used to force and accelerate the convergence. It is constantly updated, by the scheme described and justified in Appendix B. With this scheme, convergence is generally attained in 2 to 4 iterations. The general flow chart of the algorithm is described in Fig. 5.2.

4. Stability, accuracy of the solution, and simulation speed

The stability and the accuracy of the solution, as well as the simulation speed are essentially affected by the size of the space and time increments. In simple cases, a Fourier analysis of the mathematical system can provide a stability criterion in terms of the ratio $\frac{\Delta t}{\Delta x^2}$. It often results in a maximum value for this ratio, beyond which the solution becomes unstable (i.e., the numerical solution oscillates about the true solution).

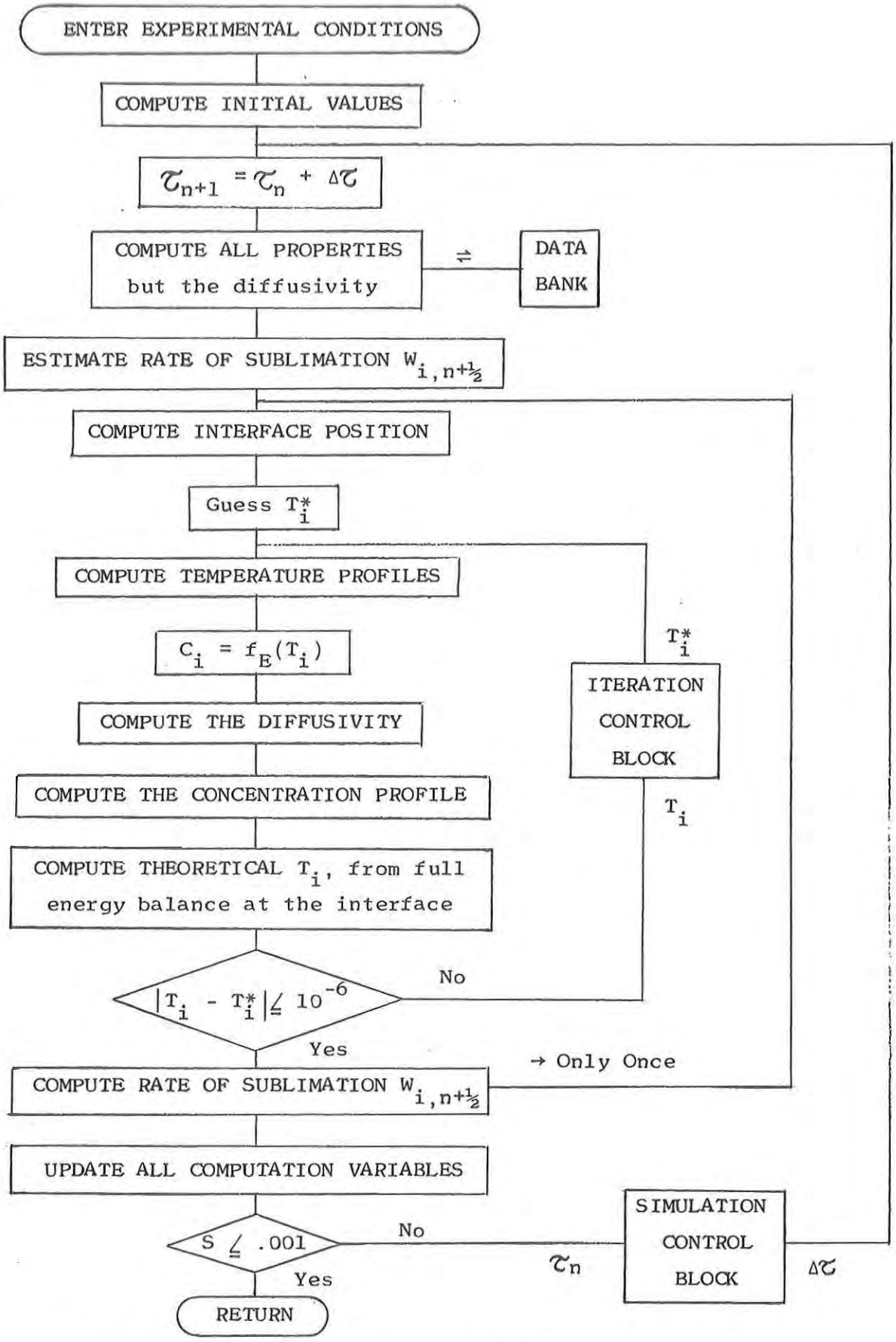

Figure 5.2- General algorithm flow chart - Subroutine MFWD.

Unfortunately, due to the high degree of complexity of the mathematical system encountered here, such an analysis is expected to be extremely cumbersome. Thus, variations of $\frac{\Delta t}{\Delta x^2}$ are used to study the behavior of the solution.

The space increment is usually fixed and its value decided on the ground of the accuracy desired in the determination of the profiles of the dependent variables. When the profiles are smooth curves with no sharp slope changes, 20 space intervals are sufficient to give a good description of the curves. This is done here. Both the frozen region and the dried layer are divided into 20 equal intervals ($\Delta z = \Delta y = 0.05$). As the time-variation of the variables is small, one may think that a large value of the time increment Δt can be used without an appreciable loss of accuracy. For instance, for a total drying time of 6 hours (216,000 sec), one might be able to use a Δt as high as 3.6 min (216 sec) with a reasonable accuracy, and thus a high simulation speed. However, the stability requirement is such that much smaller values of Δt had to be used, especially at the beginning of the simulation. Table 5.1 shows the results of the stability study for different Δt, as a function of time for a typical calculation.

Table 5.1 - stability of the numerical solution

Time increment number	Value of the time increment Δt		
	0.072 sec	0.72 sec	7.2 sec
0 - 100	stable	unstable	unstable
100 - 500	stable	stable	unstable
500 - ∞	stable	stable	stable

Hence, a Δt of .072 sec is used for the first 100 time increments. A Δt of .72 sec is used for the next 400 time increments and a Δt of 7.2 sec was used for the rest of the computation. The corresponding, normalized time increment $\Delta\tau$ is computed from the normalization equation (4.23). The total number of time increments necessary to reach the end point (S = 0.001) varied from 1,500

to 8,000 depending on the total drying time. The average total number of iterations per time increment is of the order of 6 to 10. The computer time required is of the order of 3 to 5 min of CPU time per hour of total drying time on a PDP-10 digital computer.

- PART II -

APPLICATION TO THE FREEZE-DRYING OF BEEF MEAT AT 2450 MHz

Chapter VI: Numerical Data Used in the Calculations

Chapter VII: Theoretical Results and Discussion

- Chapter VI -

NUMERICAL DATA USED IN THE CALCULATIONS

This chapter is concerned with the presentation of the numerical values of the physical constants and the functional relationships of the non-constant properties used in the mathemathical simulation of the freeze-drying of a one-dimensional beef meat slab using microwave dielectric heating at 2450 MHz. The slab is cut normal to the fibers.

1. The constants

The numerical values used for the physical constants are summarized in Table 6.1. Some were assumed because of the lack of experimental data in the literature. This was the case for the heat transfer coefficient. Although vacuum freeze-drying has been on the industrial scene for many years, no value of the heat transfer coefficient could be found. This is apparently due to the general feeling that it is not a significant parameter and, should be determined according to a particular design. The value given in Table 6.1 was estimated from the initial slope of a preliminary experimental drying curve. Introduction of a continuous recording of the sample weight during drying permitted a more accurate estimation of the heat transfer coefficient from the start-up portion of the drying curve (see Chapter IX). It was then found that an h value of the order of 2×10^{-4} cal/cm^2/sec/°C

Table 6.1 - Numerical values of the constants used in the simulation.

Constant	Numerical value used	Origin
h	5×10^{-4} cal/cm^2/sec/°C	assumed
ρ	.92 g/cm^3	CRC Hdbk
ρ_D	.32 g/cm^3	measured
ρ_F	.96 g/cm^3	measured
C_{pw}	.5 cal/g/°C	assumed
C_D	.36 cal/g/°C	Awberry & Griffiths (1933)
C_F	.43 cal/g/°C	Rey (1964)
ΔH_s	675 cal/g	Hohner (1970) after Threlkeld (1962)

would be more suitable for the freeze-dryer used in the experiments. This value is used for the comparison of the experimental drying curves with those predicted.

It was also assumed that the specific heat of the water vapor at the usual freeze-drying operating conditions (-50°C to 60°C; .05 to 1 mmHg) could be approximated by that at 100°C and 1 atm. (exactly .4836 cal/g/°C after Lange's Handbook of Chemistry). It may be somewhat different, due to the difference in temperature and pressure as well as the relative importance of the wall effects in the transition flow regime.

The average porosity (void fraction) is computed from the initial moisture content and the densities of pure ice and frozen meat,

$$\sigma = x_w \frac{\rho_F}{\rho} \tag{6.1}$$

The shrinkage effect occuring on the dried product is neglected and the same porosity value is used for the frozen region and the dried layer. It is taken as that of the frozen meat.

2. Effective thermal conductivity of frozen beef

Numerical data from various literature sources were gathered for heat flow parallel to the fibers. An attempt was made to fit the data with a functional relationship of the following form,

$$k_F = a + b\sqrt{T_f - T} \tag{6.2}$$

This form is chosen because a plot of k_F vs temperature resembles a parabola with axis parallel to the horizontal temperature axis, and tangent at the vertex parallel to the vertical axis at about 0°C. A rather good fit, as shown in Fig. 6.1 was obtained. The parameter T_f is adjusted in order to reach the best fit, and could correspond to to the average fusion temperature of the frozen meat.

Some further interesting correlations were found. A plot of a in Equation (6.2) vs fat content shows that a varies linearly with the fat content while it does not seem to vary significantly with the water content. On the contrary, Fig. 6.3, b does not seem to depend on the fat content but varies linearly with the water content. It is found that, approximately

$$a = (2.95 - 25\ x_f) \times 10^{-3},\ \text{cal/sec/cm/°K} \tag{6.3}$$

$$b = \left[.02 + 1.8\ (x_w - .65)\right] \times 10^{-3},\ \text{cal/sec/cm/(°K)}^{1.5} \tag{6.4}$$

and on the average,

$$T_f = 271.5°K \tag{6.5}$$

Equation (6.2), along with (6.3), (6.4), and (6.5), is used to determine k_F in the simulation, with the temperature T expressed in °K. a and b are determined from the fat and water content of a given choice of meat by Equations (6.3) and (6.4).

3. Effective thermal conductivity of dried beef

The experimental data, obtained at various pressures by Harper (1962), are used to determine a functional relationship between the thermal conductivity and the total pressure. For this purpose a 4th degree polynomial is least square fit to Harper's data in terms of the natural logarithm of the pressure expressed in mmHg (see Fig. 6.4). The following expression was obtained

$$k_D = 10^{-4}(1.126 + 0.1351\ \text{Log}\ P + .01565(\text{Log}\ P)^2 - 3.187 \times 10^{-3}(\text{Log}\ P)^3 - 5.483 \times 10^{-4}(\text{Log}\ P)^4 \tag{6.6}$$

where P is in mmHg and k_D in cal/sec/cm/°C.

Additional data have been obtained by other investigators, particularly by Massey & Sunderland (1967). However, they are mostly the results of calculations for typical treeze-drying

Figure 6.1 - Thermal conductivity of frozen beef vs $\sqrt{T_f - T}$ for various moisture and fat contents.

Symbol	Literature Source	% moisture	% fat
▲	Lentz (1961)	75	.9
●	Miller & Sunderland (1963)	69.5	--
⬢	Hill et al. (1967)	76.5	2.35
■	Hill et al. (1967)	78.7	1.4

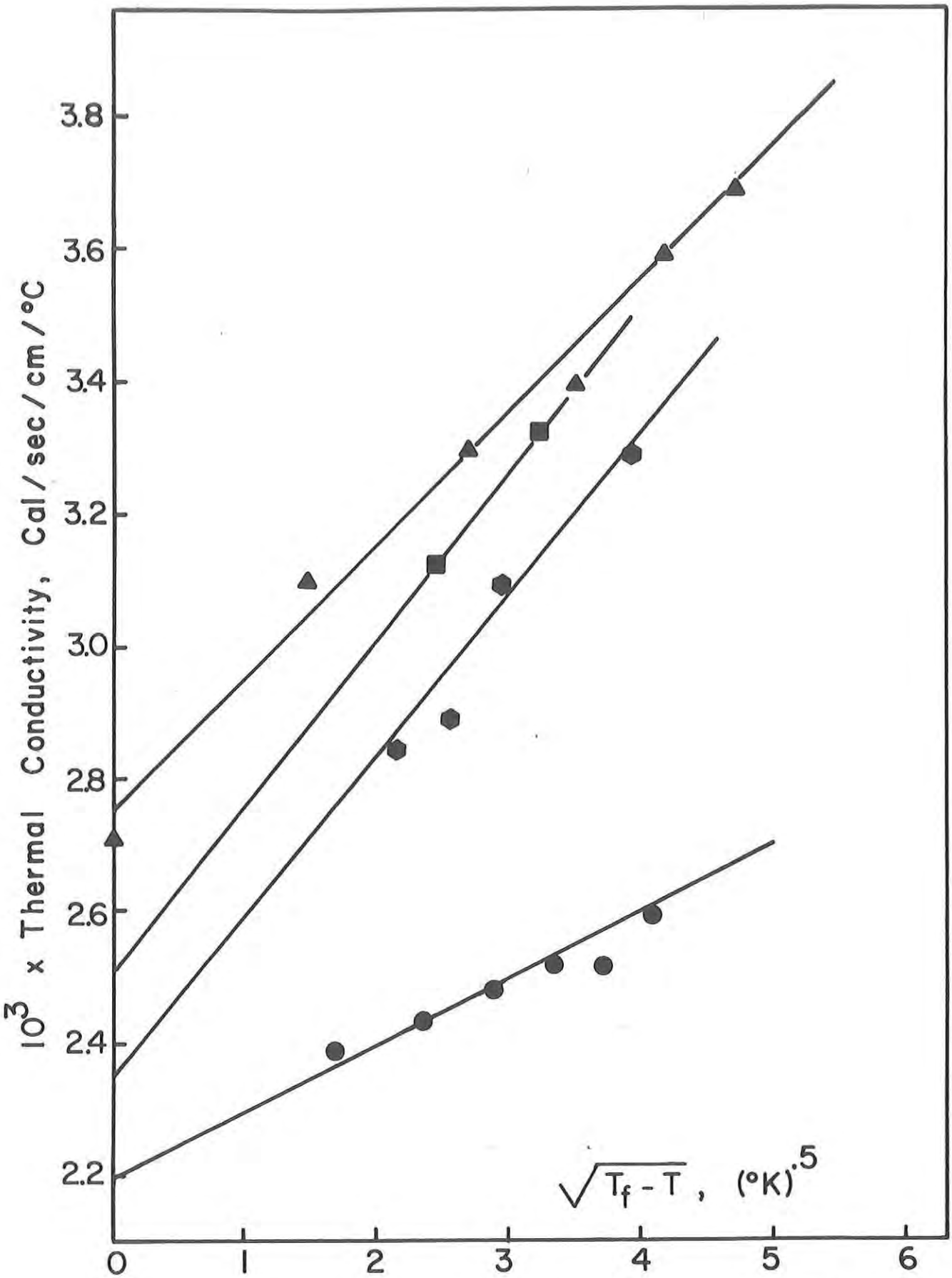

Figure 6.1 - Thermal conductivity of frozen beef vs $\sqrt{T_f - T}$. for various moisture and fat contents.

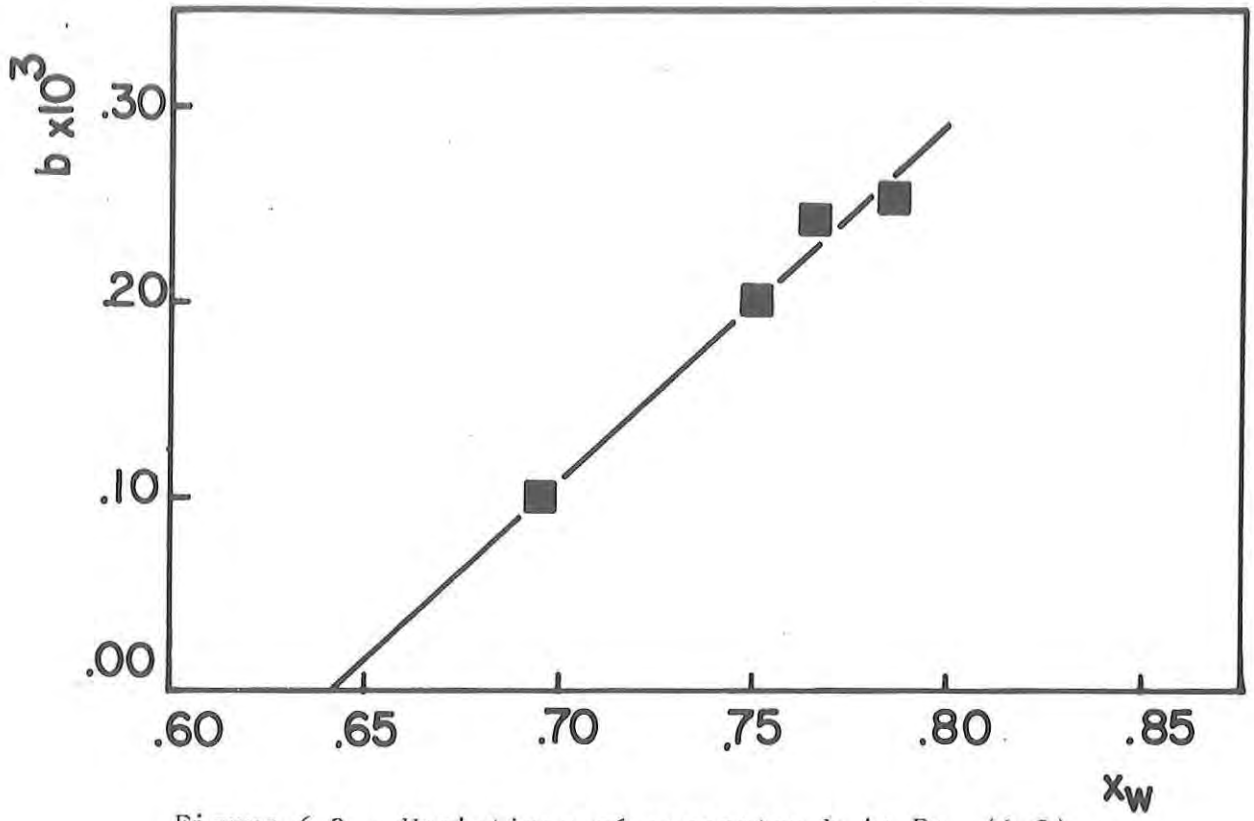

Figure 6.3 - Variations of parameter b in Eq. (6.3) vs moisture content of frozen beef.

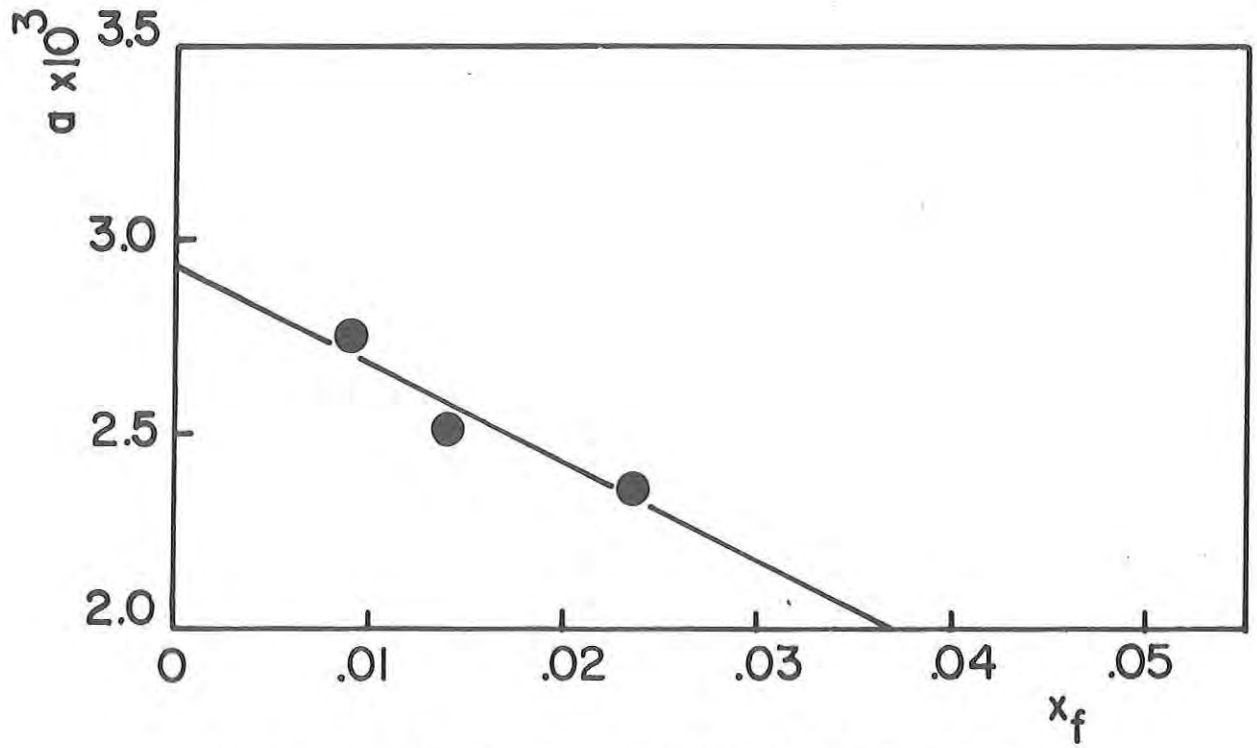

Figure 6.2 - Variations of parameter a in Eq. (6.2) vs fat content of frozen beef.

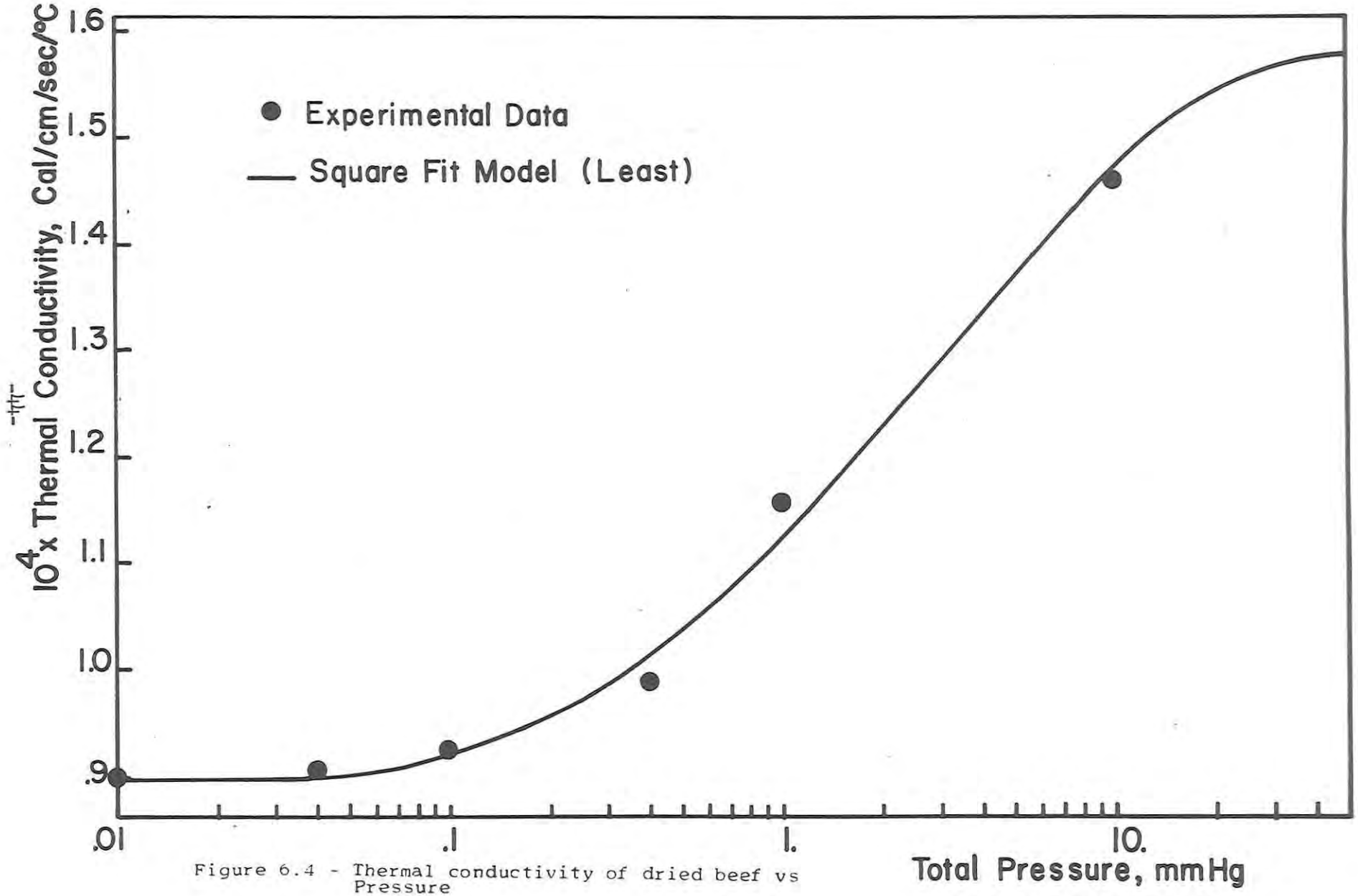

Figure 6.4 - Thermal conductivity of dried beef vs Pressure

experiments, based on a quasi-steady state model.

4. Effective diffusivity

A simplified two-parameter model, as proposed by Sandall et al. (1967), is used to describe the variations of the effective diffusivity D with the pressure in the transition flow regime,

$$D = \frac{D^o}{D^o/D_K + P} \tag{6.7}$$

where P is the pressure in atm, D° the bulb diffusivity at 1 atm, and D_K the Knudsen diffusivity.

Although the description of the water vapor mass transfer in vacuum freeze-drying processes by Fick's Equation seems widely accepted, few experimental data could be found on the diffusivity for dried beef in the transition flow regime. Sandall et al. (1967) diffusivity measurements for D° and D_K in the case of turkey breast were used in the theoretical study. They were corrected to the expected average temperature of the dried layer (20°C), assuming that D° varies as $T^{1.5}$ and D_K as $T^{0.5}$. Further temperature effects were neglected in the model as the relative variation on D is less than 20%. So that the following relationship was finally used to calculate the diffusivity as a function of pressure,

$$D = \frac{78.5}{3.4 + P} \tag{6.8}$$

where P is in mmHg and D in cm^2/sec. This was done as an approximation, due to the lack of experimental data on D_K for beef meat. It seems to be a reasonable approximation at low pressures if one considers the rather good agreement between the diffusivity calculated at 1.44 mmHg, from Sandall's D° and D_K values (for turkey breast) by Eq. (4.7), and that reported by Dyer & Sunderland (1966) for beef meat at the same pressure. These data are shown in Table 6.2.

Table 6.2 - Reported diffusivity data and computed values (superscripted)

Material used	T °K	D_K cm^2/sec	$D°$ cm^2/sec	$D_{1.44\ torr}$ cm^2/sec	Tortuosity	Porosity	Literature Source
Turkey/.	265	22	.09	15^c	1.5^a	--	Sandall et al. (1967)
breast	265	20	.1345	16^c	1.0^a	--	Sandall et al. (1967)
Beef	311	--	.045	--	4.4	.64	Harper (1962)
Beef	265	--	$.037^b$	10^c	4.4	.64	Harper (1962)
Beef	--	--	--	14	--	--	Dyer & Sunderland (1966)

a - Computed in this investigation from the ratio $D°/D°_{free\ gas}$ reported by them, assuming a porosity of .64 for the dried material.

b - Corrected at 265°K for comparison to Sandall s value, assuming that D° varies as $T^{1.5}$.

c - Computed by Equation (4.7) for comparison to Dyer & Sunderland's value, assuming D_K = 21 cm^2/sec.

5. Dissipation coefficient of frozen and dried beef

The dielectric properties of frozen and dried beef are expected to be a function of the fat, moisture and salt contents as well as the temperature and the frequency of the microwave field. Unfortunately, only the temperature effect for frozen and dried beef is available at 3000 MHz as reported by Kan and Yeaton (1961). Kan and Yeaton's data were assumed to hold at 2450 MHz and used to determine the dissipation coefficient K defined by Equation (3.6). Figures 6.5 and 6.6 show the plots of K_D and K_F vs temperature. The analytical expressions reached for these polynomials are (K is in cal/sec/cm^3/(V/cm)^2; T in °K):

$$K_D = 10^{-6} \times (14.39 - .1577\ T + 5.577 \times 10^{-4} T^2 - 5.924 \times 10^{-7} T^3) \tag{6.9}$$

$$K_F = 10^{-6} \times (294.7 - 3.628\ T + 1.464 \times 10^{-2} T^2 - 1.922 \times 10^{-5} T^3) \tag{6.10}$$

6. Ice-water vapor equilibrium relationship

The equilibrium data of pure ice, were used in this work although a depletion of the equilibrium vapor pressure of as much as 20% may occur in frozen beef as reported by Dyer et al. (1966). The equilibrium vapor pressure at the ice front was related to the concentration of water vapor in the pore using the perfect gas law. Fig. 6.7 shows the plot of the equilibrium water vapor concentration and pressure in the pore vs ice temperature. The following analytical expression is used in the simulation to depict the ice-vapor equilibrium,

$$C_i = \exp(-63.23 + 0.2969\ T_i - 4.038 \times 10^{-4} T_i^2) \tag{6.11}$$

where C_i is the equilibrium concentration of water vapor at the ice-front inside the pore, in g/cm^3, and T_i is the ice equilibrium

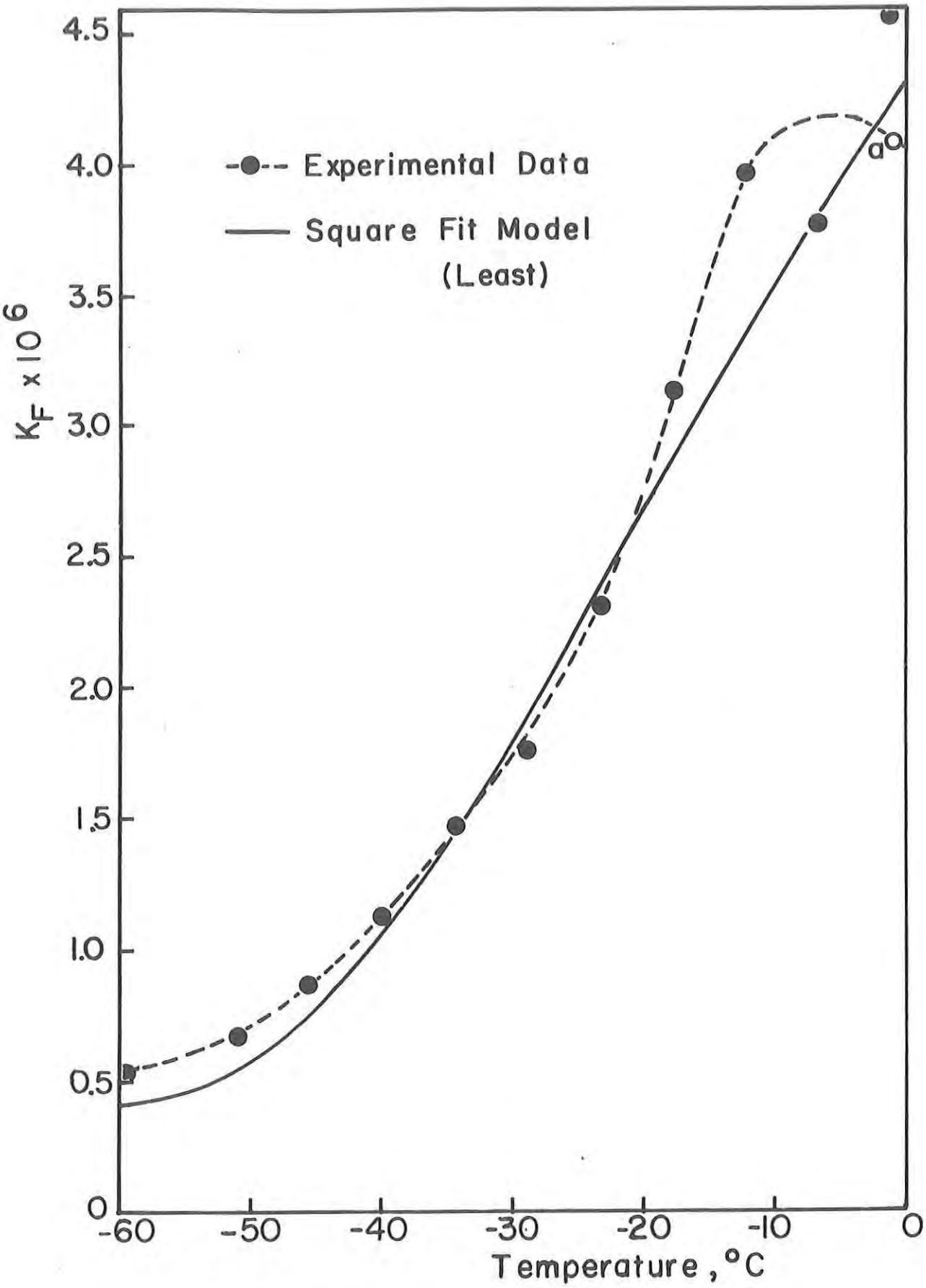

Figure 6.5 - Variations of K_F (cal/sec/cm^2/(V/cm)^2) with temperature
a- average between three consecutive points

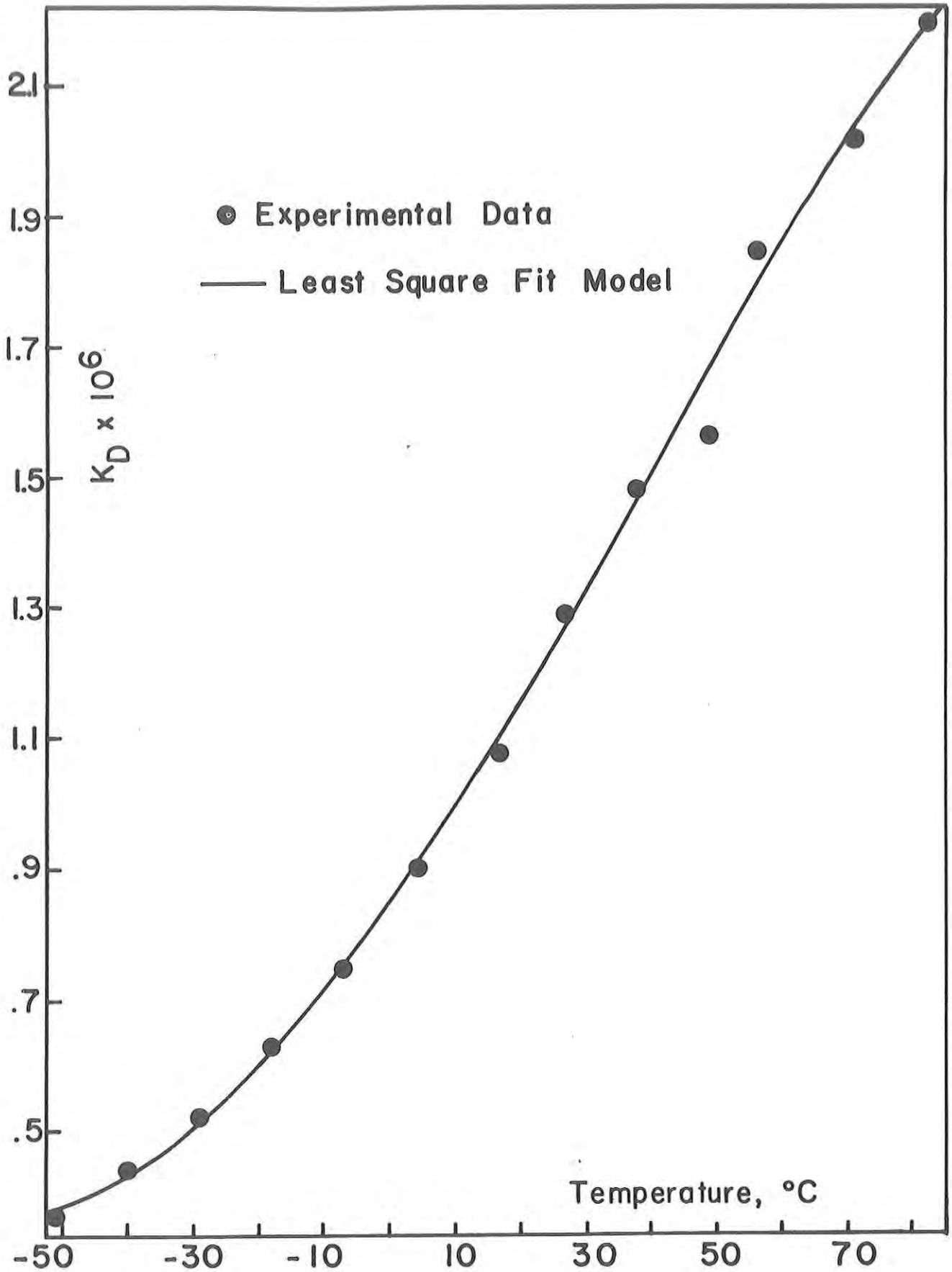

Figure 6.6 - Variations of K_D (cal/sec/cm^2/(V/cm)^2) with temperature.

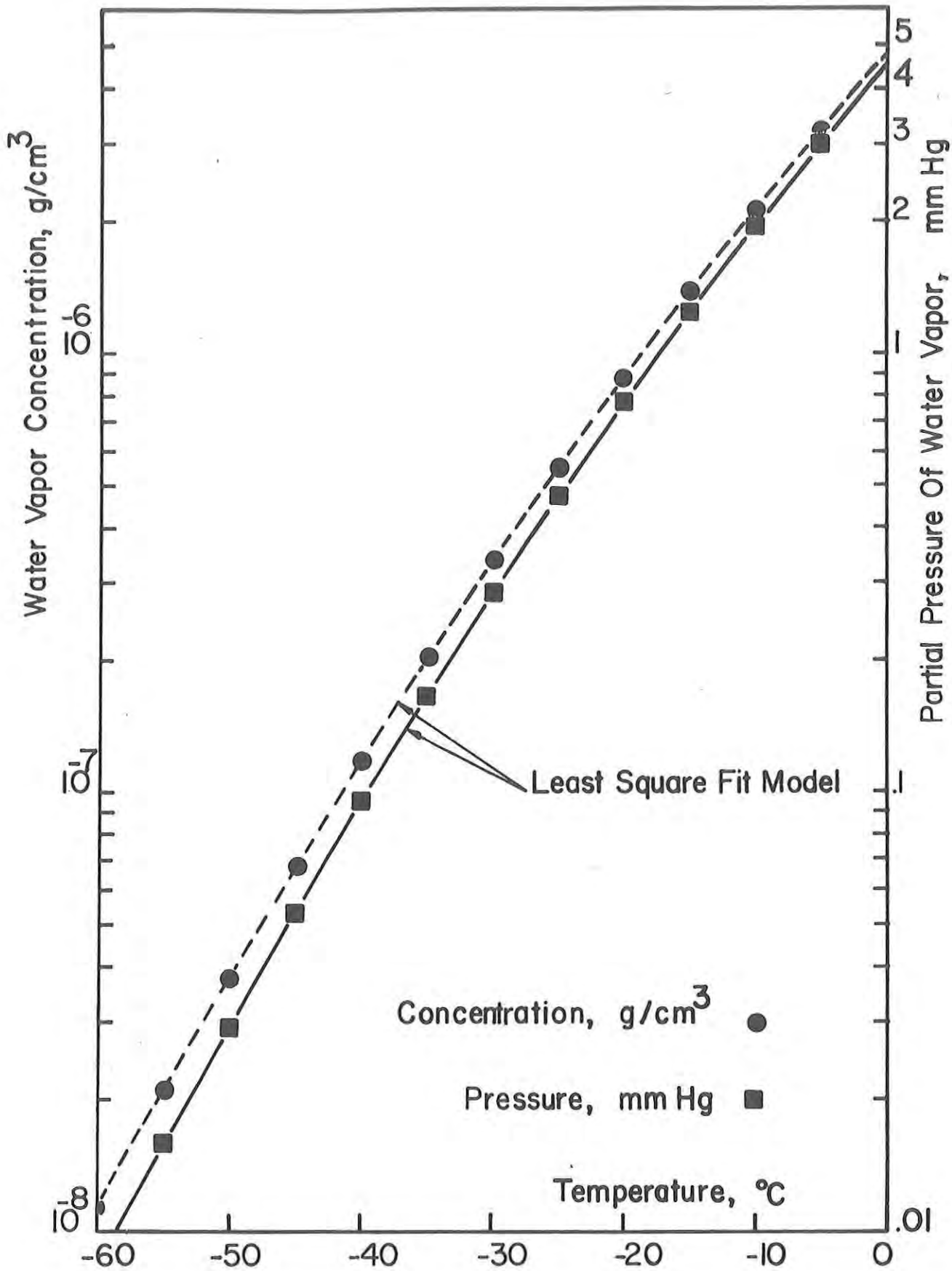

Figure 6.7 - Ice-vapor equilibrium relationship

temperature, °K.

- Chapter VII -

THEORETICAL RESULTS

The mathematical model derived earlier has been applied to the freeze-drying of beef meat with microwave energy at 2450 MHz. The sample is assumed to have the geometry of a one-dimensional symmetric slab with drying on both sides. Using the previous numerical data (Chapter VI), calculations were carried out in order to study the effects of the physical constraints of the process upon the total drying time as a function of the process variables. The results of these calculations are presented and discussed below.

It should be noted that the following results are obtained by employing a typical set of numerical data. Care must be exerted to extend the present results to other "practical" systems as it is important to have more specific and comprehensive experimental data. These results are primarily intended as a verification of the response of the mathematical model under typical operating conditions to serve as design guidelines.

1. Typical simulation outcome

It is possible to investigate quantitatively the variations of any characteristic properties through simulation. Of special interest are the temperature and water vapor concentration profiles within the sample. The variations of the sample weight (or the

ice-front position) and the characteristic temperatures with time are also of interest as they reflect the general freeze-drying performance for given operating conditions.

Of importance, too is the question of energy conversion efficiency for sublimation, which can be illustrated by the comparative histories of the microwave power absorbed in the sample and the power consumed by the sublimation.

The operating conditions used in the calculations are shown in Table 7.1.

Fig. 7.1 shows typical concentration and temperature profiles during the freeze-drying process.

The concentration profiles in the dried layer exhibit a rather small curvature. In a previous study (Ma & Peltre (1973)) of the same process using a simpler model in which the properties were assumed uniform and constant, the concentration profiles were found to be essentially straight lines. Thus, this small curvature may be attributed to the variation of the diffusivity with location, as the time derivative in the mass balance equation is negligible compared to the space derivatives, due to the slow motion of the interface and high value of the diffusivity.

On the other hand, the temperature profiles in both the frozen and dried regions are parabolic in shape which is expected from a quasi-steady state analysis. The locations of the temperature maxima in both the frozen and dried layers have specific significance as they represent the maximum temperature in these regions at any time. In fact, the temperature in the frozen region always should be kept below the melting point of the frozen material (around -1.5°C) while an upper limit of 60°C is often quoted for the dried layer in order to avoid the thermal degradation of the dried product. As shown in Fig. 7.1, the maximum temperature is at the insulated wall (center line) in the frozen region while in the dried layer it is located at the external surface during the major portion of the dehydration process. However,

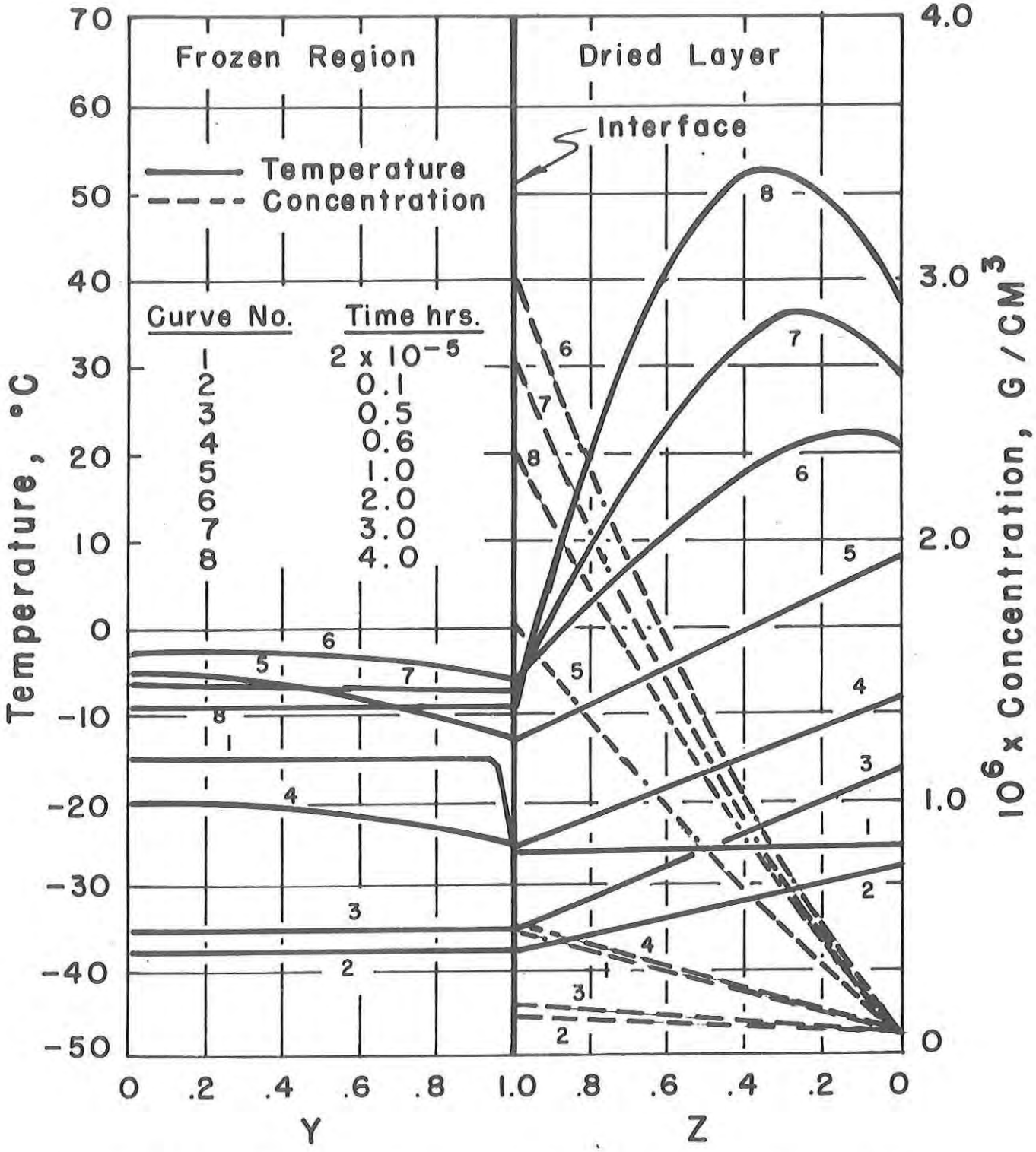

Figure 7.1 - Typical concentration and temperature profiles for the microwave freeze-drying process.

the vertex of the parabola shifts from right to left as time elapses. Near the end of the process, the maximum temperature is located inside the dried layer. Thus, hot spots inside the dried layer may be created.

Fig. 7.2 shows the maximum temperatures in the frozen and dried regions, and the interface temperature and position as a function of time.

The temperatures drop to a minimum at the beginning of the process, during the start-up stage as the ice-front temperature drops to the "wet bulb" temperature of the chamber. This may be attributed to the high mass transfer rate resulting from the small initial thickness of the dried layer, as indicated on Fig. 7.3 by the high initial value of the power consumed by sublimation. The power consumed by sublimation at the interface is given by,

$$Q_i = \Delta H_s W_i \tag{7.1}$$

Table 7.1 - Assumed operating conditions

E	125 V/cm
P_R	.29 mmHg
P_R^W	.075 mmHg
T_R	20°C
T_o	-15°C
L	1.27 cm
x_w	.73
x_f	.009

The high sublimation rate causes the loss in sensible heat of the frozen core.

As the "wet bulb" temperature is different from the frost temperature in the chamber, a small drying rate exists due to

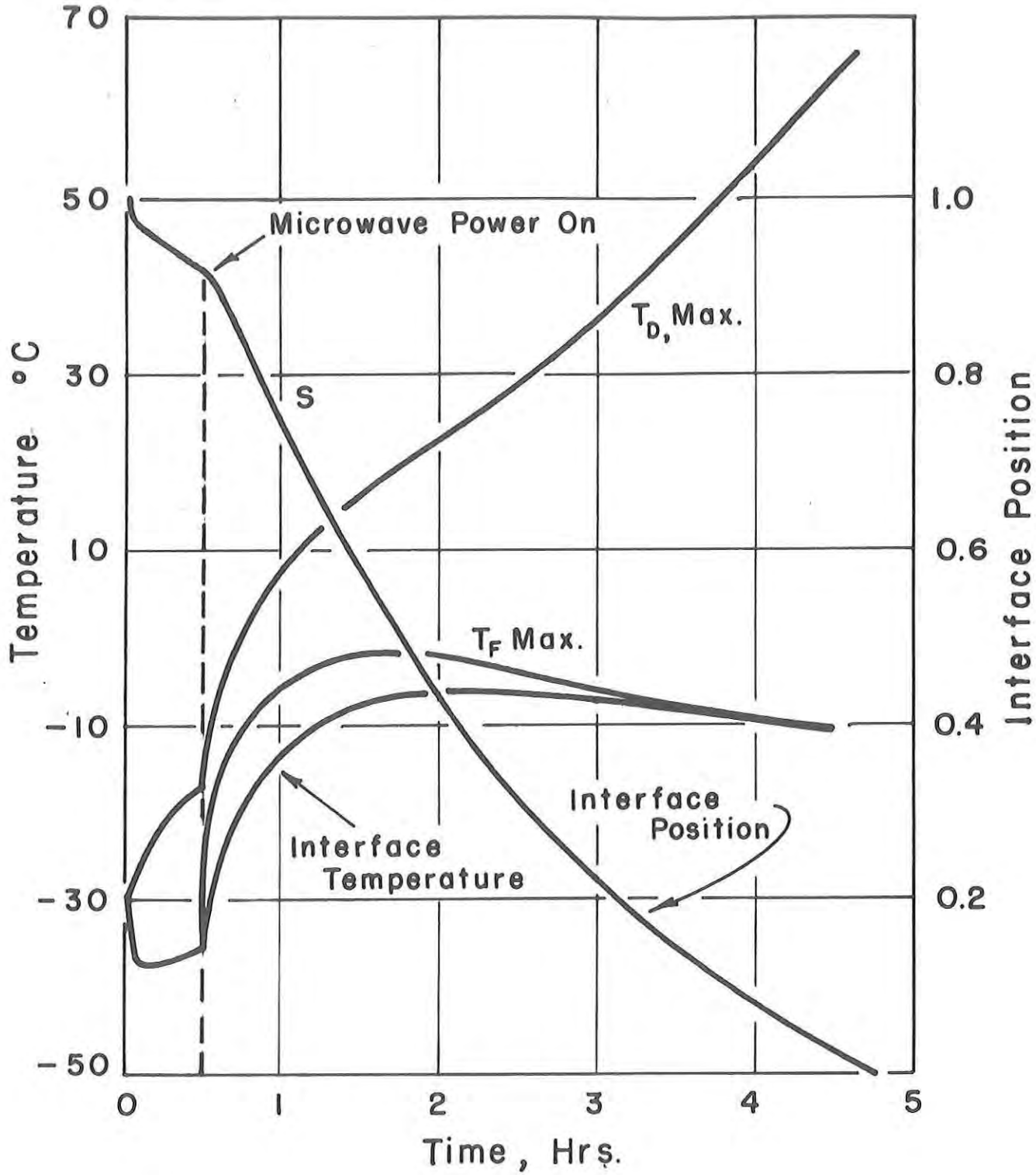

Figure 7.2 - Variations of the temperatures and of the interface position as a function of time.

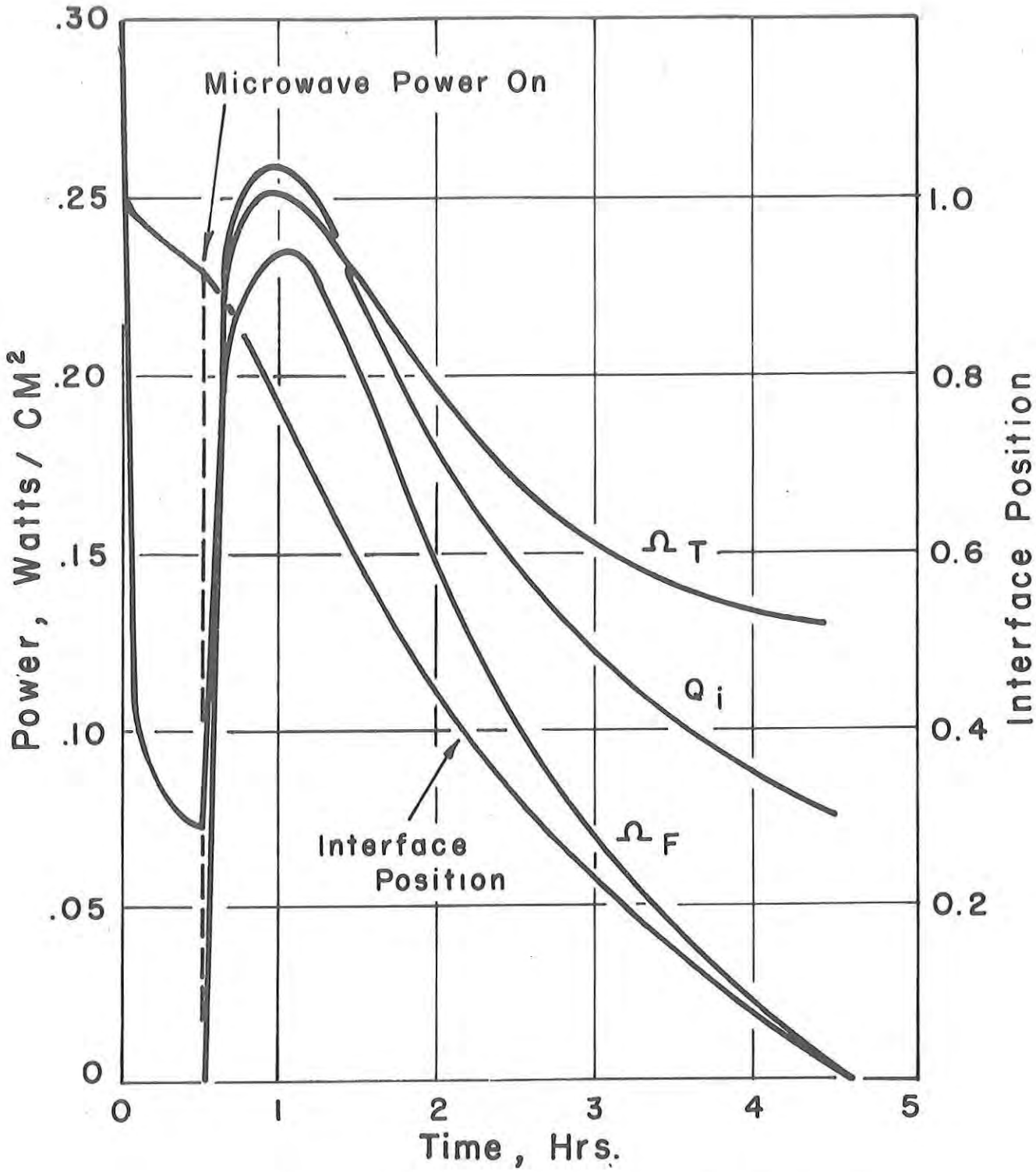

Figure 7.3 - Variations of the powers absorbed in the sample and of the interface position as a function of time.

heat supplied from the surrounding atmosphere to the sample. As the thickness of the dried layer increases due to the sublimation, the mass transfer resistance through the dried layer increases. Thus, the ice-front pressure and temperature increase. The slow decrease of the power consumed by the sublimation (supplied from the surrounding) at the interface in Fig. 7.3 reflects the augmentation of the resistance to the heat transfer as the thickness of the dried layer increases.

As the microwave power is turned on at time t = 30 min, and as the mass transfer resistance is increased due to the relatively fast receding of the ice-front, the temperatures start to rise to a maximum and then decrease again. As the majority of the microwave power is absorbed by the frozen region, it will absorb less energy when its volume is reduced as shown in Fig. 7.3. Thus, as the power input decreases the drying rate slows down. The decrease of the ice-front temperature indicates that the continuous increase of the resistance to the mass transfer (due to the growth of the dried layer) is less significant than the slow down of the drying rate (as the power input decreases). It indicates that the process is essentially heat transfer controlled. As the ice-front temperature decreases the entire frozen core cools down.

The maxima of the total microwave power absorbed (Ω_T) and, in the frozen region only (Ω_F), (Fig. 7.3) reflects the fact that the dissipation coefficient increases with the temperature in the frozen and dried regions. Ω_T and Ω_F in Fig. 7.3 have been calculated by,

$$\Omega_T = \Omega_F + \Omega_D \tag{7.2}$$

$$\Omega_F(t) = \int_0^{X(t)} \omega_F(x,t)dx \tag{7.3}$$

and similarly for Ω_D. The ω's are defined by Eq. (3.5).

The strong similarity of the drying rate curve with that

of the power input, suggests again that the heat transfer is the controlling mechanism. However, the resistance to the mass transfer and the driving force are significant as they cause the actual sample temperature variations.

The relative positions of the power input and the drying rate curve (Fig. 7.3) require additional comments. As the microwave power has just been turned on, the power input is slightly less than the actual power consumed by the sublimation. This is due to the extra energy coming from the heat supplied from the surrounding atmosphere to the sample, as its surface temperature is well below the chamber temperature. As more microwave power is absorbed in the dried layer the external surface temperature continuously increases (Fig. 7.2) and exceeds the chamber temperature. Thus, the heat flux at the surface, which is initially from the surrounding to the sample, continuously decreases, and finally reverses itself as T_S becomes greater than T_R. This effect is shown on Fig. 7.1 by the shape of the temperature profiles in the dried layer and by the time history of T_S (Fig. 7.2). It accounts for the fact that Ω_T crosses over Q_i in Fig. 7.3.

2. Process variables

For a given sample composition, the microwave freeze drying process can be characterized by the following process variables: the vacuum chamber total pressure P_R, the vacuum chamber partial pressure of water vapor P_R^w, the ambient temperature T_R, the initial temperature T_o, the sample size or thickness for the one-dimensional case, and the electric field peak strength in the vacuum E. The operating conditions are determined by a given set (E, P_R, P_R^w, T_R, T_o, L) of the process variables which will be referred to as operation point. It should be noted that the solution of the mathematical model does not require that the process variables be constants and they could be programmed as a function of time. However, this possibility is not considered in this application.

Also, the chamber temperature is really mentioned here for reference, but is taken constant and equal to 20°C as it is not expected to be a significant parameter. Moreover, its measurement is questionable under vacuum since heat conduction is limited and mostly radiant heat transfer predominates. Indeed, one could think of the heat transfer coefficient h as a lumped parameter which contains all possible forms of heat exchanges between the sample and the surrounding vacuum at T_R (20°C here).

Similarly, the initial temperature of the frozen sample is a difficult parameter to control due to the various manipulations which precede the actual drying. Fortunately, it is not expected to be a significant parameter either, as dielectric heating is a rapid process. In effect, a very small amount of time is necessary to bring the material up to the same state as the one which would have been obtained with a different initial temperature. Calculations were made for a one-inch thick slab at two different initial temperatures: -15°C and -30°C with an electric field E = 125 V/cm and pressures $P_R = P_R^w = .075$ mmHg. The drying curves were found to be practically identical. The difference on the normalized interface position S is less than .002 for most of the drying. The temperature profiles in both the frozen and dried regions are essentially the same except during the start-up stage of the process. But the temperature difference is only significant in a short period of time at the beginning of the process and reduces to less than 1°C. As the microwave power is turned on, the original temperature difference becomes unnoticeable. Thus, a constant initial temperature of -15°C is assumed.

3. Feasible domain of operation

The operating range for the process variables is limited to a finite domain which will be referred to as feasible domain of operation. This is due to the fact that there exist upper limits on the electric field strength in the vacuum and the

temperature maxima in the frozen and dried portion of the material being dried. These physical constraints which have been discussed earlier can be expressed mathematically by,

$$E \leqq E_B(P_R) \tag{7.4}$$

$$T_{F,max.}(E, P_R, P_R^W, L) \leqq T_{melting} \quad \text{(around -1.5°C)} \tag{7.5}$$

$$T_{D,max.}(E, P_R, P_R^W, L) \leqq T_{therm.\ degrad.} \quad \text{(60°C)} \tag{7.6}$$

Constraints (7.4), (7.5), and (7.6) are to be satisfied at any time in order to ensure a satisfactory operation without corona discharge, melting of the frozen material and thermal degradation of the dried product.

It has been demonstrated (Gould and Kenyon (1971)) that the break-down electric field strength in an industrial microwave applicator for given gases is a function of the vacuum pressure and the design of the microwave applicator. It is particularly sensitive to the geometry of the applicator. Thus, although Constraint (7.4) has a great practical importance, it cannot be incorporated in this theoretical application as it must be determined for each particular design.

The feasible operation domain is then determined by Constraints (7.5), and (7.6). In the four-dimensional space of the process variables (E, P_R, P_R^W, L) this domain corresponds to the innermost volume enclosed by the coordinate frame planes and the two limiting surfaces defined by the tight constraints,

$$T_{F,max.}(E, P_R, P_R^W, L) = -1.5°C \tag{7.7}$$

$$T_{D,max.}(E, P_R, P_R^W, L) = 60°C \tag{7.8}$$

This is illustrated in Fig. 7.4. The limiting surface defined by the tight constraint

$$T_{F,max.}(E, P_R, P_R^W, 1.27) = -1.5°C \tag{7.9}$$

has been calculated for a one-inch thick symmetric slab (L = ½" or 1.27 cm). The maximum electric field strength, allowable before melting of the frozen material occurs, was determined at various pressures. The accuracy of the electric field is 5 V/cm. The feasible domain with respect to Constraint (7.5) is the inner volume comprised between the limiting surface, the first bisector plane $P_R = P_R^W$ (since $P_R \geqslant P_R^W$) and the planes E = 0 and $P_R^W = 0$. Thus, if the operating conditions correspond to a point inside this volume, no melting will occur at any time during the process. On the contrary, if an operation point is taken outside this domain it will result in melting of the frozen material in the course of drying. However, Constraint (7.5) is not necessarily satisfied and the upper limit of 60°C may well be exceeded.

Figs. 7.5 and 7.6 show the orthogonal projections of the limiting surface in the plane $P_R = 0$, and $P_R^W = 0$. Fig. 7.6 shows the variations of the maximum allowable electric field strength $E_{max.}$, (such that no melting occurs) with the water vapor partial pressure at various total pressures. Fig. 7.5 shows the variations of $E_{max.}$ with the total pressure at various partial pressures. Fig. 7.5 indicates that melting occurs at a lower E value as the pressure increases. This is to be expected as the diffusivity in the dried layer decreases with increasing total pressure, resulting in a higher mass transfer resistance of the dried layer. This gives a higher ice-front pressure and temperature for a similar drying rate (same E). As the pressure approaches 100 mmHg, the electric field has to be decreased drastically in order to ensure drying without melting. Similarly, Fig. 7.6 shows that at a given pressure, an increase of the partial pressure of water vapor in the vacuum requires that the electric field be decreased. Thus, the mass transfer driving force is decreased, which results in a higher pressure and temperature at the ice-front in order to maintain the same drying rate. However, the plateau in the curves indicates that at higher pressures P_R this effect becomes insignificant

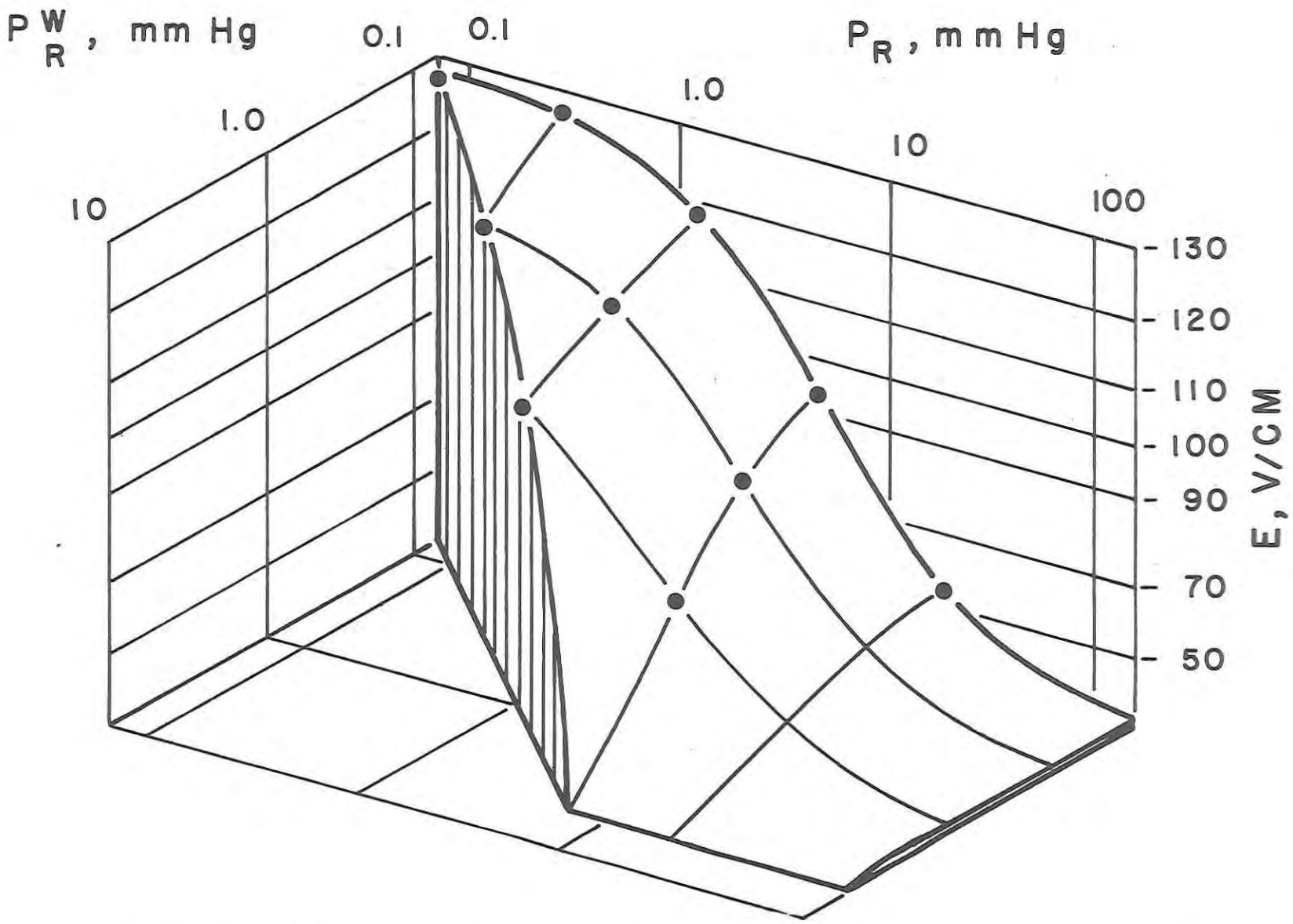

Figure 7.4 - Limiting surface for the feasible operation domain corresponding to the no melting Constraint (L = 1.27 cm).

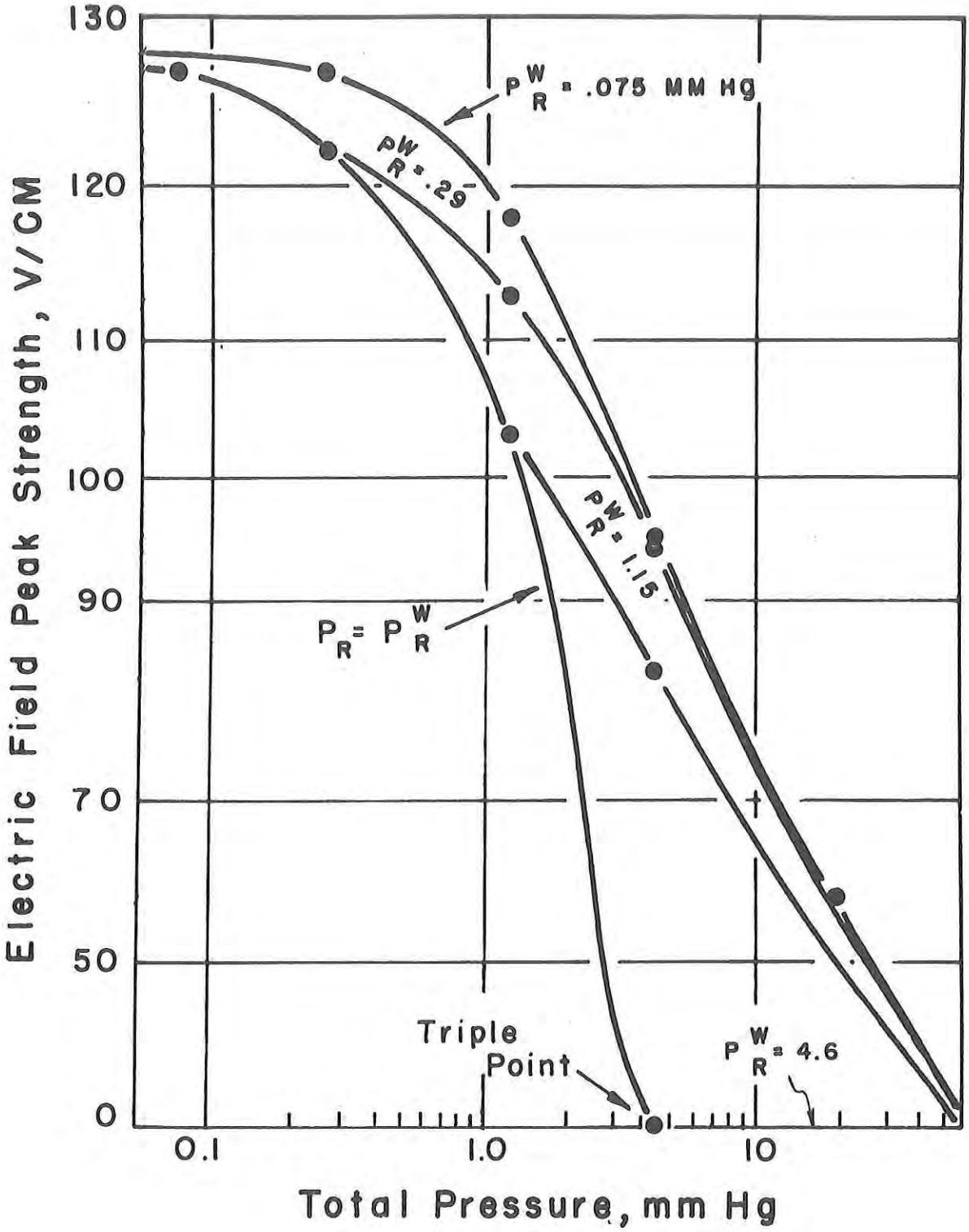

Figure 7.5 - Maximum allowable electric field (for no melting) as a function of the total pressure in the vacuum, at various partial pressures of water vapor. L = 1.27 cm

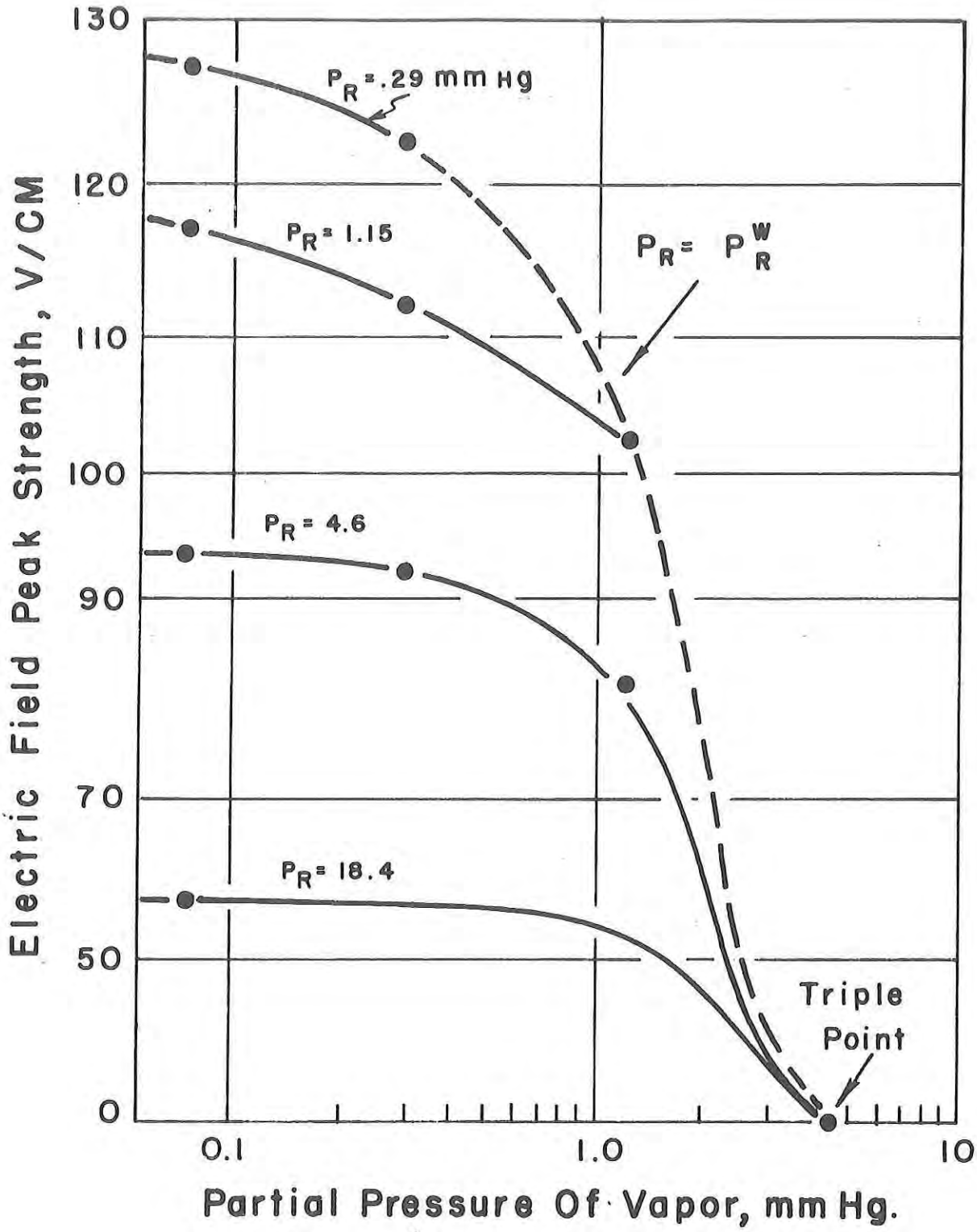

Figure 7.6 - Maximum allowable electric field (for no melting) as a function of the partial pressure of water vapor in the vacuum, at various total pressures. L = 1.27 cm

until the partial pressure P_R^W reaches a high enough value, then the electric field must be decreased drastically again in order to keep the sample frozen. The triple point, which corresponds approximately to $P_R^W = 4.6$ mmHg, constitutes an absolute limit beyond which it is not possible to keep the sample from melting. Another absolute limit is constituted by the curve $P_R^W = P_R$ on both Figs. 7.5 and 7.6. It reflects the physical constraint $P_R^W \leq P_R$ since a partial pressure cannot be greater than the total pressure.

Considering the fact that the drying time is expected to decrease substantially as the electric field is increased, Fig. 7.4 shows that an optimal operation would be to use pressures P_R and P_R^W as low as possible, as a higher field strength could be applied without melting. Figs. 7.5 and 7.6 also show that as P_R or P_R^W decrease and approach .2 mmHg, little gain is made on the maximum allowable field strength. This is due to the fact that at low pressures the vapor flow regime in the dried layer is mostly Knudsen diffusion and thus the diffusivity becomes independent of the pressure. This is why a lower limit of about 50 μHg is considered for vacuum freeze-drying. Lower pressures would represent cost increase for the vacuum system but no significant gain in keeping the sample frozen. A likely point of operation is at pressures $P_R \leq .2$ mmHg and P_R^W close to 75 μHg, using a low temperature condenser (vapor trap; below -40°C).

The entire feasible operation domain would be determined by a similar study conducted at various thicknesses, including the last Constraints (7.6) in order to ensure also that no thermal degradation of the dried product will occur due to excessive heating of the dried layer.

Figs. 7.7 and 7.8, show typical variations of the maximum temperatures at any time in the frozen and dried layers with the electric field strength at various pressures, for a vapor pressure $P_R^W = .075$ mmHg. The temperature maximum at any time in the frozen region is found to vary linearly with the square of the electric

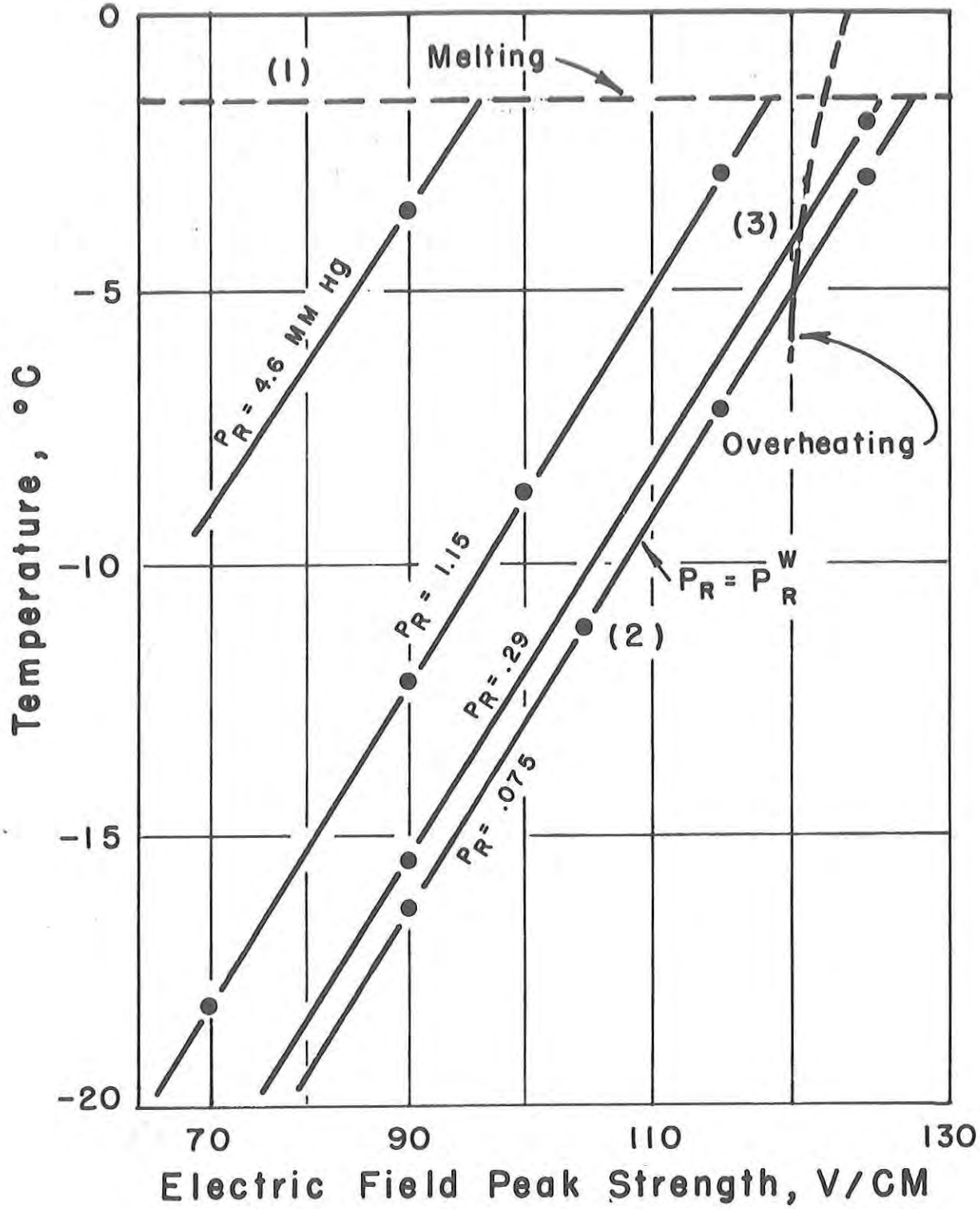

Figure 7.7 - Variations of the maximum temperature in the frozen region (at any time) with the electric field, at various total pressures. L = 1.27 cm; P_R^W = .075 cmHg.

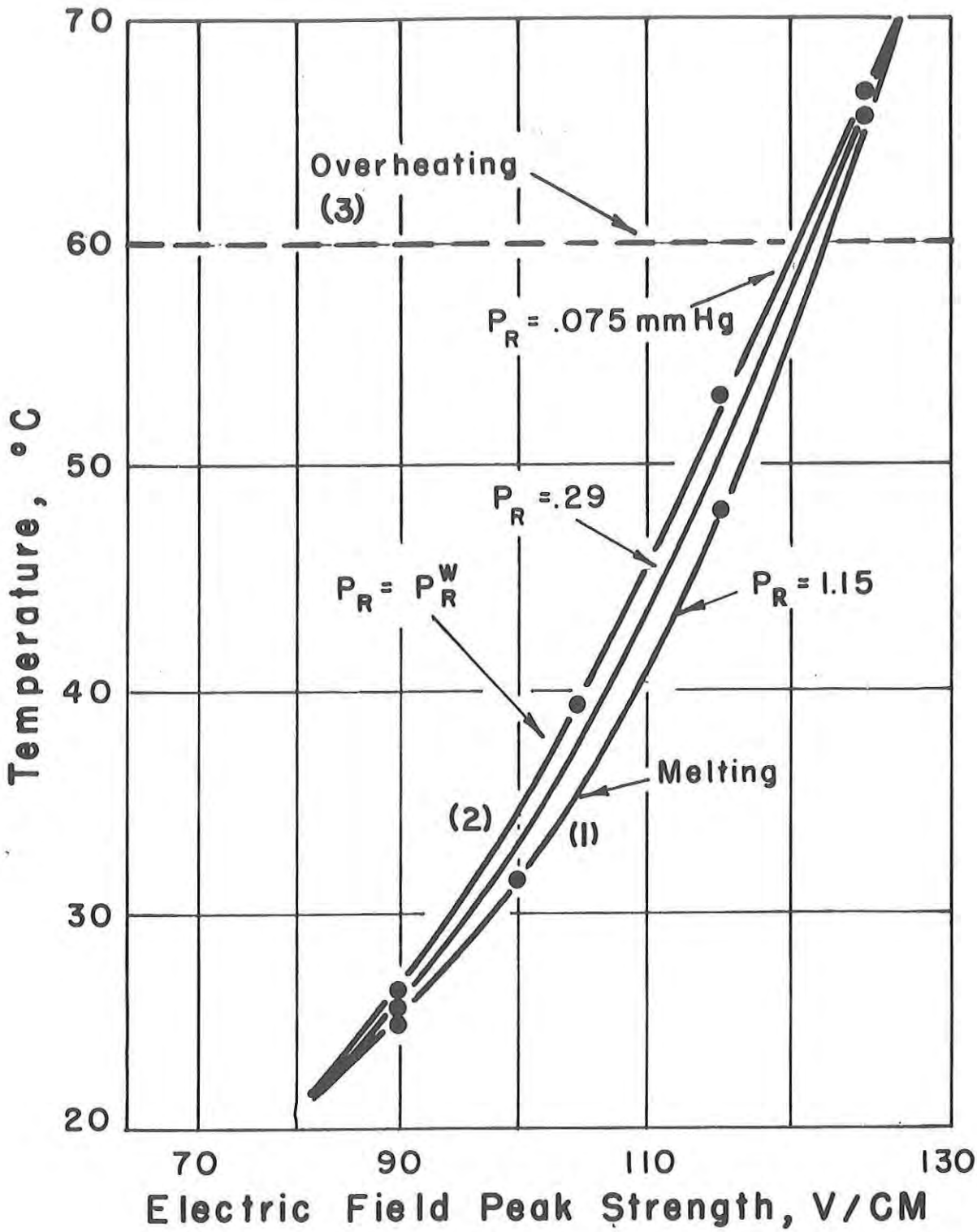

Figure 7.8 - Variations of the maximum temperature in the dried layer (at any time) with the electric field, at various total pressures. L = 1.27 cm; P_R^W = .075 mmHg

field strength in the vacuum. The operation domain is limited to the region enclosed within the lines (1), (2), and (3) on both figures. Line (1) reflects the no melting constraint ($T_{F,max.} \leq -1.5°C$) while line (2) corresponds to the physical constraint ($P_R^W \leq P_R$). Line (3) corresponds to the constraint of no thermal degradation ($T_{D,max.} \leq 60°C$). It is also found that while the temperature maximum at any time in the frozen region is relatively sensitive to variations of the total pressure, particularly at higher pressures, the temperature maximum in the dried layer does not vary significantly with it. It has been pointed out earlier that the temperatures in the frozen region are expected to increase as the resistance to the mass transfer through the dried layer is increased when the total pressure becomes higher. The decrease of the temperature maximum in the dried layer as the total pressure is increased can be attributed to the increase of the effective thermal conductivity (Fig. 6.4). Thus, for the same heat transfer, the temperature in the dried layer is expected to be somewhat lower. Both temperature maxima are found to be strong functions of the electric field. It can be also seen from Fig. 7.7 and 7.8 that for pressures P_R of .075 and .29 mmHg, the process will be actually limited by the overheating of the dried layer as the temperature exceeds 60°C before melting of the frozen core.

Figs. 7.9 and 7.10 show typical variations of the maximum temperature reached in the frozen region ($T_{F,max.}$) and in the dried layer ($T_{D,max.}$), with respect to the sample size (slab half thickness L). The calculations have been carried out for $P_R = P_R^W = .075$ mmHg, a reduction of a 1/4" thick slab by 1/64" would result approximately in a 40°C drop of the temperature maximum. Although one may not have expected such a strong dependency of the temperature maxima upon the slab thickness, it is comprehensible for the temperature and pressure of the ice-front to decrease as the slab thickness is reduced because of the lower resistance to the mass transfer in the dried layer, which results in a general

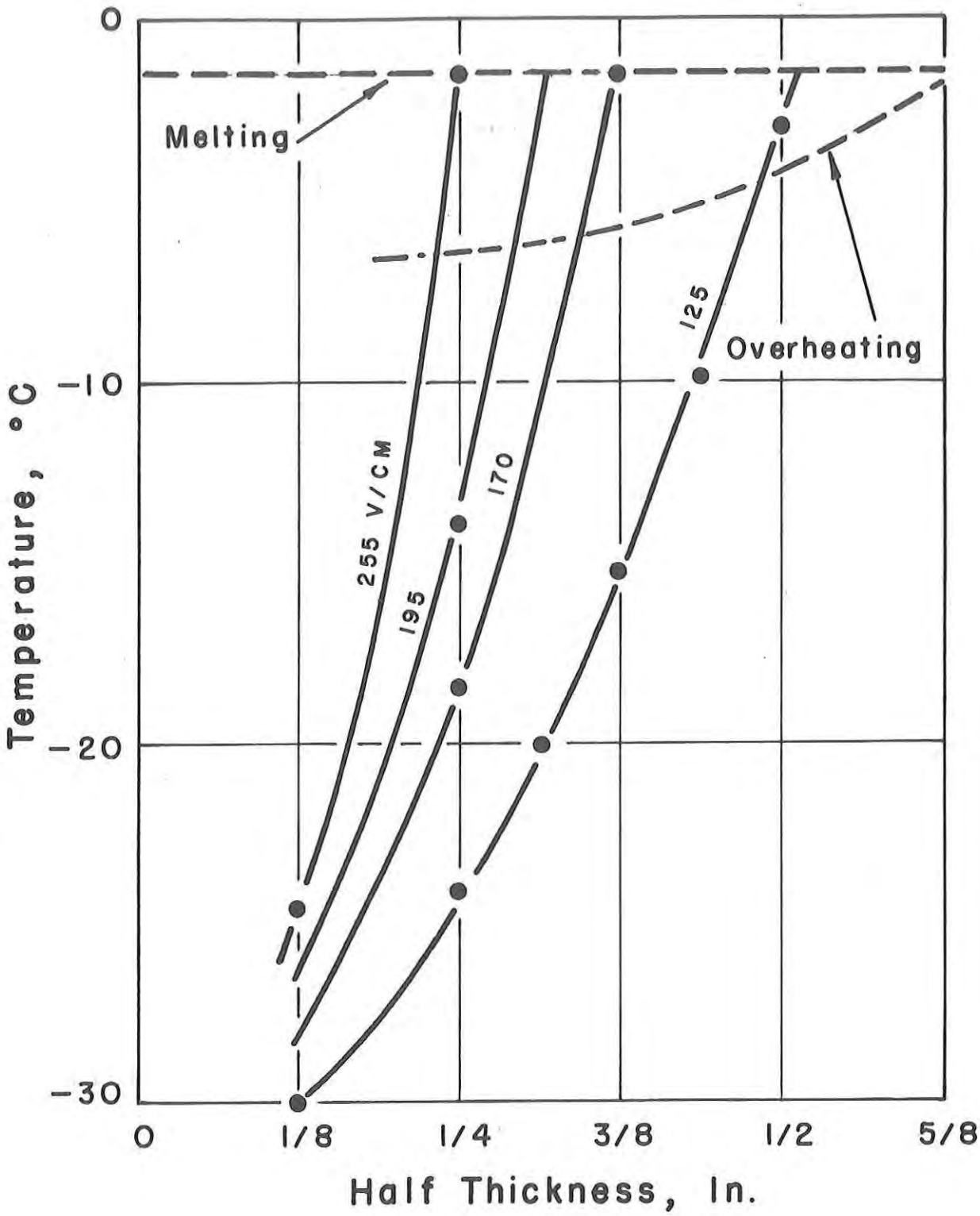

Table 7.9 - Effects of the sample half thickness on the maximum temperature in the frozen region (at any time). $P_R = P_R^w = .075$ mmHg.

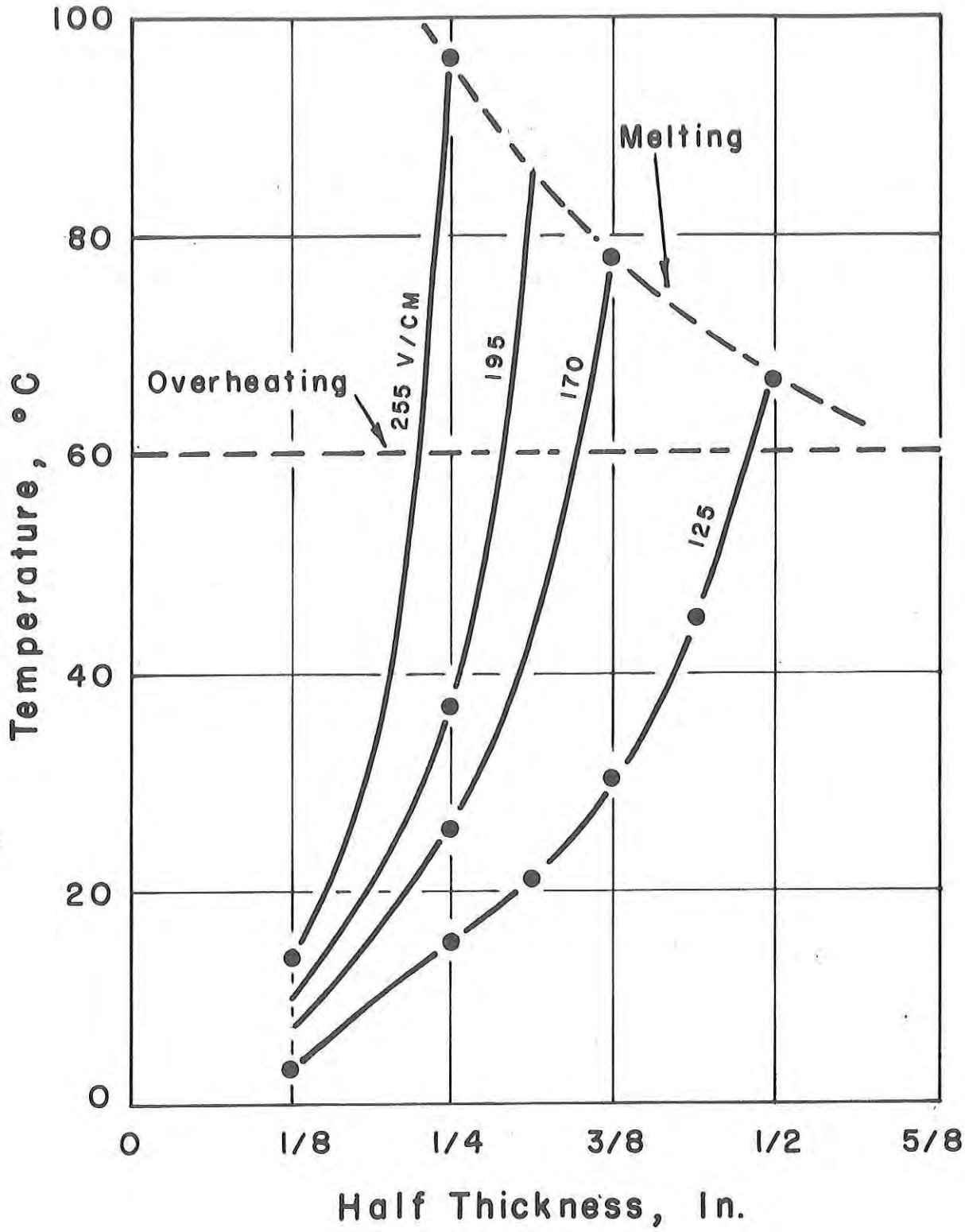

Table 7.10 - Effects of the sample half thickness L on the maximum temperature in the dried layer (at any time). $P_R = P_R^W = .075$ mmHg.

cooling of the sample. The sharpness of the dependency at high electric field strengths may be attributed to the fact that the energy generated in the sample for a given thickness varies as E^2. Thus, the quantitative variations of the temperature maxima at various field strengths will constitute a very critical information for the designer when deciding on an optimal slab thickness. Lower temperatures will allow one to increase the microwave power input and thus shorten the drying time. This point will be discussed in the next section.

Figs. 7.9 and 7.10 show that the 60°C limit is exceeded at the assumed operating pressures before melting occurs for all values of L considered. However, it must be noted that these findings depend on the assumptions which we made for the numerical value of certain properties (particularly the diffusivity). It was found (Part III) that the effective diffusivity might have been overestimated. The true temperatures in the frozen region may, thus, be substantially higher than those indicated here.

4. Effects of the process variables on the drying time

Calculations have been carried out at various total pressures, electric field strengths and sample size in order to study the variations of the total drying time (including the start-up period) with these parameters. The partial pressure of the water vapor in the vacuum is a less important parameter. In effect, the drying time is not expected to vary significantly over the small feasible range of the partial pressure of water vapor.

As one may have expected, the drying time is a strong function of the electric field strength. The drying time has been plotted in Fig. 7.11 vs the square of the electric field (the abscissa of Fig. 7.11 is a quadratic scale) at various pressures and a vapor partial pressure of .075 mmHg. From the small curvature of the curves it can be seen that the drying time varies approximately with E^2, within a relatively small range. In other words, the drying time is approximately proportional to the microwave

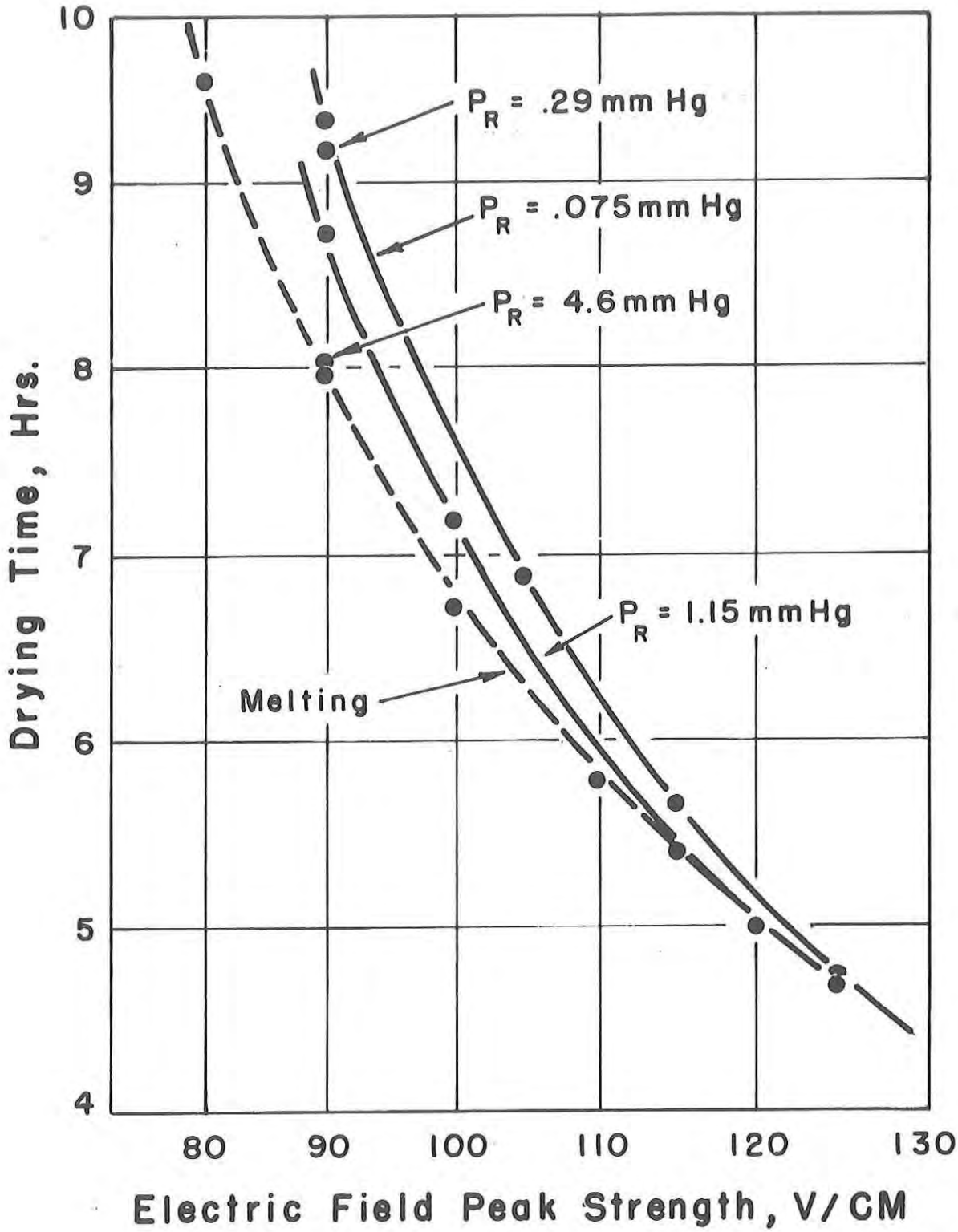

Figure 7.11 - Variations of the total drying time as a function of the electric field, at various pressures of the vacuum chamber. L = 1.27 cm; P_R^w = .075 mmHg.

power input.

It is found also that an increase of the total pressure has an appreciable effect, although small, in decreasing the drying time, as shown on Fig. 7.12. This is due to the increase of the dissipation coefficient (mainly in the frozen region) as the temperature increases in the sample with the resistance to the mass transfer. This effect has been discussed earlier. On the other hand, the increase of the resistance to the mass transfer should result in a slow down of the mass transfer rate. The fact that the drying time actually decreases rather than increases is another indication that the freeze-drying process using dielectric heating is heat transfer controlled. However, if the pressure is further increased the upper curve on Fig. 7.12 would be expected to go to a minimum and start to rise as the process becomes mass transfer controlled. However, for this to happen a field strength low enough would have to be used, otherwise melting of the frozen core would occur first. The lower curve on Fig. 7.12 illustrates the effect of the pressure increase in raising the frozen core temperature due to the higher resistance to the mass transfer in the dried layer.

The different calculation points used to determine the limiting surface in Sec. 3 of the melting-free domain of operation, have also been plotted in Fig. 7.11. It is interesting to note that, although they were obtained at different pressures and vapor partial pressures of water, they all fall on the same smooth curve. This suggests that the drying time depends only on the electric field strength. This supports the argument presented in the previous paragraph. The pressures affect the drying time because of their effect on the temperatures, which in turn affect the dissipation coefficient. Thus, if the temperatures are approximately the same, as it is the case along the limiting surface, the effects of the pressures on the drying time are nil.

The variations of the total drying time with L in Fig. 7.13 seem to be in contradiction with Hoover et al. (1966) results,

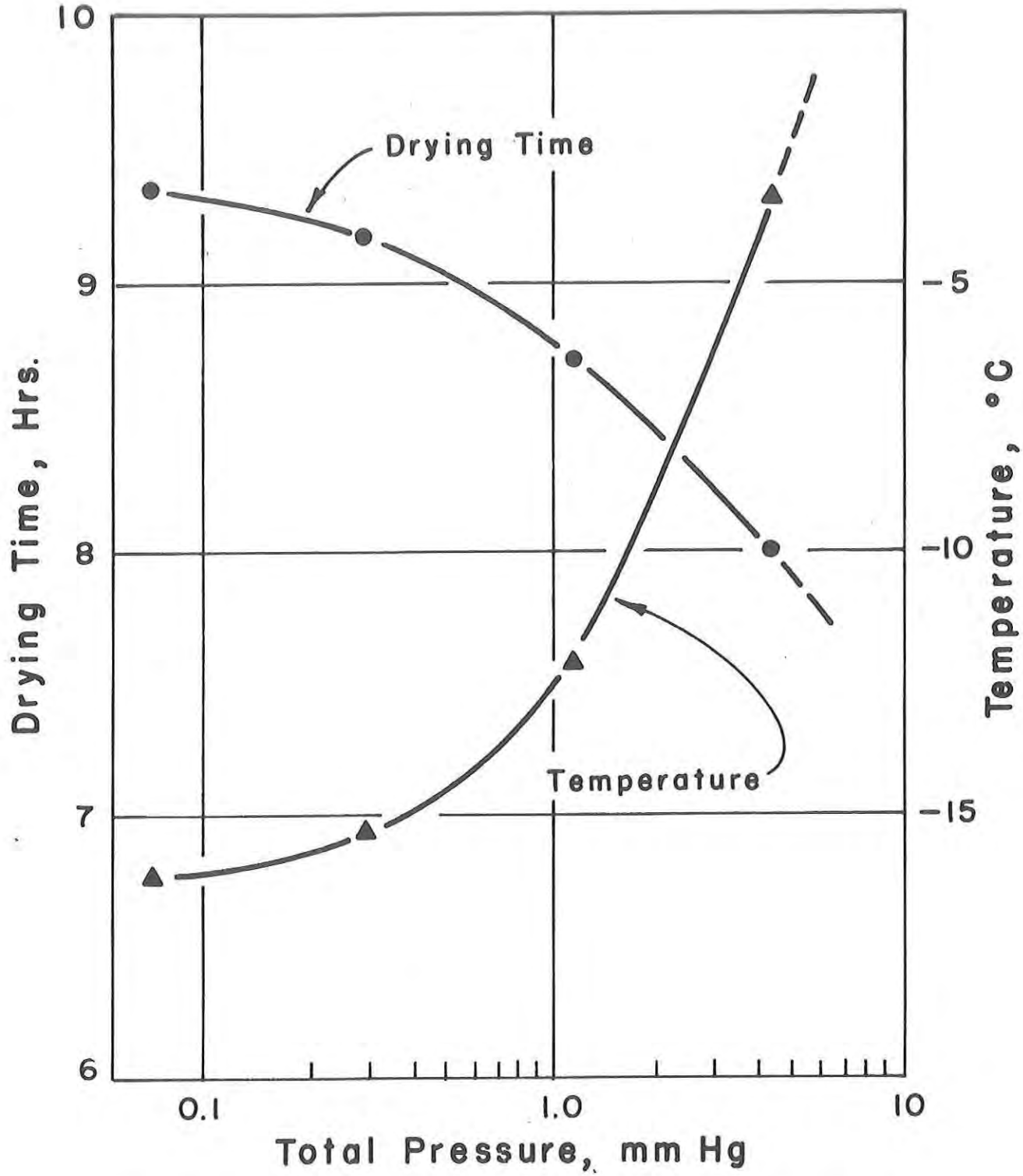

Figure 7.12 - Effects of the total pressures in the vacuum on the drying time and the maximum temperature reached by the frozen core. E = 90 V/cm, P_R^W = .075 mmHg. L = 1.27 cm.

who have obtained experimental drying times essentially independent of the thickness. The results shown in Fig. 7.13 may be supported by an approximate calculation of the total drying time t_2 as shown below. The total drying time can be obtained by rearranging Equation (4.17) to give

$$dt = -\rho \, \sigma \frac{dX}{W_i} \tag{7.10}$$

The drying rate W_i can be related to the microwave power input, by neglecting the variations of the sensible heat and the losses at the outer surface. A combination of Equations (7.1) and (3.5) gives

$$W_i = \frac{1}{\Delta H_s} \left[K_F \, X + K_D \, (L - X) \right] E^2 \tag{7.11}$$

where the variations of K_F and K_D with location have been neglected. Thus,

$$dt = - \frac{\rho \, \sigma \, \Delta H_s}{E^2} \frac{dX}{K_F X + K_D (L-X)} \tag{7.12}$$

Integration of Equation (7.12) between $t = 0$ and $t = t_2$, or $X = L$ and $X = 0$, gives (neglecting the variations of K_F and K_D with time),

$$t_2 = t_1 + \frac{\rho \, \sigma \, \Delta H_s}{(K_F - K_D) \, E^2} \, \mathrm{Log} \left(1 + \frac{K_F - K_D}{K_D} \, \frac{X_1}{L} \right) \tag{7.13}$$

Equation (7.13) shows that when the sample thickness is reduced, the overall drying time t_2 decreases as the fraction of product, $\frac{X_1}{L}$, remaining to dry at the end of the start-up period decreases. If the thickness is further reduced, t_2 reaches eventually t_1 as $\frac{X_1}{L}$ goes to zero (all frozen material removed at the end of the start-up period). The drying process then becomes only radiant heating, for which the drying time goes to zero with the sample thickness L.

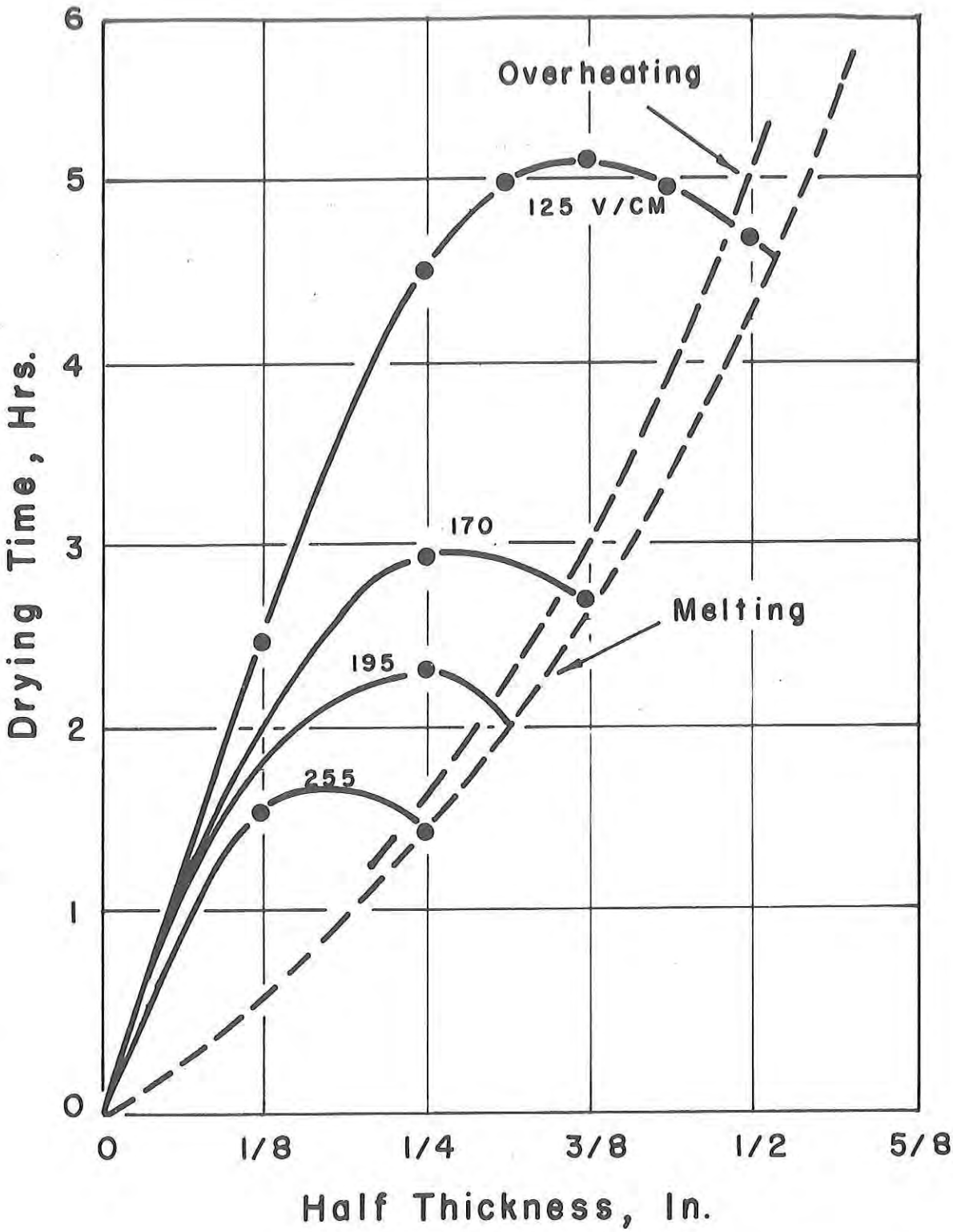

Figure 7.13 - Effects of the sample thickness on the total drying time for various field strengths. $P_R = P_R^W = .075$ mmHg.

The above variations of t_2 with L are in agreement and confirm those predicted by the model as shown in Fig. 7.13. It should be added that the dissipation coefficients K_D and K_F are expected to affect the drying time as the thickness is changed. In effect, they vary with the temperature which is a function of the thickness L (see Figs. 7.9 and 7.10). Similarly, although the mass transfer is not the controlling mechanism, a variation in L results in a different resistance to the mass transfer which in turn may, directly or indirectly, vary the drying time.

The maximum of the curves at higher thicknesses in Fig. 7.13 can be attributed to the temperature increase (mainly in the frozen core) due to the increase of the mass transfer resistance when the thickness is augmented, as discussed previously. The higher temperatures in the sample increase the dissipation coefficient in both the frozen and dried regions, which causes more microwave power to be absorbed by the sample, and thus, shortens the drying time. Fig. 7.13 seems also to indicate that smaller slab thicknesses would enable one to use higher electric field strengths to shorten drastically the drying time without melting.

Fig. 7.14 shows a plot of the amount of frozen product dried per hour (per unit area) vs the sample half thickness L at various electric field strengths. It can be seen from this figure that as the slab thickness is reduced the output of the microwave freeze-dryer continuously decreases. Thus, for a given electric field strength the optimal thickness yielding the highest output of dried product is the largest thickness without occurrence of melting of the frozen material or overheating of the dried product. Fig. 7.14 shows that, under the assumptions made here, that overheating of the dried product would occur earlier than melting of the frozen core. However, it should be mentioned again, and as it will be discussed in the experimental part of this study, that the numerical value of the diffusivity may have been overestimated in this case. This would mean that

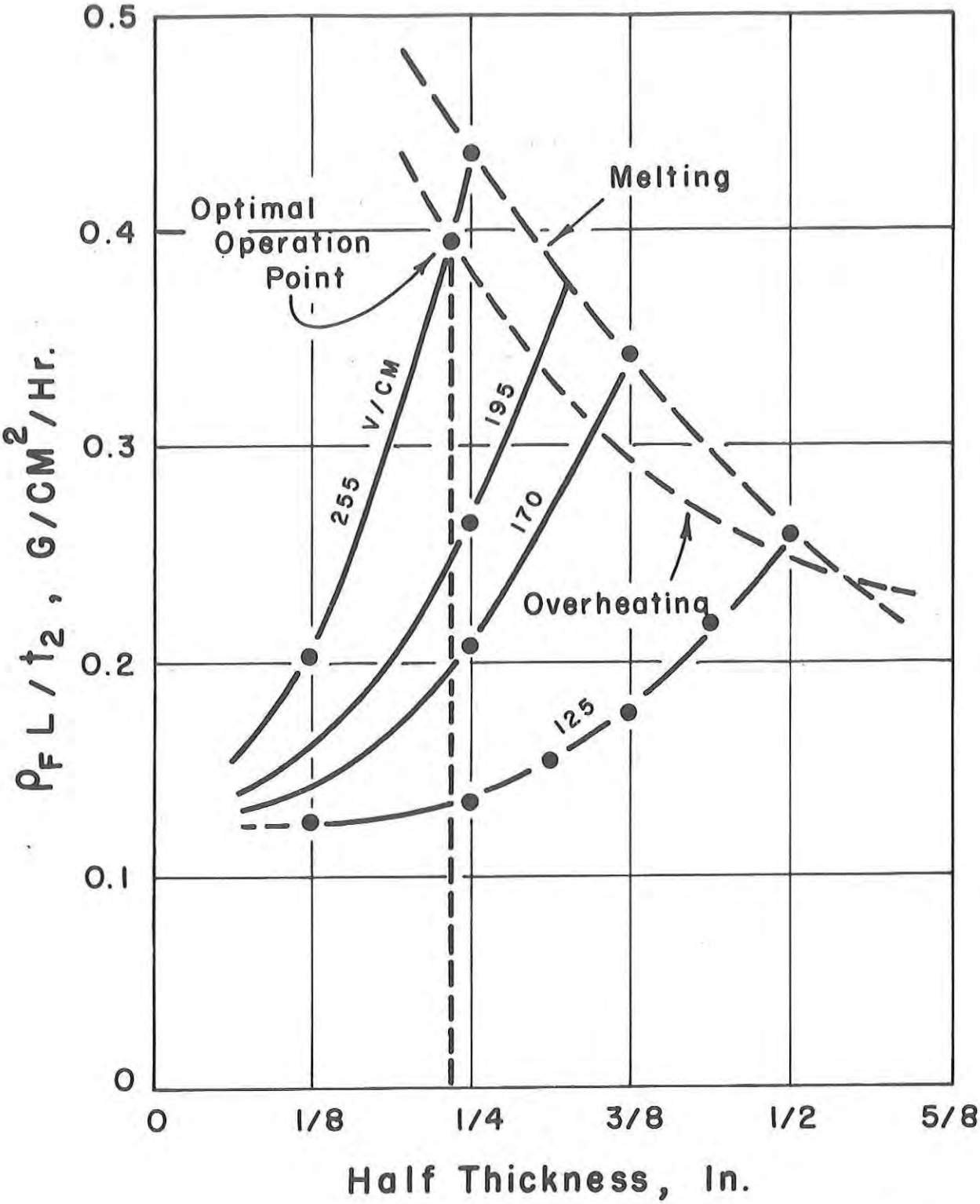

Figure 7.14 - Effects of the sample size on the output of the microwave freeze-dryer. for various electric field strengths. $P_R = P_R^W = .075$ mmHg

the actual temperatures in the sample are indeed somewhat higher than those computed here and thus melting may occur earlier than predicted.

On the other hand, the negative slope of the "overheating" limiting curve in Fig. 7.14, indicates that use of smaller thicknesses would increase the freeze-dryer output as higher field strengths are made possible. However, as the electric field strength is increased, a corona discharge may develop in the microwave applicator, reducing drastically the power conversion efficiency and possibly inducing burns of the product. Thus, the optimal thickness yielding the maximum freeze-dryer output is that which would correspond to an operation near corona and overheating occurrence (or melting). For instance, if corona was to develop slightly above 255 V/cm the optimal thickness would correspond to the optimal operation point shown in Fig. 7.14. It is important to note that the previous discussion had assumed an operation under low pressures ($P_R = P_R^w = .075$ mmHg) in order to ensure the lowest possible temperatures in the frozen region and the dried layer.

Under these conditions and the assumptions made, if corona were to occur beyond 255 V/cm, drying times as short as an hour and one half (including the 30 min start-up period), should be possible for a ½" symmetric slab. This would result in a maximum freeze-dryer output of approximately 0.4 grams of frozen product per hour, per unit area.

- PART III -

CORRELATION WITH EXPERIMENTAL DRYING CURVES

Chapter VIII: Experimental Set-Up and Procedure

Chapter IX: Experimental Results - Correlation with Simulation

- Chapter VIII -

EXPERIMENTAL SET-UP AND PROCEDURE

1. Experimental set-up

1.1 The microwave freeze-dryer

A schematic of the experimental system is given in Fig. 8.1. The microwave generator (A) is a converted microwave oven (Speed Range 110) which uses a magnetron Amperex DX-206 to deliver 1 KW of adjustable power at 2450 MHz $\pm$ 25 MHz. The microwave applicator cavity (B) is located inside a vacuum chamber (C) and contains the sample to be dried (D). The microwave power is transmitted to the cavity (B) by a rectangular wave guide WR-284, through various control, monitoring and tuning devices. The power from the generator is sent by a four-port circulator (E) into the line section where an H-tuner (F) varies the admittance to a dry resistor (G) (matched load of less than 1% reflection). The fraction of power reflected at the H-tuner (determined by the plunger location) travels back to the circulator where it is diverted into the termination line section (microwave applicator and freeze-dryer). It encounters a bidirectional coupler (H) which separates the power traveling forward from that traveling reverse (reflected from the termination). The reverse power travels back to the circulator where it is sent to a second dry resistor (I) in order to prevent harmful reflections to the

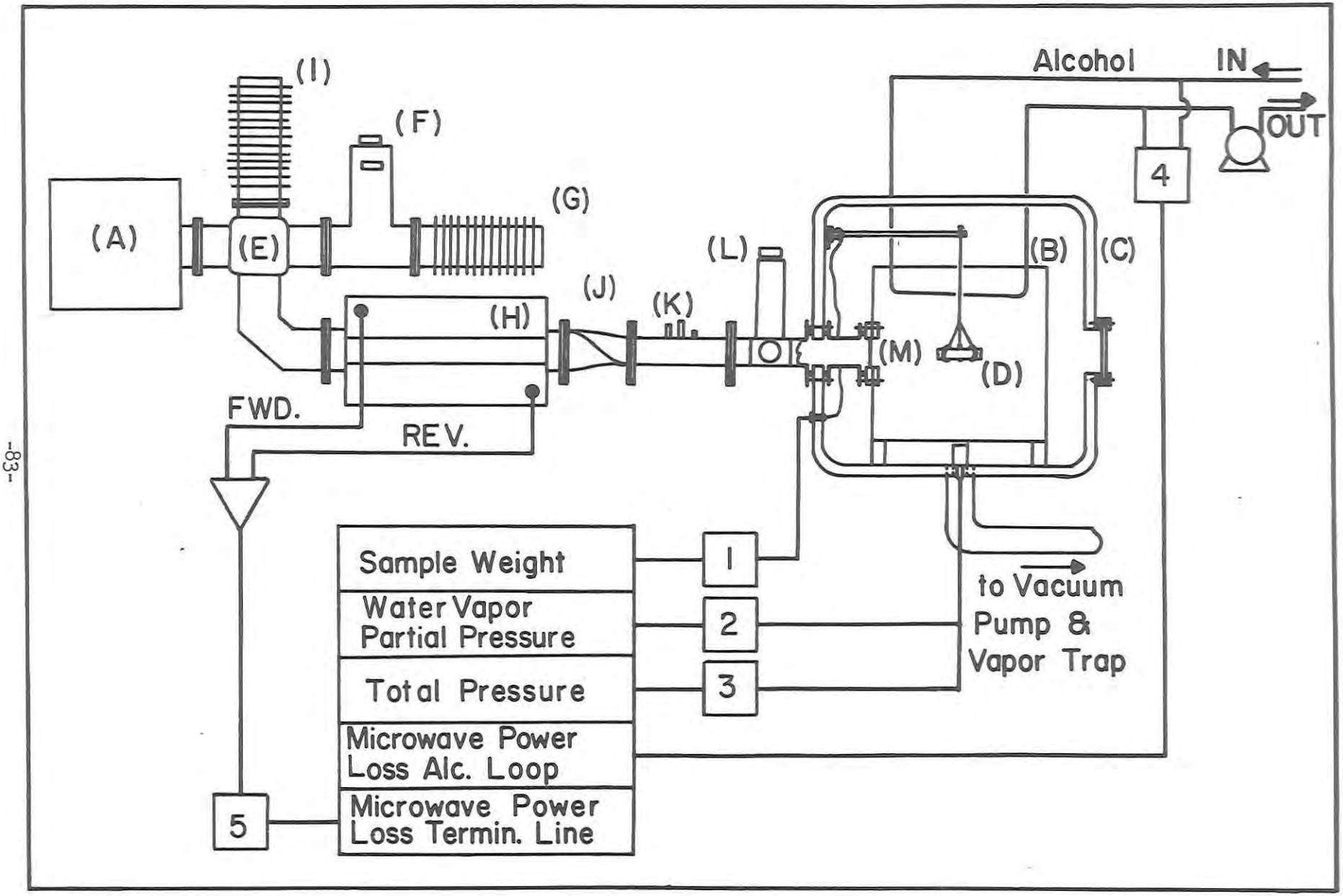

Figure 8.1 - Schematic of the experimental set-up

magnetron. The forward and reverse powers in the bidirectional coupler are sampled by two small antenna probes. The bidirectional coupler is connected to a twist (J) which rotates 90° the original polarization of the electric field. The electric field enters the cavity (B) with a vertical polarization (parallel to the figure plane). A 3-Stub tuner (K) is used in conjunction with an E-H tuner (L) to tune the cavity (B). The microwave power enters the cavity (B) through a wave guide vacuum transition (M) using a fiber glass window.

The multimode rectangular cavity (B) has dimensions 39 x 39 x 51 cm and is made of perforated aluminum sheet in order to retain the microwave power, but let the water vapor from the dehydration flow through to the main chamber (C) and finally the vapor trap. An oversized condenser is used for the vapor trap. The sample to be freeze-dried (D) is hung inside the cavity (B) with its main surface horizontal and is located in front of the wave guide mouth as shown in Fig. 8.1. It is suspended to a cantilever beam, used in the weight measuring system, by means of teflon hooks and fiber glass strings.

Finally, n-propyl alcohol is circulated at a constant flow rate in a glass loop inside the cavity. It was intended to serve a double purpose. First, in order to obtain a fairly uniform field in the multimode cavity, a reasonable load is necessary. By increasing the load one decreases the Q of the cavity and broadens its frequency band at resonance. Thus, more modes (eigen frequencies) can be admitted inside the cavity which superimpose and average out to yield a relatively uniform field. The increase of the load was found necessary, due to the small size of the sample used (about 60 to 90 cm^3) as compared to the large volume of the cavity (about 7.5×10^4 cm^3). n-propyl alcohol was chosen as the circulating fluid because its dielectric constant ($\epsilon' = 3.7$) is comparable to that of frozen beef meat ($\epsilon' = 3.6$). Second, it was intended as a means of monitoring the electric field inside the cavity, as it will be discussed below.

1.2 The data acquisition system

A special system was designed by this investigator to allow continuous recording of the sample weight in the course of the dehydration. The sample is suspended by means of a fiber glass string to the free end of a cantilever beam through a knife edge. The strain induced at the fixed end by the sample weight is measured by four strain gages mounted in a Wheatstone bridge (two in compression and two in tension). The bridge is excited with a 1.5 V DC voltage and balanced for no load conditions (no sample hung). The DC signal resulting from the imbalance of the bridge in the measuring circuit, when the sample is hung, is a measure of the weight. This DC signal, of the order of several μV, is amplified and sent to a strip chart recorder. Known weights are used to calibrate the measuring system. The recorder gain is adjusted to give a reading of 10 g/in on the chart. Surrounding machinery induces undesirable mechanical vibrations in the beam which result in a strong low frequency noise in the output of the DC amplifier. Noise of a frequency less than 10 Hz could not be suppressed by the built-in filters of the amplifier. A special filter was designed by this investigator to suppress all AC signals in the range 1 to 10 Hz and proved very successful in filtering out the electrical noise caused by the mechanical vibrations. The assembly (DC power supply, balancing unit, DC amplifier and strip chart recorder) is referred to in Fig. 8.1 as data acquisition unit 1.

The water vapor partial pressure in the vacuum chamber is measured continuously by a Panametrics model 1000 Hygrometer (unit 2) which uses an aluminum oxide transducer probe. The total pressure is monitored by a MacLeod Pressure gage (unit 3).

As mentioned above, an attempt was made to estimate the average electric field in the cavity by measuring the amount of microwave power absorbed in n-propyl alcohol circulated in a glass loop through the cavity at a constant flow rate. The microwave power loss in the alcohol is determined from the temperature

difference between the inlet and the outlet measured with a Doric digital thermocouple temperature indicator (unit 4). However, only a qualitative monitoring of the average field strength was possible due to the difficulty of measuring the effective volume of alcohol which absorbed microwave power. Moreover, the contamination of the alcohol by the Tygon tubing connections makes the validity of utilizing the dielectric data of the alcohol questionable. However, this system is used as an indicator of melting occurence in the frozen sample. In effect, when melting occurs, as the dissipation factor of the wet meat is much greater than that of the frozen meat the power absorption in the sample rises suddenly. Thus, at the same time, the microwave power absorbed in the alcohol drops as indicated by the outlet temperature drop. This is due to the fact that the microwave power fed into the cavity is relatively constant.

The total microwave power loss in the termination line (including twist, tuners, window, connectors, leakage, sample and alcohol) is measured from the forward and reverse microwave powers detected in the bidirectional coupler. The detected forward and reverse powers are determined by a Hewlett-Packard 431 B power meter which uses a thermistor mount (unit 5). A manual switch allows one to select either powers. The power measurement was initially intended to monitor the power loss in the sample. However, a quantitative measurement was impracticable due to the relatively high fraction of power lost in leakage. Determination of this fraction was not possible as it was found to be a function of the load in the cavity, and the tuning adjustment. Thus, the results of the power measuring unit were limited to comparisons between runs. The Hewlett-Packard power meter reading (mW) was calibrated against a factory calibrated power meter (Bird Electronic, Thru-line). The latter power meter could not be kept for on-line direct power measurements as it could only give reliable readings under low reflection ratios.

2 General experimental procedure

2.1 Tuning of cavity

Tuning of the cavity is necessary in order to obtain a relatively uniform electric field. The uniformity of the field was checked on a test run by visual examination of a partially dried sample, cut in several directions. A planar ice-front was observed which indicated a relatively uniform heating. The tuning consists in performing an analysis of the admittance vs frequency of the termination line for a calibrated signal generated by a sweep oscillator (cold-test). The frequency band swept by the test oscillator corresponds to the frequency band of the magnetron: 2450 MHz $\pm$ 25 MHz. The tuning criterion is to adjust the 3-Stub or the E-H tuner in order to obtain a flat profile of the power dissipated in the termination line vs frequency. A flat power profile means that microwave power will be admitted into the termination line equally for each frequencies of the frequency band generated by the magnetron. It was hoped that this would also correspond to a maximum number of modes (a mode corresponds to a given eigen-frequency or resonant frequency of the cavity) admitted in the cavity and thus yield a more uniform field. With this tuning criterion it is believed that a relatively uniform field distribution can be obtained.

The termination line section tested consisted of the line section located to the right hand side of the bidirectional coupler in Fig. 8.1.

2.2 Sample preparation

Two batches of samples of different choices of beef meat with different preparation were used. The first one, used in the study of the effects of the power input on the drying curves consisted of an eye of the round choice which offers a rather homogeneous fat free texture (moisture: 71%). The outer fat was trimmed and the meat deep frozen to approximately -37°C. Slabs

of approximately 1.5 cm thickness were cut perpendicularly to the fibers from the frozen muscle with an electric band saw. The samples were then wrapped separately and stored in a freezer until later use. However, there were two drawbacks to this method of preparation. The thickness and the contour of the slab were irregular and difficult to reproduce. Thus another preparation method was employed in the study of the effects of pressure on the drying curves. However, since a larger muscle cross section was needed, a different choice of meat was used. It consisted of top of the round (average moisture: 67%, average fat: 2%). The whole muscle was tempered at about -4°C and then pressed and formed in a cylindrical die, with the general orientation of the fibers parallel to the cylinder axis. The meat cylinder was then chopped automatically in slabs of a relatively constant thickness (approximately 1.5 cm). 7.5 cm diameter discs were then punched out of the meat slab with a metal cutting form and then placed on a metal tray and re-frozen in a blast freezer. It should be noted that the freezing method does not seem adequate since the fast freezing from the bottom of the sample resting on the tray yields a concave top surface. A different method might have given better results. The frozen samples were again wrapped separately in paper and stored in a freezer at about -37°C.

2.3 Experimental procedure for a run

Before each run, a known weight was suspended to the cantilever beam in place of the sample and the reading of the weight on the recorder was allowed to reach a constant value. This normally took one to two hours. Once the reading was constant, the gain of the recorder was adjusted for a direct reading in grams. The refrigeration system and vacuum pump were started 30 min to 1 hr prior to each run with the vacuum chamber isolated in order to achieve a constant condenser temperature of approximately -40°C.

The meat sample was then taken from the storage freezer, weighed and its cross section area and thickness were measured.

The sample was then attached to the fiber glass string from the cantilever beam weighing system by means of three teflon hooks, its surface horizontal and its edge facing the mouth of the microwave power feed (wave guide). Thus, the polarization of the electric field at the sample surface was expected to be mainly that in the wave guide ($TE_{1,0}$), i.e., vertical (normal to the sample surface).

The doors of the microwave cavity and vacuum chamber were then shut and the chamber opened to the vacuum. The desired vacuum was found to establish in less than 5 min. A pressure less than 200 μHg was not possible due to air leakage.

After usually 30 min the microwave power was turned on. The desired power input was selected by using the H-tuner (F in Fig. 8.1). The sample was then allowed to dry. It was considered fully dried when the weight reading on the recorder reached a constant value. Readings were taken at variable time intervals for the following parameters: partial pressure of water vapor, total pressure, forward and reverse microwave power, temperature IN and OUT of the alcohol glass loop, and flow rate of the circulated alcohol (a constant flow rate could not be achieved).

The drying curve (sample weight vs time) was directly given by the reading on the strip chart recorder.

It should be noted that in certain instances, especially during the runs at high pressure (3.5 mmHg), a corona discharge occured at the end of the dehydration. The high pressure runs (3.5 mmHg) were not relevant due to local melting and vaporization of the frozen core. An otherwise, corona-free operation was reached.

The microwave power measurements were not quantitative, as mentioned earlier. Thus, the electric field peak strength in the vacuum near the sample surface was evaluated from the drying rate using the dielectric data of Kan and Yeaton (1961). This point will be discussed in the next chapter, sec. 2.

- Chapter IX -

EXPERIMENTAL RESULTS AND CORRELATION WITH MATHEMATICAL MODEL

Freeze-drying experiments have been conducted for beef samples with microwave dielectric heating at 2450 MHz in order to compare experimental drying curves with those predicted by the theory. The experimental set-up and procedure which were used in the experiments are described in the previous chapter. The beef samples had the geometry of a slab of about 7.5 cm in diameter and a thickness of approximately 1.5 cm. Two different choices of beef meat were used (eye of the round and top of the round). The frozen samples were prepared by two different methods (see chapter VIII, sec. 2.2).

1. Experimental results

Drying curves have been obtained at various microwave power inputs for a constant vacuum pressure of approximately .3 mmHg (referred to as power runs) and at various pressures for a fixed microwave power input (referred to as pressure runs) corresponding to an electric field peak strength of about 125 V/cm.

Two different batches of samples were used for the power and pressure runs. An eye of the round choice of meat was used for the power runs, while the pressure runs were performed with top of the round. The two batches further differed by the geometry of the slabs and the preparation of the samples, as discussed

in the previous chapter. It should be noted that the thickness of the slabs was not uniform for any sample and varied between different samples due to difficulties in their preparation. A variation of 1 to 2 mm about the mean thickness (approximately 1.5 cm) was observed for a sample.

Table 9.1 shows the operating conditions used for each run and the average value used to calculate the theoretical drying curves. The values given for the vacuum pressure and partial pressure of water vapor correspond to the starting point when the microwave power is turned on. They were observed to decrease slowly during most of the drying (a drop of about .05 to .1 mmHg) and relatively faster in the final stage during which an additional drop of approximately .05 mmHg was observed. The initial temperature is not given as it was not possible to measure it directly from the sample when enclosed in the microwave oven. The results from the theoretical study have shown (Chapter VII) that the starting temperature is not a significant parameter of the process.

As discussed in the previous chapter, the net microwave power fed into the cavity could not be used to determine the power input into the sample or the corresponding electric field strength in the vacuum. This was due to unknown power losses in the termination line. Moreover, the field distribution in the cavity and thus the power loss in the load were observed to be a function of the load and the tuning adjustment. Therefore, the power measurement was used primarily for comparison between runs (although this was not always possible as the tuning adjustment was changed) and for detecting anomalies during a run. It was particularly helpful to detect occurence of melting (shown by a drop of the power absorbed in the alcohol loop as more power is absorbed in the sample) and of a corona discharge in the cavity (shown by a jump of the reflected power in the transmission line as the admittance of the cavity drops).

Assuming that the variations of the sensible heat of the sample and the heat losses to or from the surrounding atmosphere

Table 9.1 - Experimental conditions

Run Number	$E^a_{exp.}$	P_R	P_R^w	L	x_w	$\frac{m_1 - m_f}{m_o - m_f}$	$h^b \times 10^4$	t_1	Type
	V/cm	mmHg	mmHg	cm	--	--	cal/cm^2 /sec/°C	min	
25	125	1.0	.4	.8	.66	.923	2.1	30	
27	125	.2	.2	.8	.69	.944	1.6	30	PRESSURE
29	125	3.5	.5	.75	.67	.952	1.4	30	RUNS
Average	125	NA	NA	.78	.67	.94	1.7	30	
12	103	.32	.23	.71	.71	.957	1.3	24	
13	107	.29	.27	.74	.72	.950	--	19	
14	145	.24	.23	.71	.70	.905	1.9	35	
15	125	.30	.30	.78	.72	.936	2.1	30	POWER
16	135	.31	.30	.76	.71	.941	2.3	30	RUNS
17	120	.27	.26	.71	.71	--	--	--	
Average	NA	.29	.26	.735	.71	.94	1.9	NA	

a - Estimated from drying curve as discussed in sec. 1 (Eq. (9.1) and (9.2)).
b - Estimated from start-up portion of drying curve by Eq. (9.5), see sec. 2.

were negligible compared to the microwave power generated in the sample, the electric field strength in the vacuum (near the sample surface) was estimated from the drying rate. With this assumption the power generated by the microwave field in the sample could be equated to that consumed by the sublimation:

$$\Phi_T = \Phi_F + \Phi_D = \Delta H_s \dot{m} \tag{9.1}$$

where the total microwave power generated Φ_T can be further related to the electric field strength by Eq. (3.5) to give

$$\Phi_T = \left[K_F(T_F)\ V_F + K_D(T_D)\ V_D\right] E^2 \tag{9.2}$$

The dissipation factors K_F and K_D which are a function of the temperature were estimated from the numerical data shown in Chapter VI by assuming average temperatures for the frozen region and dried layer. An average temperature of 5°C was assumed for the dried layer. An average temperature between -10°C and -1.5°C was assumed for the frozen region, as K_F does not vary significantly between -10°C and 0°C (see Chapter VI). However, a temperature lower than -10°C may be expected in the frozen region for the run at the lowest power level (100 V/cm in Fig. 9.1). Thus, feedback from the theory was used to estimate the temperature in the frozen core (-20°C). The volumes V_F and V_D of the frozen and dried regions were determined using the interface position, derived from the drying curve at the point where the calculations were made (usually half dehydration point and/or maximum of the drying rate curve). An average 16% shrinkage (as observed experimentally) was further allowed for the determination of the volume of the dried layer. Table 9.1 shows the results of the calculations for the electric field peak strength in the vacuum.

The starting fraction of the initial moisture content, $\mu_1 = (m_1 - m_f)/(m_o - m_f)$ (corresponds to the time when the microwave power is turned on), varied from one run to the other due to difficulties in reproducing the operating conditions. Thus, the microwave drying curves have been first normalized to permit

their comparison. The normalized values were then corrected to the average starting moisture content (.94) to include the start-up stage of the process under average operating conditions. Thus, the following quantity:

$$\mu' = \frac{m - m_f}{m_1 - m_f} \mu_{1,aver.} \tag{9.3}$$

has been plotted vs time in Figs. 9.1 and 9.2. The average value of μ_1 observed for both the pressure and the power runs is .94. Typical start-up portions of the drying curve have been plotted in Fig. 9.1, using data of Run 16 and Fig. 9.2, using data of Run 27.

Fig. 9.1 shows the drying curves obtained at various electric field strengths for an average chamber pressure of .3 mmHg. The common portion during the start-up stage of the process (before the microwave power is turned on) exhibits the same characteristics as that predicted by the theory in Chapter VII. An initially high drying rate exists as the dried layer is very small and the mass transfer driving force high due to the low partial pressure of vapor in the vacuum. It decreases rapidly as the temperature of the frozen material drops to the wet-bulb temperature of the vacuum and becomes practically constant until the microwave power is turned on. The drying rate starts to increase as microwave energy is absorbed in the sample.

It can be seen from Fig. 9.1 that the drying rate increases substantially when the electric field strength is increased as expected from the theory. Toward the end of the drying the curves start to level off. This corresponds to the stage in which the frozen core has disappeared and the residual adsorbed moisture is being removed from the dried product. This latter stage is usually of little interest as only removal of the frozen moisture content is sought in industrial freeze-drying operations. The residual moisture content can be determined from a plot of the drying rate vs time as the curve exhibits a sudden decrease of the slope when

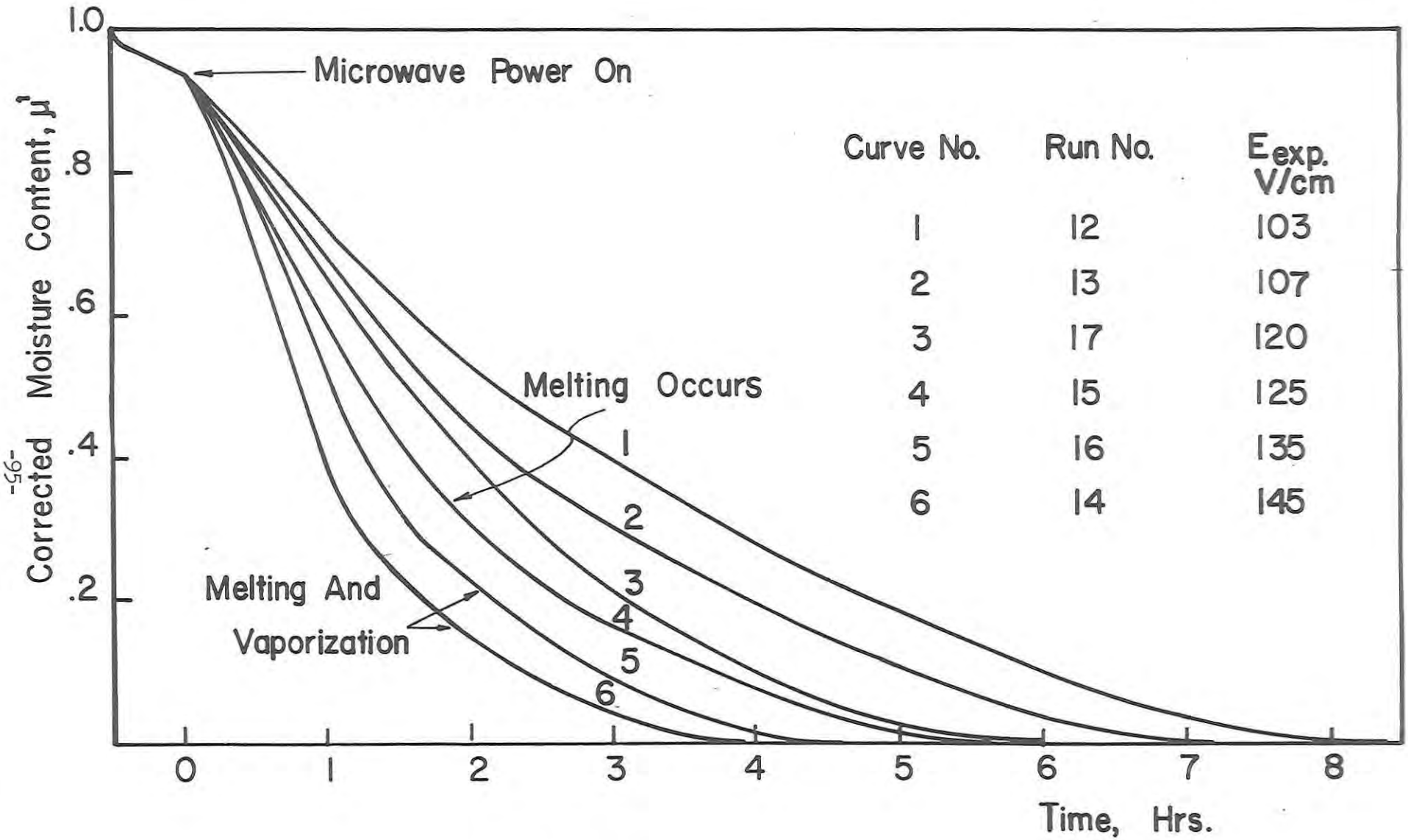

Figure 9.1 - Experimental drying curves (power runs). P_R = .3 mmHg

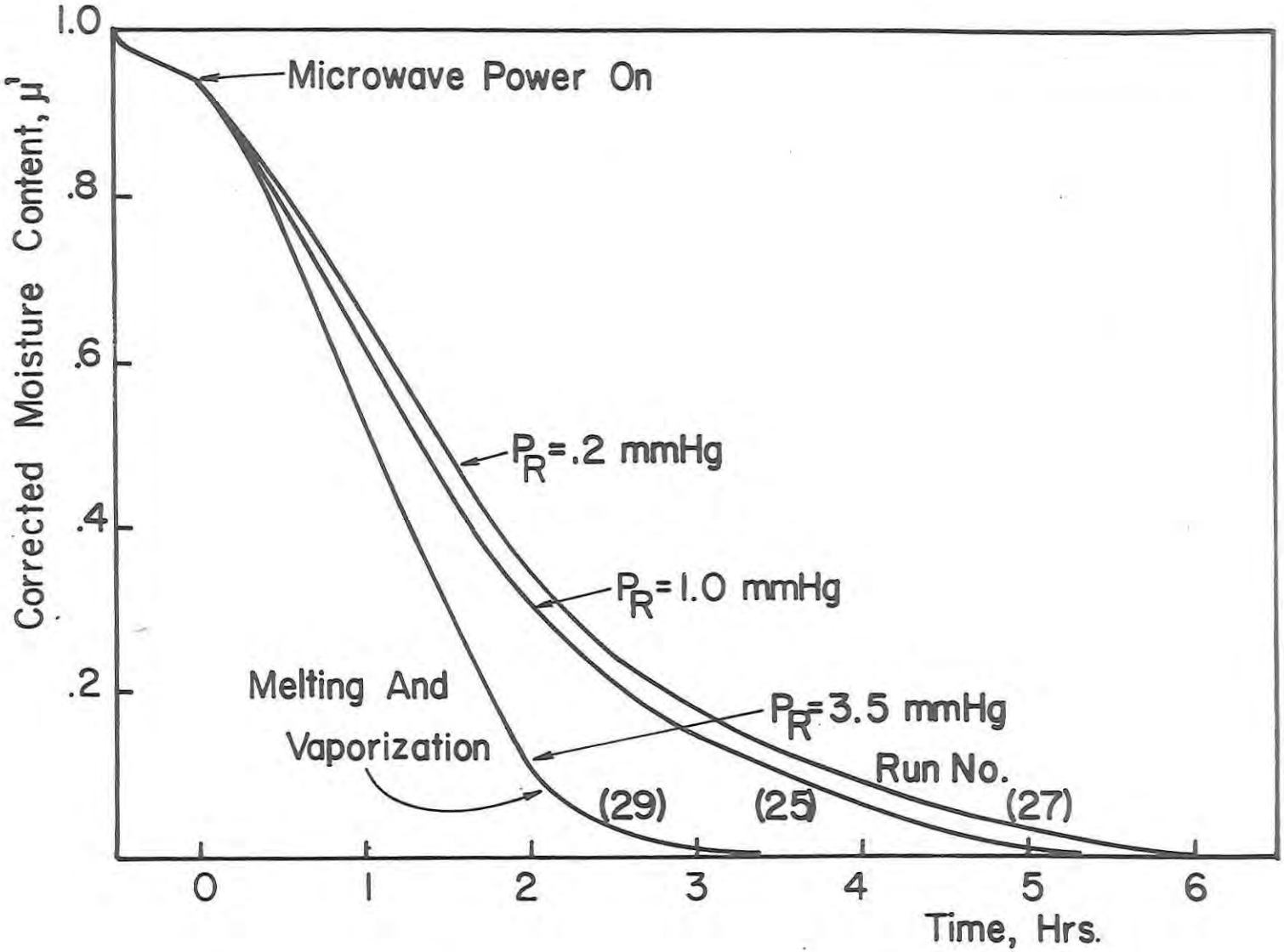

Figure 9.2 - Experimental drying curves (pressure runs).

the frozen core disappears (less microwave power is absorbed by the sample). This is shown in Figs. 9.3, 9.4, 9.5, and 9.6. It has been found by this technique that the residual moisture content is less than 5% of the initial sample weight or 7% of the initial weight of water. The actual residual moisture content was found to be approximately 1.5% of the initial sample weight for all runs except, Runs No. 12 and 15 for which it was of the order of 4.5%. This is reflected on Fig. 9.1 by the early leveling off of the corresponding drying curves.

It should be noted that a visual examination of the dried sample obtained in Run No. 13 showed local burns of the material which indicated a non uniform field distribution for this run. The tuning of the cavity was readjusted following this run and the problem was corrected.

When a higher microwave power is used, melting of the frozen material starts to occur (Run No. 15), followed by a local vaporization (Runs No. 16 and No. 14). The local vaporization indicates that the dielectric heating is not perfectly uniform although a relatively planar ice-front has been observed at medium and low power levels. This was done by cutting in different directions a partially dried sample. It seems that for the lower power input, the drying rate is small enough to permit the temperature non-uniformities in a cross section to level out. This is less likely to occur at the higher power levels. Thus, a non planar ice-front and hot spots may develop in the frozen region inducing an early melting of the frozen core.

Melting is believed to start occuring with Run No. 15 as the drying rate exhibits (Fig. 9.3) a sudden increase at time t = .8 hr. This was confirmed during the experiments by the observed drop of the microwave power loss in the alcohol loop. Indeed, as a higher microwave power is used (Run No. 16 and No. 14) local vaporization takes place. As the ice melts and vaporization occurs a much higher drying rate develops locally due to the higher dissipation factor of the wet material. This phenomenon

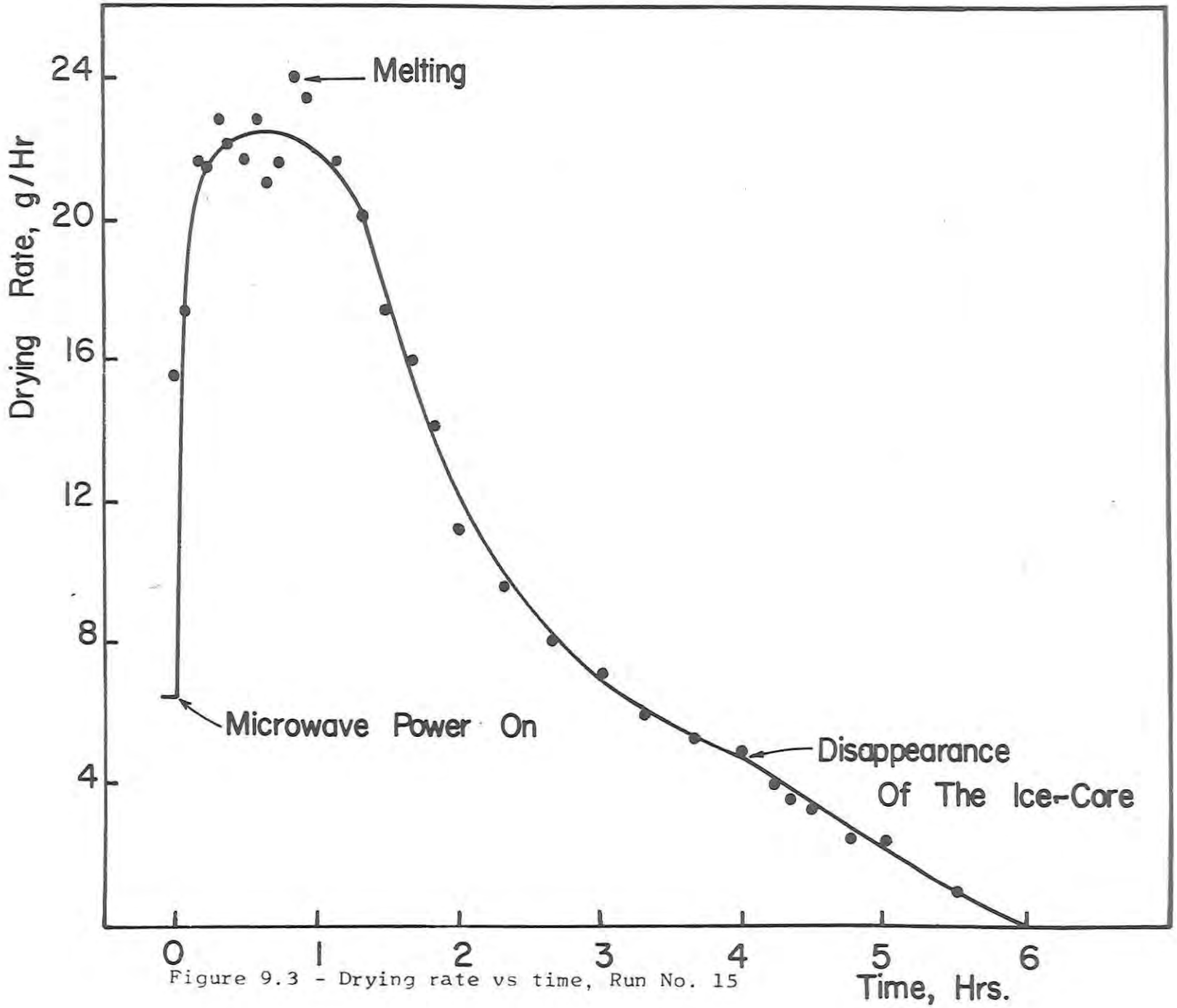

Figure 9.3 - Drying rate vs time, Run No. 15

can be observed visually as a dark spot and puffing develop at the surface of the sample. The occurence of vaporization is also reflected by the drying curve as its slope increases due to the higher drying rate (see Fig. 9.1).

Fig. 9.2 shows similar plots for the drying curves at various pressures and a fixed microwave power input. An electric field peak strength of 125 V/cm has been estimated for the three runs by the method outlined earlier. It can be seen from this figure that the sample dried faster for a pressure of 1 mmHg than for .2 mmHg as expected from the theory. This can be explained by the increase of the dissipation coefficient with the temperature, mainly in the frozen core, due to the higher resistance of the mass transfer in the dried layer. In fact, when the pressure of the vacuum chamber is increased to 3.5 mmHg, melting of the frozen core occurs, early during the dehydration, and is followed by a local vaporization.

2. Comparison with simulated drying curves

In order to obtain theoretical drying curves for comparison with those obtained experimentally, the heat transfer coefficient has been estimated from the start-up portion of the drying curves. This was done by assuming a linear temperature profile in the dried layer. The Dew-Point temperature corresponding to the pressure in the vacuum chamber was used to approximate the ice-front temperature (essentially equal to the wet-bulb temperature of the vacuum) as the drying rate was small. It can be seen from an energy balance on the dried layer that,

$$h(T_R - T_{S,1}) = K_D \frac{(T_S - T_i)_1}{\delta_1} = Q_{S,1} \doteq \Delta H_s W_1 \qquad (9.4)$$

h can then be related to the drying rate before the microwave power is turned on by

$$h = \Delta H_s \frac{1 + \beta}{T_R - T_{i,1}} W_1 \qquad (9.5)$$

where β is given by

$$\beta = \text{Biot Number} = \frac{h\ \delta_1}{k_D} \tag{9.6}$$

and δ_1 is the dried layer thickness.

Values of h calculated in this manner are shown in Table 9.1 for each run. The average value of 1.9×10^{-4} cal/cm^2/sec/°C found for the first batch (eye of the round) was used in the simulation. Due to the concave shape of the slab in the second batch, the thickness of the dried layer, could not be determined accurately. Thus, this might result in a higher uncertainty on h.

It has been found from preliminary computer runs using the average operating conditions of the power runs, that melting would occur for an electric field peak strength of 205 V/cm. However, an experimental value of approximately 125 V/cm was observed. Although this discrepancy could be attributed experimentally to a non-uniform heating, it was felt that the diffusivity values used in the calculations might be overestimated. The actual values for the beef samples could be somewhat lower by as much as a factor 2. Consequently, Eq. (6.8) in Chapter VI was modified using Harper's value of D° for beef (corrected at 265°K) and data on D_K (at 265°K) for turkey breast (no experimental value of D_K could be found for beef in the literature). It constitutes a reduction of the diffusivity by as much as 40% at high pressures (several mmHg and over). The difference becomes negligible at low pressures (near .1 mmHg). This modification led to a new value of the maximum field (without melting) of 170 V/cm (peak strength).

Theoretical drying curves were calculated using the average operation conditions (shown in Table 9.1).

In order to compare the theoretical curves with experimental values, the experimental drying curves were modified in order to represent the variations of the ice-front position with time.

In effect, the ice-front position can be related to the weight loss by,

$$S(t) = \frac{m - (m_f + m_r)}{m_o - m_f} = \frac{m(t) - m_f}{m_o - m_f} - \frac{m_r(t)}{m_o - m_f} \qquad (9.7)$$

m_r is the weight of residual water adsorbed in the dried layer, and $m_r / (m_o - m_f)$ the fraction of adsorbed moisture.

Since $m_r(t)$ was not known it was estimated from its final value $m_{r,2}$ assuming a linear variation with time. $m_{r,2}$ was obtained from the drying rate curves (Figs. 9.3, 9.4, 9.5, and 9.6). The following formula was used to determine the position of the interface at any time from the experimental drying curves,

$$S(t) = \frac{m(t) - m_f}{m_o - m_f} - \frac{m_{r,2}}{m_o - m_f} \frac{t}{t_2} \qquad (9.8)$$

Figs. 9.7, 9.8, 9.9, 9.10, and 9.11 show plots of the variations of the interface position determined from the experimental results by the above method. The theoretical curves predicted by the simulation are also shown in these figures. The electric field strengths used in the simulation were adjusted in order to give the best fit. It should be pointed out that the final values of the electric field strength used to calculate the curves shown in Figs. 9.7, 9.8, 9.9, 9.10, and 9.11 agree within 4% of those determined experimentally. A generally good agreement is also found between the theoretical and experimental drying curves as shown by Figs. 9.7, 9.8, 9.9, 9.10, and 9.11. The small differences observed may just be the inherent differences between the model and the experiments. However, they may also reflect an uncertainty in the numerical data used in the model (especially diffusivity and dissipation factor) or non-ideal experimental conditions, e.g.,

1. non-uniform field distribution in the sample
2. non-constant standing wave pattern in the cavity
3. non-constant microwave power fed into the cavity
4. non-uniform thickness of the sample

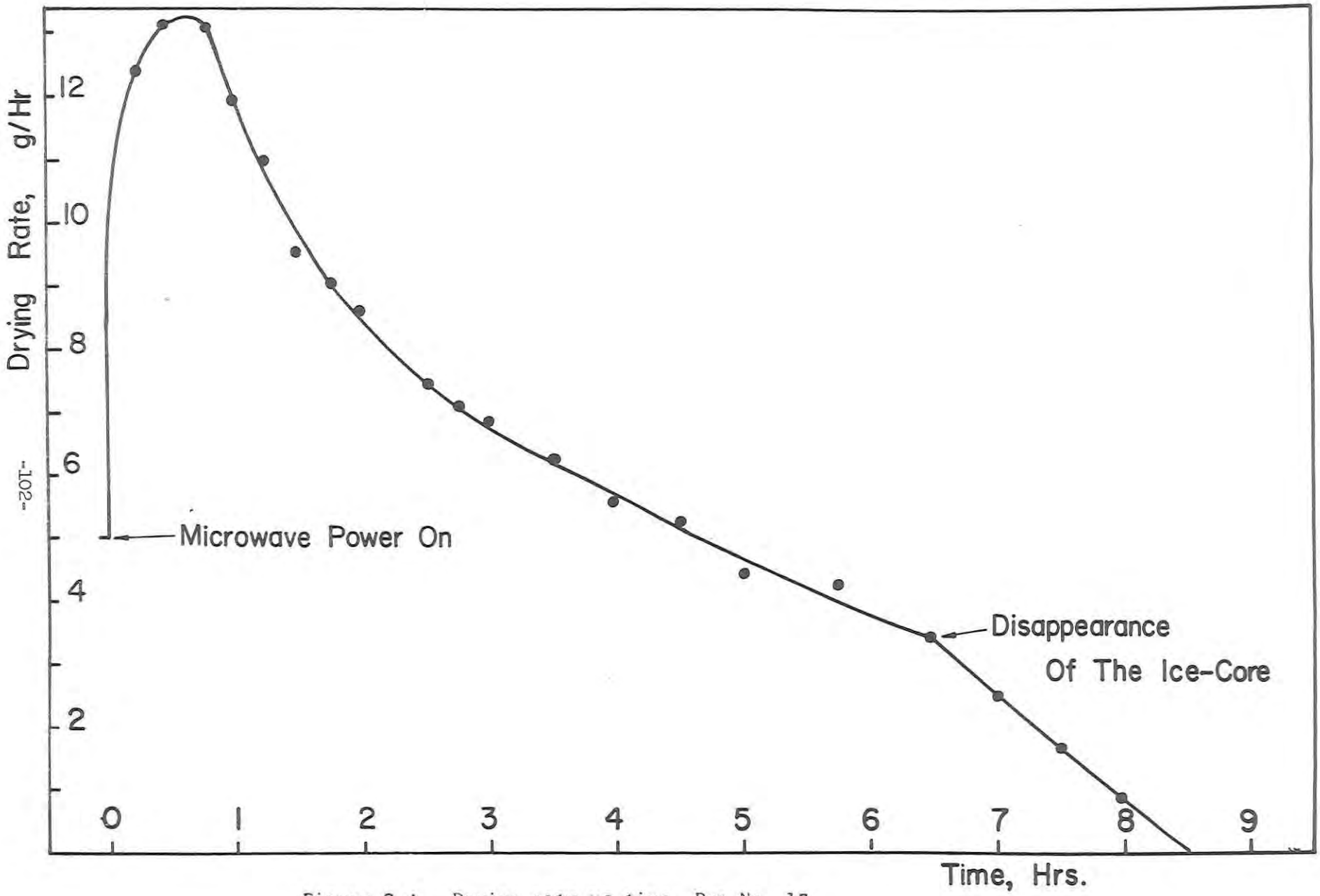

Figure 9.4 - Drying rate vs time. Run No. 12

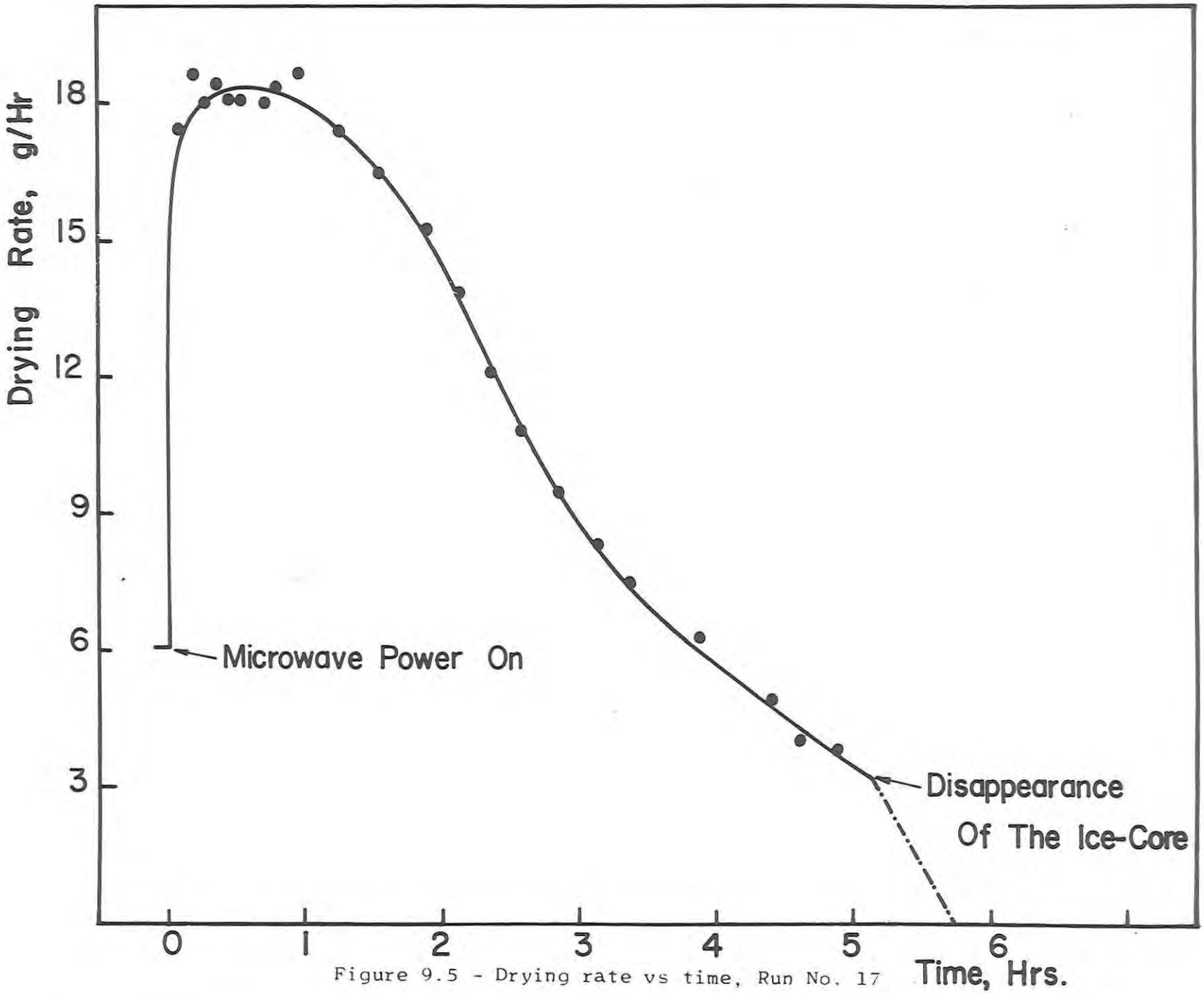

Figure 9.5 - Drying rate vs time, Run No. 17

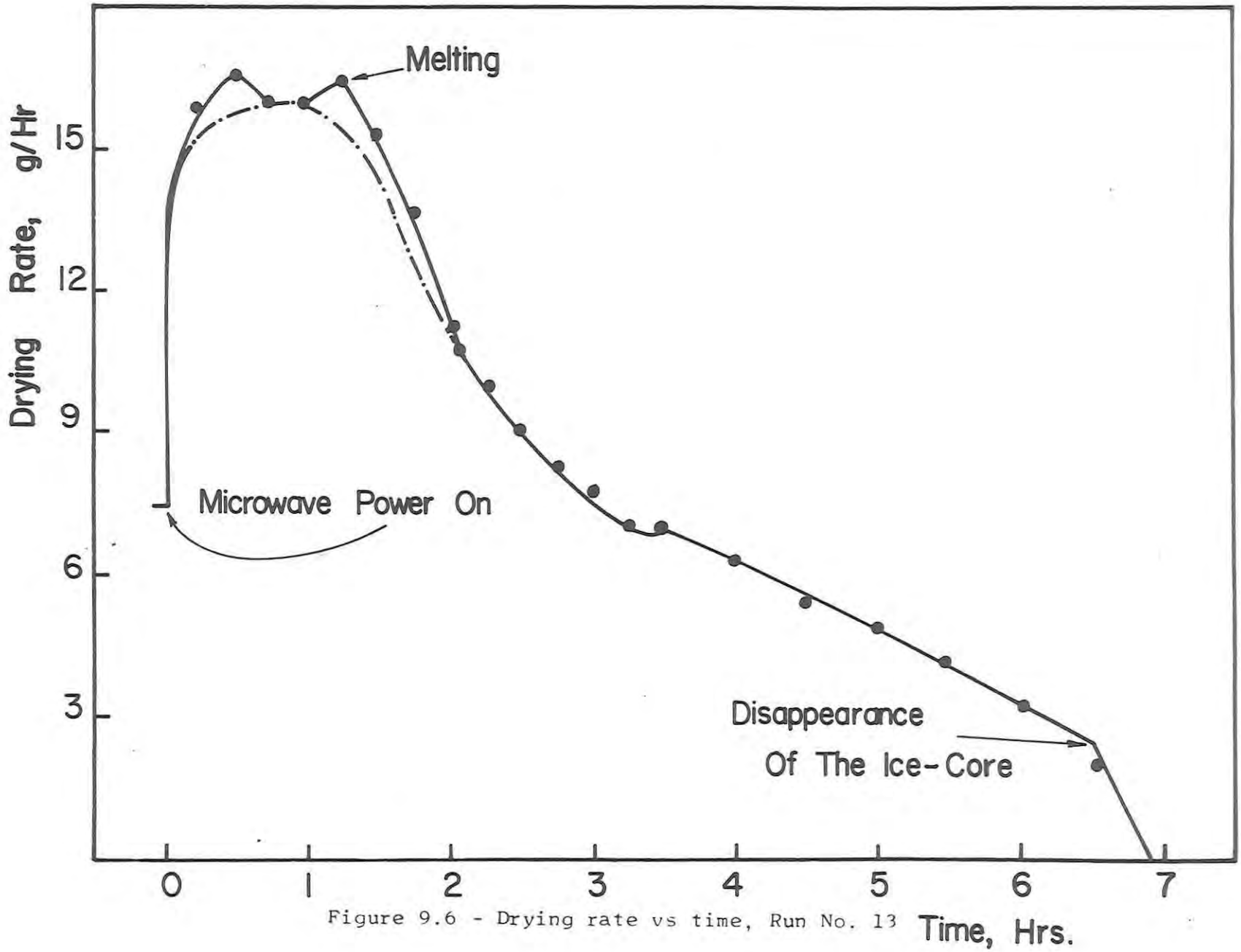

Figure 9.6 - Drying rate vs time, Run No. 13

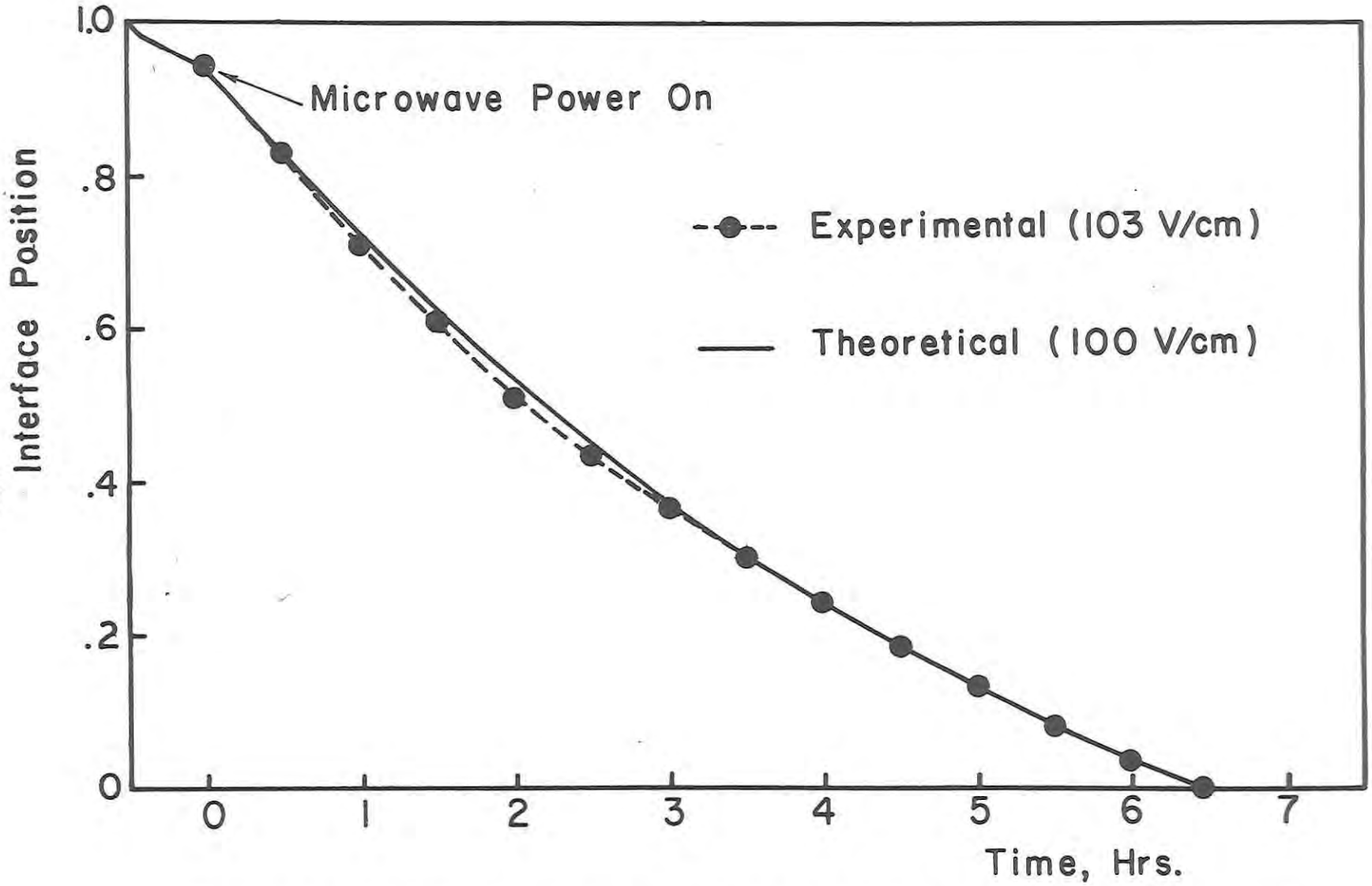

Figure 9.7 - Experimental (Run No. 12) and simulated drying curves. P_R = .3 mmHg

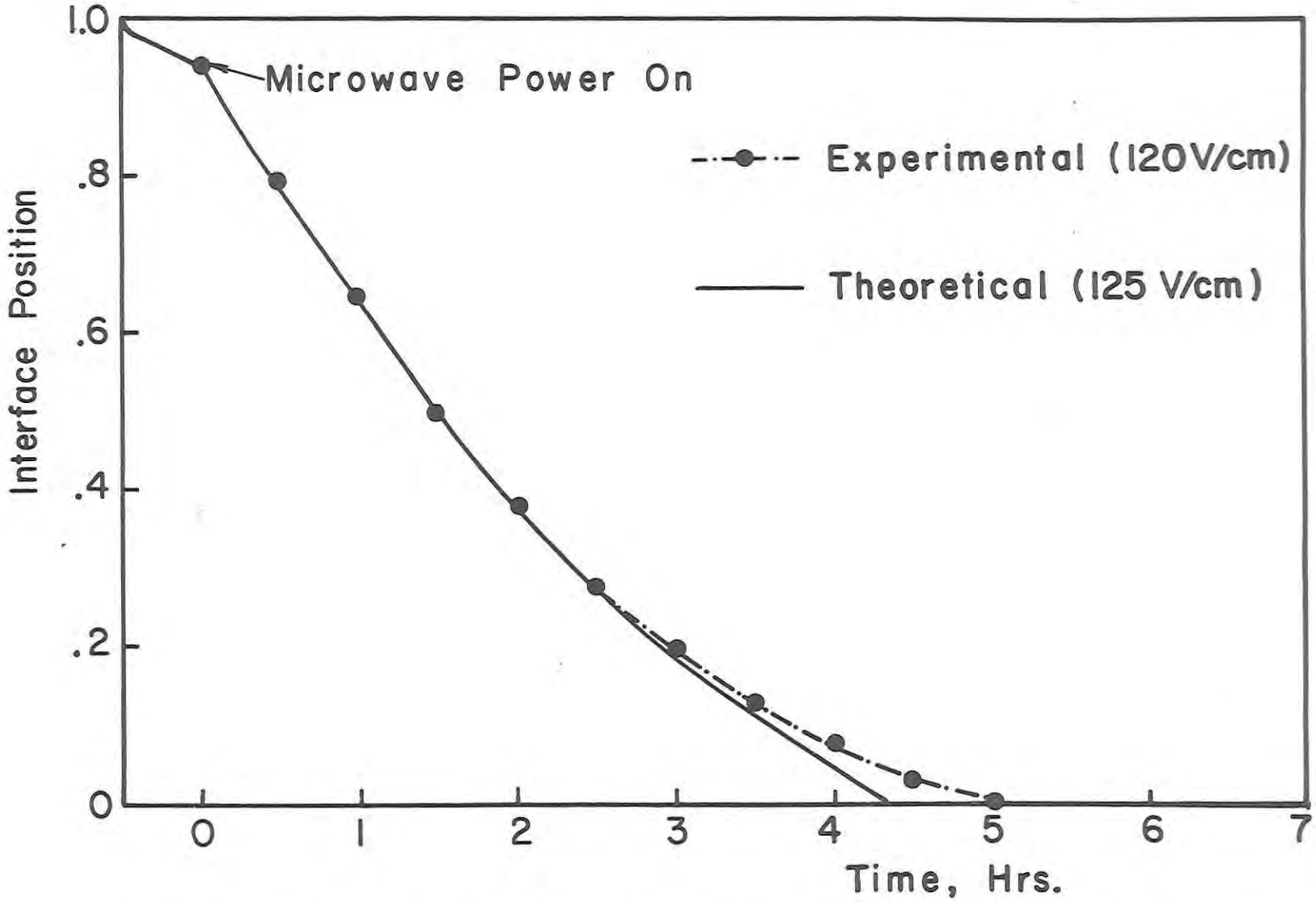

Figure 9.8 - Experimental (Run No. 17) and simulated drying curves. P_R = .3 mmHg

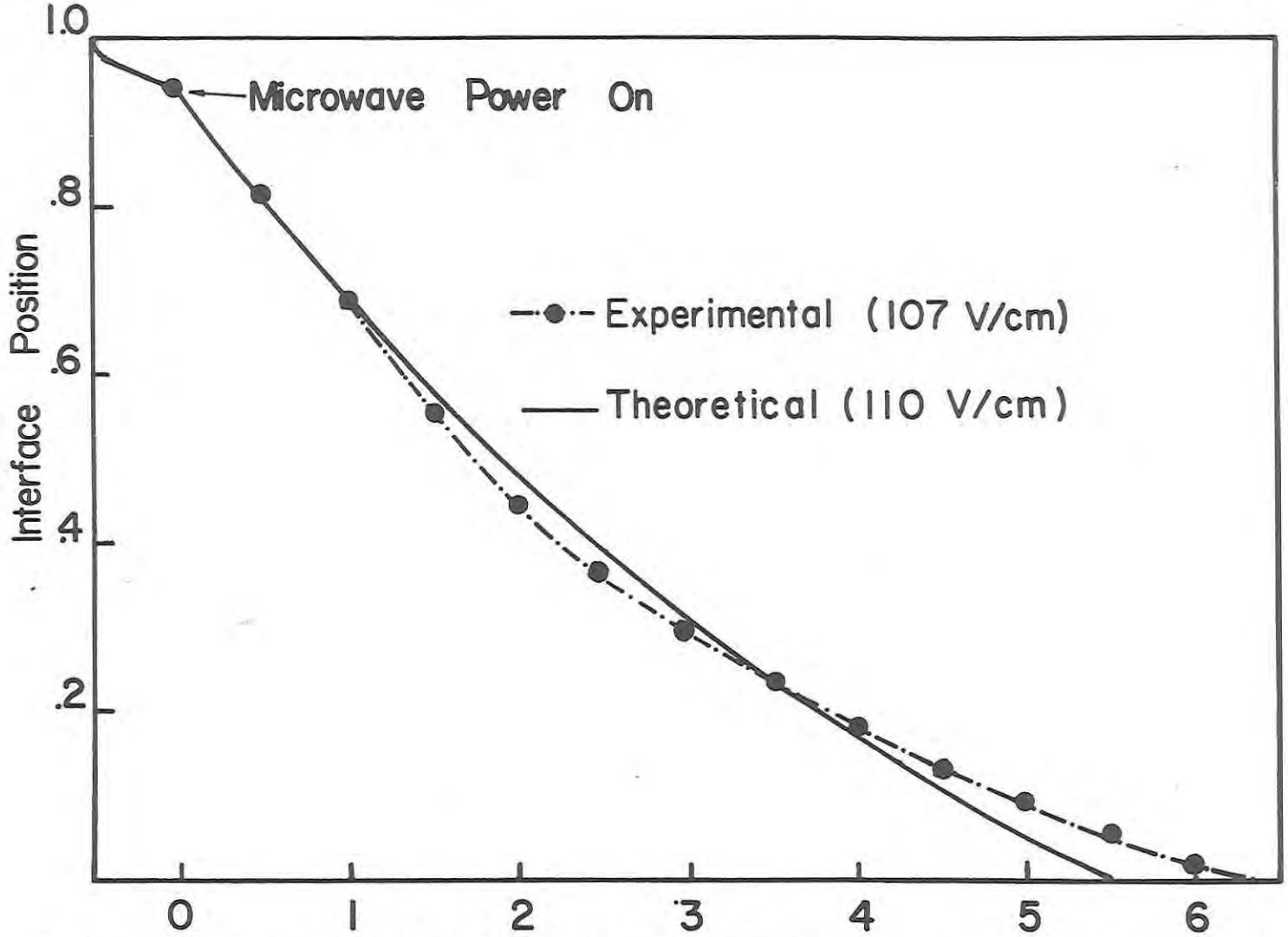

Figure 9.9 - Experimental (Run No. 13) and simulated drying curves. P_R = .3 mmHg

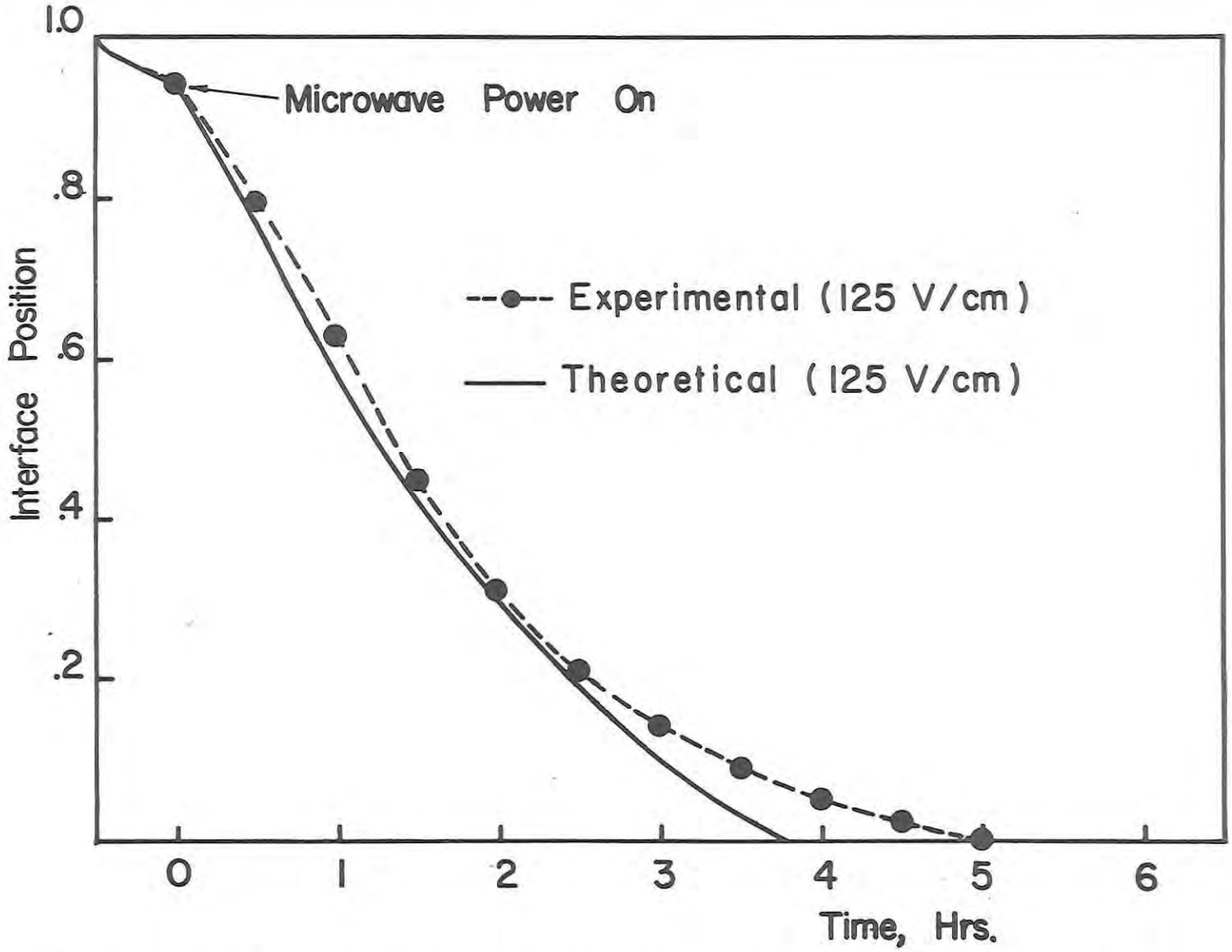

Figure 9.10 - Experimental (Run No. 25) and simulation drying curves. P_R = 1 mmHg

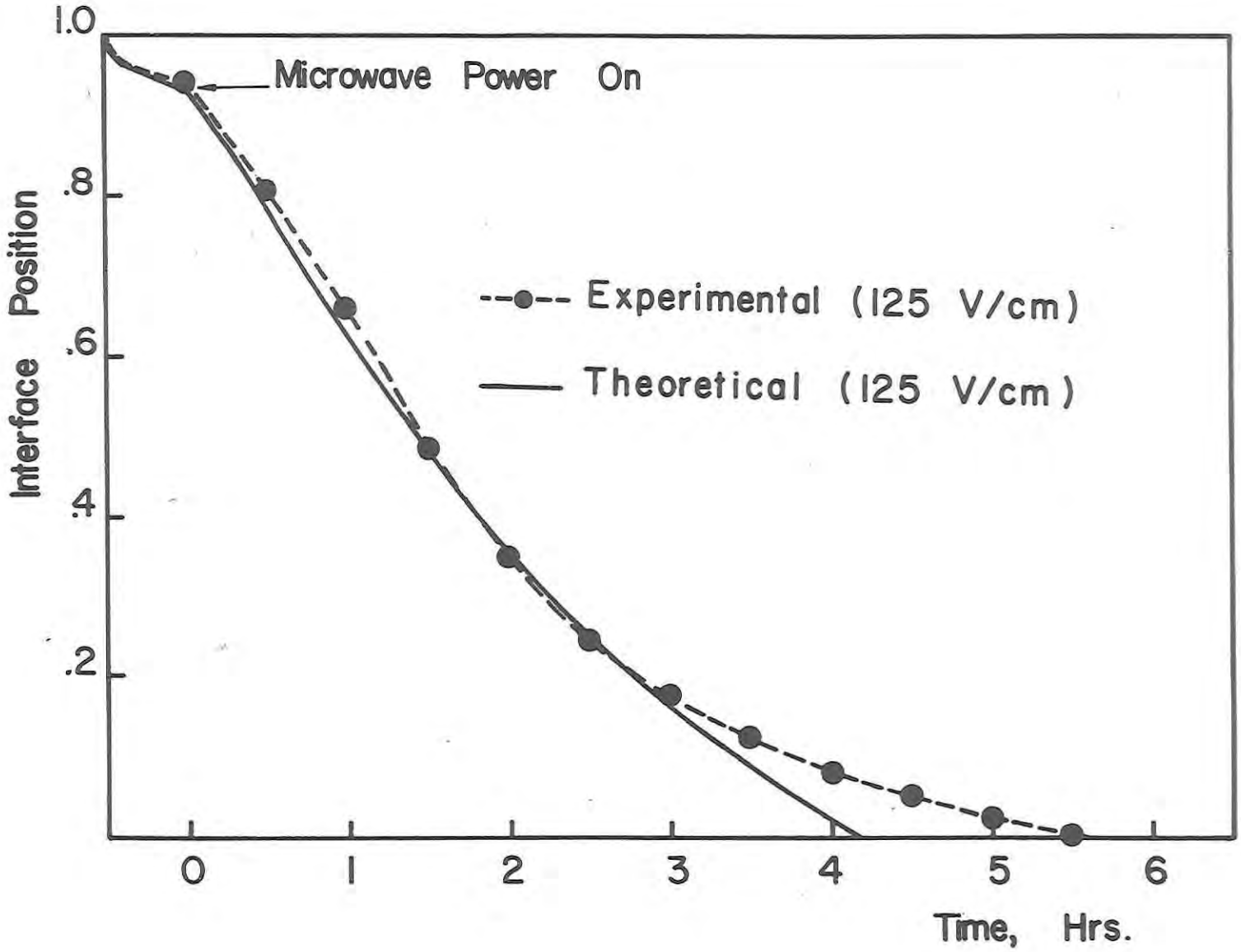

Figure 9.11 - Experimental (Run No. 27) and simulated drying curves. P_R = .2 mmHg

The possibility for a non-uniform field is indicated by the local vaporization which occured in Runs No. 14 and 16, and the local burns of the sample observed in Run No. 13. It would explain the greater discrepancy observed for this latter run between simulated and experimental drying curves (Fig. 9.9). Indeed the sudden decrease of slope in Fig. 9.9 of the experimental drying curve, with respect to the theoretical one, corresponds to a peak of the drying rate curve (Fig. 9.6) at t = 1 hr., which may have been caused by a local melting.

A non-constant standing wave pattern or a non-uniform field distribution in the sample may have caused the difference observed in Figs. 9.8, 9.9, 9.10, and 9.11 toward the end of the dehydration. Although it may have been the fact of the non-uniform thickness (this stands particularly for the pressure runs, Figs. 9.10, and 9.11). Indeed, it is not possible to differentiate between the multiple causes of non ideality. Given the uncertainties on the experimental conditions, the general agreement obtained between the theoretical and experimental drying curves can be considered as good, considering the small differences observed.

- Chapter X -

CONCLUSIONS

1. A one-dimensional model of the freeze-drying process using microwave energy has been derived from the analysis of the transport phenomena, assuming an infinitely sharp sublimation front. The complete transient mass and energy transfer equations have been written in both the frozen and dried regions. The transport and dielectric properties are allowed to vary with both time and location in the sample as a function of temperature and pressure. The adsorption effect of the water vapor in the dried layer is neglected. Fick's equation is used to describe the flow of water vapor in the dried layer.

2. The model enables one to describe the sublimation of the frozen moisture content before and after the microwave power is turned on. The final drying stage, of little industrial significance, in which all frozen material has disappeared and the adsorbed residual moisture (less than 5% of the initial sample weight) is being removed, is not covered by this study.

3. A numerical solution of the transient energy and mass transfer equations in both the frozen and dried layer is proposed. It is based on an approximation of the partial differential equations by Crank-Nicolson method. The finite-difference equations are

solved by Gauss's elimination technique. An iteration of the interface temperature is used to handle the energy and mass transfer equations which are coupled at the interface. A second iteration loop is used to predict the interface motion.

4. A new numerical method is proposed to accelerate and control the convergence of an iteration scheme. Use of this method enables one to reach convergence in 2 to 4 iterations.

5. The results of the theoretical study show that the freeze-drying process is heat transfer limited. Drying rates are essentially a function of the microwave power input. The total pressure and the partial pressure of water vapor in the vacuum mainly affect the temperature within the sample during freeze-drying and have little effect on the drying time. Low pressures should be used in order to ensure temperatures as low as possible in the sample and thus allow one to shorten the drying time by using a higher microwave power input. However, pressures below 75 μHg are useless as their effect becomes insignificant while the flow regime in the pores becomes mainly Knudsen Diffusion.

The initial temperature of the sample, prior to drying, is not an important parameter.

6. A reduction of the sample size results in shorter drying times and a greater output of the freeze-dryer as a higher microwave power level is possible without melting or overheating. An optimal operation, yielding a maximum freeze-dryer output, would correspond to an operation near corona and overheating (or melting) conditions.

7. With the assumption that a corona discharge would occur in the microwave applicator beyond 255 V/cm (peak strength) and that the diffusivity values of turkey breast are applicable to beef meat, drying time as short as 1½ hours would be possible for a ½ in. thick

8. A value of the heat transfer coefficient (1.9×10^{-4} cal/cm^2/sec/°C) has been determined from the start-up portion of the experimental drying curves. Use of this value in the prediction of the drying curves gave an excellent agreement between the theoretical and experimental start-up portions of the drying curves.

9. Comparison of the theoretical (170 V/cm) and experimental (125 V/cm) electrical field peak strengths at which melting starts to occur in the frozen core, seems to indicate that the actual diffusivity in the experiments may be somewhat lower than that assumed in the calculations. However, the difference may also reflect experimental heating non-uniformities.

10. Finally, the predicted drying curves are in good agreement with those obtained experimentally. The small differences observed may be due to an uncertainty on the value of the diffusivity (or that of the dielectric properties) or non-ideal experimental conditions, e.g.,

1. non-uniform electric field distribution in the sample
2. non-constant standing wave pattern in the cavity
3. non-uniform thickness of the sample

11. The mathematical model can be used to simulate with a good accuracy the sublimation-dehydration process using microwave dielectric heating.

- Chapter XI -

RECOMMENDATIONS

1. Future improvement of the mathematical model may include the moisture adsorption effect in the dried layer. This would enable one to account for the variations of the dissipation factor of the dried product with the sorbed moisture content, as experimental data are obtained. It would also permit one to describe the final drying stage in which the residual sorbed moisture is removed from the dried product.

2. There is a need for more experimental data on the physical properties of frozen and dried beef meat. These data should include especially the following:

   1. the effective diffusivity in the operating pressure range (.05 to 1 mmHg)
   2. the dielectric properties in the temperature range, -50°C to 0°C for frozen beef and -50°C to 60°C for dried beef as a function of composition (moisture, fat, and salt contents)

3. Shorter computer times in the mathematical simulation may be obtained through a more efficient organization of the numerical scheme and the determination of an optimal time increment size strategy. The latter would require an extensive stability analysis.

4. More extensive and comprehensive experimental data on the microwave freeze-drying process are still needed. There is a need

for a systematic experimental study of the effects of the process constraints and variables on the drying time, in order to support the theory.

5. Special care should be used in the design of an experimental freeze-dryer in order to ensure conditions of:

1. corona-free operation
2. uniform electric field distribution in the sample
3. constant standing wave pattern in the microwave applicator
4. in-process determination of the electric field strength in the vacuum near the sample and/or the microwave power loss in the sample.

A.1 FINITE DIFFERENCE EQUATIONS

Mass transfer equation (dried layer):

$$\frac{\Gamma_{k+1,n+1} - 2\Gamma_{k,n+1} + \Gamma_{k-1,n+1}}{\Delta z^2} + \left(\frac{1}{D_k^*}\,\frac{D_{k+1}^* - D_{k-1}^*}{2\Delta z} - \frac{1}{D_k^*}(k-1)\Delta z\,(1-S_{n+1})\,\frac{S_{n+1}-S_n}{\Delta\tau}\right)\frac{\Gamma_{k+1,n+1}-\Gamma_{k-1,n+1}}{2\Delta z} - \frac{\sigma}{D_k^*}(1-S_{n+1})^2\,\frac{\Gamma_{k,n+1}-\Gamma_{k,n}}{\Delta\tau}$$

$$+\frac{\Gamma_{k+1,n} - 2\Gamma_{k,n} + \Gamma_{k-1,n}}{\Delta z^2} + \left(\frac{1}{D_k^*}\,\frac{D_{k+1}^* - D_{k-1}^*}{2\Delta z} - \frac{1}{D_k^*}(k-1)\Delta z\,(1-S_n)\,\frac{S_{n+1}-S_n}{\Delta\tau}\right)\frac{\Gamma_{k+1,n}-\Gamma_{k-1,n}}{2\Delta z} - \frac{\sigma}{D_k^*}(1-S_n)^2\,\frac{\Gamma_{k,n+1}-\Gamma_{k,n}}{\Delta\tau} = 0 \qquad (A.1.1)$$

Heat transfer equation in the dried layer:

$$\frac{\theta_{k+1,n+1}^D - 2\theta_{k,n+1}^D + \theta_{k-1,n+1}^D}{\Delta z^2} + \left[\frac{1}{\alpha_{D_k}^*}\,\frac{\alpha_{D_{k+1}}^* - \alpha_{D_{k-1}}^*}{2\Delta z} - \left(\frac{C_{pw}\,\rho\sigma}{\rho_D C_D \alpha_{D_k}^*} + \frac{1}{\alpha_{D_k}^*}(k-1)\Delta z\right)(1-S_{n+1})\,\frac{S_{n+1}-S_n}{\Delta\tau}\right]\frac{\theta_{k+1,n+1}^D - \theta_{k-1,n+1}^D}{2\Delta z} - \frac{1}{\alpha_{D_k}^*}(1-S_{n+1})^2\,\frac{\theta_{k,n+1}^D - \theta_{k,n}^D}{\Delta\tau}$$

$$+\frac{\omega_{D_k}^*}{\alpha_{D_k}^*}\,\frac{\rho_F C_F}{\rho_D C_D}\,\frac{\omega_F^\circ L^2 (1-S_{n+1})^2}{k_F^\circ (T_R - T_0)}$$

$$+\frac{\theta_{k+1,n}^D - 2\theta_{k,n}^D + \theta_{k-1,n}^D}{\Delta z^2} + \left[\frac{1}{\alpha_{D_k}^*}\,\frac{\alpha_{D_{k+1}}^* - \alpha_{D_{k-1}}^*}{2\Delta z} - \left(\frac{C_{pw}\,\rho\sigma}{\rho_D C_D \alpha_{D_k}^*} + \frac{1}{\alpha_{D_k}^*}(k-1)\Delta z\right)(1-S_{n+1})\,\frac{S_{n+1}-S_n}{\Delta\tau}\right]\frac{\theta_{k+1,n}^D - \theta_{k-1,n}^D}{2\Delta z} - \frac{1}{\alpha_{D_k}^*}(1-S_n)^2\,\frac{\theta_{k,n+1}^D - \theta_{k,n}^D}{\Delta\tau}$$

$$+\frac{\omega_{D_k}^*}{\alpha_{D_k}^*}\,\frac{\rho_F C_F}{\rho_D C_D}\,\frac{\omega_F^\circ L^2 (1-S_n)^2}{k_F^\circ (T_R - T_0)} = 0 \qquad (A.1.2)$$

Heat transfer equation in the frozen region:

$$\frac{\theta^F_{m+1,n+1} - 2\theta^F_{m,n+1} + \theta^F_{m-1,n+1}}{\Delta y^2} + \left[\frac{1}{\alpha^*_{Fm}}\frac{\alpha^*_{Fm+1} - \alpha^*_{Fm-1}}{2\Delta y} + \frac{1}{\alpha^*_{Fm}}(m-1)\Delta y\, S_{n+1}\frac{S_{n+1} - S_n}{\Delta\tau}\right]\frac{\theta^F_{m+1,n+1} - \theta^F_{m-1,n+1}}{2\Delta y} - \frac{1}{\alpha^*_{Fm}} S^2_{n+1}\frac{\theta^F_{m,n+1} - \theta^F_{m,n}}{\Delta\tau}$$

$$+ \frac{\omega^*_{Fm}}{\alpha^*_{Fm}}\frac{\omega^o_F L^2 S^2_{n+1}}{k^o_F(T_R - T_o)}$$

$$+ \frac{\theta^F_{m+1,n} - 2\theta^F_{m,n} + \theta^F_{m-1,n}}{\Delta y^2} + \left[\frac{1}{\alpha^*_{Fm}}\frac{\alpha^*_{Fm+1} - \alpha^*_{Fm-1}}{2\Delta y} + \frac{1}{\alpha^*_{Fm}}(m-1)\Delta y\, S_n\frac{S_{n+1} - S_n}{\Delta\tau}\right]\frac{\theta^F_{m+1,n} - \theta^F_{m-1,n}}{2\Delta y} - \frac{1}{\alpha^*_{Fm}} S^2_n\frac{\theta^F_{m,n+1} - \theta^F_{m,n}}{\Delta\tau}$$

$$+ \frac{\omega^*_{Fm}}{\alpha^*_{Fm}}\frac{\omega^o_F L^2 S^2_n}{k^o_F(T_R - T_o)} = 0 \qquad (A.1.3)$$

The properties have not been time indexed for simplicity although they are a function of time. Equations (A.1.1), (A.1.2), and (A.1.3) are rearranged into the general form of Eq. (5.9) as shown below.

Mass transfer equation:

$$\Gamma_{k+1,n+1}\left[r^c_{k,n+1} + d^c_{k,n+1} - \frac{1}{2}(k-1)(1-S_{n+1})(S_{n+1} - S_n)\right] - \Gamma_{k,n+1}\left[2r^c_{k,n+1} + \sigma(1-S_{n+1})^2 + \sigma(1-S_n)^2\right] + \Gamma_{k-1,n+1}\left[r^c_{k,n+1} - d^c_{k,n+1} + \frac{1}{2}(k-1)(1-S_{n+1})(S_{n+1} - S_n)\right]$$

$$= -\Gamma_{k+1,n}\left[r^c_{k,n} + d^c_{k,n} - \frac{1}{2}(k-1)(1-S_n)(S_{n+1} - S_n)\right] + \Gamma_{k,n}\left[2r^c_{k,n} - \sigma(1-S_{n+1})^2 - \sigma(1-S_n)^2\right] - \Gamma_{k-1,n}\left[r^c_{k,n} - d^c_{k,n} + \frac{1}{2}(k-1)(1-S_n)(S_{n+1} - S_n)\right]$$

$$(A.1.4)$$

Heat transfer equation in the dried layer:

$$\theta^D_{k+1,n+1}\left[r^D_{k,n+1}+d^D_{k,n+1}-\frac{1}{2}p_k(1-S_{n+1})(S_{n+1}-S_n)\right]-\theta^D_{k,n+1}\left[2r^D_{k,n+1}+(1-S_{n+1})^2+(1-S_n)^2\right]$$

$$+\theta^D_{k-1,n+1}\left[r^D_{k,n+1}-d^D_{k,n+1}+\frac{1}{2}p_k(1-S_{n+1})(S_{n+1}-S_n)\right]=$$

$$-\theta^D_{k+1,n}\left[r^D_{k,n}+d^D_{k,n}-\frac{1}{2}p_k(1-S_n)(S_{n+1}-S_n)\right]+\theta^D_{k,n}\left[2r^D_{k,n}-(1-S_{n+1})^2-(1-S_n)^2\right]$$

$$-\theta^D_{k-1,n}\left[r^D_{k,n}-d^D_{k,n}+\frac{1}{2}p_k(1-S_n)(S_{n+1}-S_n)\right]-q^D_{k,n+1}(1-S_{n+1})^2-q^D_{k,n}(1-S_n)^2$$

(A.1.5)

Heat transfer equation in the frozen region:

$$\theta^F_{m+1,n}\left[r^F_{m,n+1}+d^F_{m,n+1}+\frac{1}{2}(m-1)S_{n+1}(S_{n+1}-S_n)\right]-\theta^F_{m,n+1}\left[2r^F_{m,n+1}+S^2_{n+1}+S^2_n\right]$$

$$+\theta^F_{m-1,n+1}\left[r^F_{m,n+1}-d^F_{m,n+1}-\frac{1}{2}(m-1)S_{n+1}(S_{n+1}-S_n)\right]=$$

$$-\theta^F_{m+1,n}\left[r^F_{m,n}+d^F_{m,n}+\frac{1}{2}(m-1)S_n(S_{n+1}-S_n)\right]+\theta^F_{m,n}\left[2r^F_{m,n}-S^2_{n+1}-S^2_n\right]$$

$$-\theta^F_{m-1,n}\left[r^F_{m,n}-d^F_{m,n}-\frac{1}{2}(m-1)S_n(S_{n+1}-S_n)\right]-q^F_{m,n+1}S^2_{n+1}-q^F_{m,n}S^2_n$$

(A.1.6)

where:

$$r^c_{k,n}=\frac{D^*_{k,n}\Delta\tau}{\Delta z^2}\ ;\quad r^D_{k,n}=\frac{\alpha^*_{D_{k,n}}\Delta\tau}{\Delta z^2}\ ;\quad r^F_{m,n}=\frac{\alpha^*_{F_{m,n}}\Delta\tau}{\Delta y^2}$$

(A.1.7)

$$d^c_{k,n}=.25\left(D^*_{k+1,n}-D^*_{k-1,n}\right)\frac{\Delta\tau}{\Delta z^2}\ ;\quad d^D_{k,n}=.25\left(\alpha^*_{D_{k+1,n}}-\alpha^*_{D_{k-1,n}}\right)\frac{\Delta\tau}{\Delta z^2}\ ;\quad d^F_{m,n}=.25\left(\alpha^*_{F_{m+1,n}}-\alpha^*_{F_{m-1,n}}\right)\frac{\Delta\tau}{\Delta y^2}$$

(A.1.8)

And:

$$p_k = \frac{C_{pw} \rho \sigma}{\rho_D C_D \Delta z} + k - 1 \qquad (A.1.9)$$

$$q^D_{k,n} = \omega^*_{D_{k,n}} \frac{\rho_F C_F}{\rho_D C_D} \frac{\omega^0_F L^2 \Delta \tau}{k^0_F (T_R - T_0)} \qquad (A.1.10)$$

$$q^F_{m,n} = \omega^*_{F_{m,n}} \frac{\omega^0_F L^2 \Delta \tau}{k^0_F (T_R - T_0)} \qquad (A.1.11)$$

A.2 ENERGY BALANCE AT THE INTERFACE

An energy balance is made on a slab one space increment thick, centered at the interface:

$$|\text{conduction}_{IN}| - |\text{convection}_{OUT}| = |\text{accumulation}| - |\text{production}| + |\text{consumption}| \tag{A.2.1}$$

where:

$$|\text{conduction}_{IN}| = -k_F \frac{\partial T_F}{\partial x} + k_D \frac{\partial T_D}{\partial x} \tag{A.2.2}$$

$$|\text{convection}_{OUT}| = W_i\, C_{pw} \frac{\partial T_D}{\partial x} \frac{\Delta x}{2} \tag{A.2.3}$$

$$|\text{consumption}| = W_i\, \Delta H_s \tag{A.2.4}$$

$$|\text{production}| = \omega_D \frac{\Delta x}{2} + \omega_F \frac{\Delta x}{2} \tag{A.2.5}$$

$$|\text{accumulation}| = \rho_D C_D \frac{\partial T_D}{\partial t} \frac{\Delta x}{2} + \rho_F C_F \frac{\partial T_F}{\partial t} \frac{\Delta x}{2} \tag{A.2.6}$$

Substitution of the transformation and normalization equations (see Chapter IV, Sec. 4) into Equations (A.2.1), (A.2.2), (A.2.3), (A.2.4), (A.2.5), and (A.2.6) gives

$$COND = -\alpha_F^* \frac{1}{S} \frac{\partial \theta_F}{\partial y} - \frac{\rho_D C_D}{\rho_F C_F} \frac{\alpha_D^*}{1-S} \frac{\partial \theta_D}{\partial z} \tag{A.2.7}$$

$$CONV = -\frac{W_i\, C_{pw}\, L}{k_F^o} \frac{\Delta z}{2} \frac{\partial \theta_D}{\partial z} \tag{A.2.8}$$

$$CONS = \frac{W_i\, L\, \Delta H_s}{k_F^o (T_R - T_0)} \tag{A.2.9}$$

$$PROD = \frac{\omega_F^o L^2}{k_F^o (T_R - T_0)} \left[\omega_D^* (1-S) \frac{\Delta z}{2} + \omega_F^* S \frac{\Delta y}{2} \right] \tag{A.2.10}$$

$$ACCUM = \frac{\rho_D C_D}{\rho_F C_F} (1-S) \frac{\Delta z}{2} \frac{\partial \theta_D}{\partial \tau} + S \frac{\Delta y}{2} \frac{\partial \theta_F}{\partial \tau} - \frac{W_i L}{\rho \sigma \alpha_F^o} \left(\frac{\rho_D C_D}{\rho_F C_F} z \frac{\Delta z}{2} \frac{\partial \theta_D}{\partial z} - y \frac{\Delta y}{2} \frac{\partial \theta_F}{\partial y} \right) \tag{A.2.11}$$

with

$$W_i = \frac{D(C_{TP} - C_R)}{L(1-S)} \left(\frac{\partial \Gamma}{\partial z} \right)_i \tag{A.2.12}$$

The energy balance becomes

$$COND - CONV = ACCUM - PROD + CONS \qquad (A.2.13)$$

where the terms COND, CONV, ACCUM, PROD, CONS correspond respectively to the terms of conduction$_{IN}$, convection$_{OUT}$, accumulation, production (microwave), consumption (sublimation) in the energy balance athe interface.

The corresponding finite-difference equations are:

$$COND_m = -\alpha^*_{F_{M+1/2,m}} \frac{1}{S_m}\left(\frac{\partial\theta_F}{\partial y}\right)_{M+1/2,m} - \frac{\rho_D C_D}{\rho_F C_F}\alpha^*_{D_{K+1/2,m}} \frac{1}{1-S_m}\left(\frac{\partial\theta_D}{\partial z}\right)_{K+1/2,m} \qquad (A.2.14)$$

$$CONV_m = -W_{i,m}\frac{C_{pw}L}{k^o_F}\frac{\Delta z}{2}\left(\frac{\partial\theta_D}{\partial z}\right)_{K+1/2,m} \qquad (A.2.15)$$

$$CONS_m = \frac{\Delta H_s L}{k^o_F(T_R-T_o)} W_{i,m} \qquad (A.2.16)$$

$$PROD_m = \frac{1}{2}\frac{\omega^o_F L^2}{k^o_F(T_R-T_o)}\left[\omega^*_{D_{K+1/2,m}}(1-S_m)\Delta z + \omega^*_{F_{M+1/2,m}} S_m \Delta y\right] \qquad (A.2.17)$$

$$\begin{aligned} ACCUM_{m+1/2} = {} & .75\left[\frac{\rho_D C_D}{\rho_F C_F}(1-S_{m+1/2})\frac{\Delta z}{2} + S_{m+1/2}\frac{\Delta y}{2}\right]\left(\frac{\partial\theta_i}{\partial\tau}\right)_{m+1/2} \\ & + .25\left[\frac{\rho_D C_D}{\rho_F C_F}(1-S_{m+1/2})\frac{\Delta z}{2}\left(\frac{\partial\theta_D}{\partial z}\right)_{K,m+1/2} + S_{m+1/2}\frac{\Delta y}{2}\left(\frac{\partial\theta_F}{\partial y}\right)_{M,m+1/2}\right] \\ & - \frac{W_{i,m+1/2}L}{\rho\sigma\alpha^o_F}\left[\frac{\rho_D C_D}{\rho_F C_F} z\frac{\Delta z}{2}\left(\frac{\partial\theta_D}{\partial z}\right)_{M+1/2,m+1/2} - y\frac{\Delta y}{2}\left(\frac{\partial\theta_F}{\partial y}\right)_{M+1/2,m+1/2}\right] \end{aligned} \qquad (A.2.18)$$

with

$$W_{i,m} = \frac{D_{K+1/2,m}(C_{Tp}-C_{pa})}{L(1-S_m)}\left(\frac{\partial\Gamma}{\partial z}\right)_{K+1/2,m} \qquad (A.2.19)$$

Typically,

$$\left(\frac{\partial\theta_F}{\partial y}\right)_{M+1/2,m} = \frac{\theta^F_{M+1,m}-\theta^F_{M,m}}{\Delta y} \qquad (A.2.20)$$

$$\left(\frac{\partial\theta_F}{\partial\tau}\right)_{M,m+1/2} = \frac{\theta^F_{M,m+1}-\theta^F_{M,m}}{\Delta\tau} \qquad (A.2.21)$$

Calculation of the interface temperature

The temperature at the interface at τ_{n+1} which would have satisfied the energy balance (as opposed to that guessed) is given by[a]

$$\theta_{i,n+1} = \theta_{i,n} + \Delta\tau \frac{COND_{n+1/2} - CONV_{n+1/2} + PROD_{n+1/2} - CONS_{n+1/2} - ACC2_{n+1/2}}{AINT_{n+1/2}} \qquad (A.2.22)$$

Calculation of the interface position:

From Eq. (5.14):

$$S_{n+1} = S_n - \Delta\tau \frac{k_F^o (T_R - T_o)}{\rho \sigma \alpha_F^o \Delta H_s} \left(COND_{n+1/2} - CONV_{n+1/2} + PROD_{n+1/2} - ACCUM_{n+1/2} \right) \qquad (A.2.23)$$

a - ACC2 in Eq. (A.2.22) corresponds to the sum of the two latter terms in the right hand side in Eq. (A.2.18). AINT in Eq. (A.2.22) represents the coefficient of $(\Delta\Theta_i)_{n+\frac{1}{2}}$ in Eq. (A.2.18).

A.3 BOUNDARY CONDITION AT THE OUTER SURFACE

An energy balance at the outer surface of the slab (dried layer side) is used to derive the boundary condition for the temperature as of Eq. (5.10). The energy balance is made on a slab half a space increment thick:

$$h(T_R - T_S) - k_D \frac{\partial T_D}{\partial x} - C_{pw} W_i \frac{\Delta T_S}{2} = \rho_D C_D \frac{\partial T_D}{\partial t} \frac{\Delta x}{2} - \omega_D \frac{\Delta x}{2} \qquad (A.3.1)$$

Substitution of the transformation and normalization equations in Eq. (A.3.1) and use of the finite difference approximation at $\tau_{n+\frac{1}{2}}$ will lead to the desired form for the boundary condition.

Equation (A.3.1) becomes

$$\frac{hL}{k_F^o}(1-\theta_S^D) + \frac{\rho_D C_D}{\rho_F C_F}\alpha_D^* \frac{1}{1-S}\left(\frac{\partial \theta_D}{\partial z}\right)_S - \frac{\rho C_{pw}\sigma}{\rho_F C_F}\frac{dS}{d\tau}\frac{\Delta\theta_S}{2} = \frac{\rho_D C_D}{\rho_F C_F}(1-S)\frac{\Delta z}{2}\frac{\partial \theta_D}{\partial \tau}$$

$$+ \frac{\rho_D C_D}{\rho_F C_F}\frac{\Delta z}{2}\gamma \frac{dS}{d\tau}\left(\frac{\partial \theta_D}{\partial z}\right)_S + \omega_D^* \frac{\omega_F^o L^2(1-S)}{k_F^o(T_R - T_o)}\frac{\Delta z}{2} \qquad (A.3.2)$$

Let:

$$C = \frac{hL}{k_F^o} \qquad (A.3.3)$$

$$CD_m = \frac{\rho_D C_D}{\rho_F C_F}\frac{\alpha^*_{D\,3/2,m}}{(1-S_m)\Delta z} \qquad (A.3.4)$$

$$CV_{n+1/2} = \frac{1}{2}\frac{\rho C_{pw}\sigma}{\rho_F C_F}\frac{S_{n+1}-S_n}{\Delta\tau} + \frac{1}{2}\frac{\rho_D C_D}{\rho_F C_F} z_{5/4}\frac{S_{n+1}-S_n}{\Delta\tau} \qquad (A.3.5)$$

$$PR_m = \omega^*_{D\,5/4,m}\frac{\omega_F^o L^2(1-S_n)}{k_F^o(T_R - T_o)}\frac{\Delta z}{2} \qquad (A.3.6)$$

$$AC_{m+1/2} = \frac{\rho_D C_D}{\rho_F C_F}\left(1 - \frac{S_{n+1}+S_n}{2}\right)\frac{\Delta z}{2}\frac{1}{\Delta\tau} \qquad (A.3.7)$$

Then, the finite difference equation corresponding to Eq. (A.3.2) is

$$C(1-\theta^D_{1,n+1}) + CD_{n+1}(\theta^D_{2,n+1} - \theta^D_{1,n+1}) - CV_{n+1/2}(\theta^D_{2,n+1} - \theta^D_{1,n+1}) + PR_{n+1}$$

$$+ C(1-\theta^D_{1,n}) + CD_n(\theta^D_{2,n} - \theta^D_{1,n}) - CV_{n+1/2}(\theta^D_{2,n} - \theta^D_{1,n}) + PR_n =$$

$$2\,AC_{n+1/2}\left[.75(\theta^D_{1,n+1} - \theta^D_{1,n}) + .25(\theta^D_{2,n+1} - \theta^D_{2,n})\right] \qquad (A.3.8)$$

Equation (A.3.8) corresponds to an energy balance, in the fixed boundary domain, over the slab $(z_{1+\frac{1}{2}}, z_1)$ between times τ_n and τ_{n+1}. It is rearranged to give the final form of the boundary condition as required by the numerical scheme of solution (Eq. (5.10)). One has

$$\theta^D_{1,n+1} + \delta_{1,n+1}\theta^D_{2,n+1} = \lambda_{1,n+1} \qquad (A.3.9)$$

where

$$\delta_{1,n+1} = \left(CD_{n+1} - CV_{n+1/2} - .5\,AC_{n+1/2}\right) / \left(-C - CD_{n+1} + CV_{n+1/2} - 1.5\,AC_{n+1/2}\right) \qquad (A.3.10)$$

$$\begin{aligned}\lambda_{1,n+1} = -\Big[& \theta^D_{1,n}\left(-C - CD_n + CV_{n+1/2} + 1.5\,AC_{n+1/2}\right) \\ & + \theta^D_{2,n}\left(CD_n - CV_{n+1/2} + .5\,AC_{n+1/2}\right) \\ & + \left(PR_{n+1} + PR_n + 2C\right)\Big] / \left(-C - CD_{n+1} + CV_{n+1/2} - 1.5\,AC_{n+1/2}\right)\end{aligned} \qquad (A.3.11)$$

B.1 SOLUTION OF THE SYSTEM OF FINITE-DIFFERENCE EQUATIONS

The finite-difference equations of Appendix A are written under the general form

$$U_i + \alpha_i U_{i+1} + \beta_i U_{i+2} = \gamma_i \qquad i = 1,\ldots, I-1 \qquad (B.1)$$

while the boundary conditions are written as:
at the outer edge (center line or outer surface)

$$U_1 + \delta_1 U_2 = \lambda_1 \qquad (B.2)$$

and at the interface (ice-front)

$$p\, U_I + U_{I+1} = q \qquad (B.3)$$

They form a set of I+1 linear equations which are to be solved with I+1 unknowns, the U_i's at τ_{n+1}, i=1,...,I+1. One has

$$\begin{array}{ll}
U_1+\delta_1 U_2 & = \lambda_1 \\
U_1+\alpha_1 U_2+\beta_1 U_3 & = \gamma_1 \\
\ldots\ldots\ldots\ldots\ldots\ldots & \\
U_{i-1}+\alpha_{i-1} U_i+\beta_{i-1} U_{i+1} & = \gamma_{i-1} \\
U_i+\alpha_i U_{i+1}+\beta_i U_{i+2} & = \gamma_i \\
\ldots\ldots\ldots\ldots\ldots\ldots & \\
U_{I-1}+\alpha_{I-1} U_I+\beta_{I-1} U_{I+1} & = \gamma_{I-1} \\
p\, U_I + U_{I+1} & = q
\end{array}$$

A forward elimination of the lowest subscript unknown U_i, starting i=1 yields the δ_i's and the λ_i's defined by

$$U_i + \delta_i U_{i+1} = \lambda_i \qquad i=1,\ldots,I \qquad (B.5)$$

It comes

$$\delta_i = \frac{\beta_{i-1}}{\alpha_{i-1} - \delta_{i-1}} \tag{B.6}$$

$$\lambda_i = \frac{\gamma_{i-1} - \lambda_{i-1}}{\alpha_{i-1} - \delta_{i-1}} \tag{B.7}$$

for $i=2,\ldots,I$. δ_1 and λ_1 are given by the boundary condition, Eq.(B.2). A backward substitution of the numerical values of the δ's and λ's in Eq. (B.5), starting $i=I$, yields the unknowns U_i's:

$$U_{I+1} = \frac{q - p_I}{1 - p\,\delta_I} \tag{B.8}$$

$$U_i = \lambda_i - \delta_i\, U_{i+1} \qquad i = I,\ldots, 1 \tag{B.9}$$

The corresponding FORTRAN IV computer program is given in Appendix F (subroutine EMMA).

B.2 FORCING AND ACCELERATING THE CONVERGENCE OF AN ITERATION SCHEME

Theoretically, iterative procedures encountered in the solution of mathematical problems correspond to the solution of the equation

$$x = \psi(x) \tag{B.10}$$

by an organized method of trial and error. The variable x in Equation (B.10) may not be a scalar variable, while the functional ψ is not necessarily known explicitly. ψ may for instance result of the solution of a more complex problem for a given value of the "parameter" x.

In order to solve the above equation a value x^* of the variable x is "tried". The corresponding value $\psi(x^*)$ of the functional is then obtained and compared to that of x according to a predetermined convergence criterion.

The usual iteration scheme is such that , if the convergence criterion is not satisfied, the current value of the functional ψ is fed back as the next trial for the value of x. This procedure is repeated (iterated) until the convergence criterion is satisfied, i.e. until the difference $|x - \psi(x)|$ is less than a given number. Mathematically, the iteration scheme is given by

$$x^*_{j+1} = \psi(x^*_j) \tag{B.11}$$

where x^*_j represents the jth trial. Geometrically, this iteration scheme correspond to the search of the intersection of the curve $y = \psi(x)$ with the first bisector $y = x$ in a coordinate frame of abscissa x and ordinate y (see Fig. B.2.1). Unfortunately, this scheme is not always convergent. Indeed, in many instances it may converge very slowly, resulting in long and therefore costly machine calculations. In effect, theoretically this scheme converges only if the slope of the curve $y = \psi(x)$, at the solution point, is less than 1 in absolute value:

$$-1 \angle \frac{d\psi}{dx} \angle 1 \tag{B.12}$$

An alternate scheme is proposed here to force and accelerate the convergence of an iteration. This scheme is such that the next trial is computed from the previous trial and the previous value of the

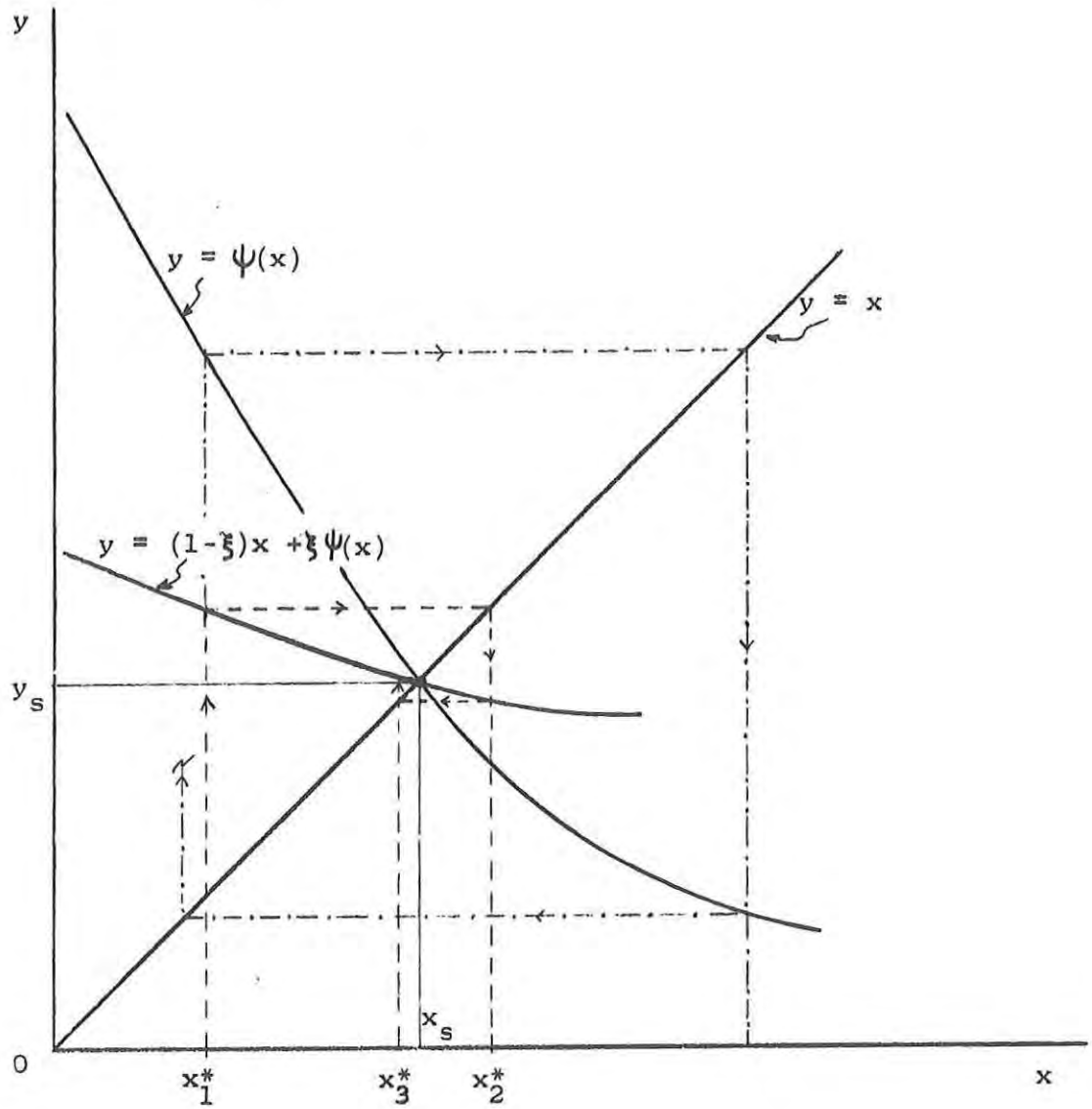

Figure B.2.1- Geometrical representation of the iteration schemes.

functional ψ according to

$$x^*_{j+1} = (1-\xi)\ x^*_j + \xi\,\psi(x^*_j) \tag{B.13}$$

where the parameter ξ, which will be referred to as acceleration coefficient may be adjusted to force and accelerate the convergence of the iteration scheme. Geometrically (see Fig. B.2.1), this scheme correspond to the search of the intersection of the curve

$$y = (1-\xi)x + \xi\,\psi(x) \tag{B.14}$$

with the first bisector $y = x$. The change is possible since the two functionals $\psi(x)$ and $(1-\xi)x + \xi\ \psi(x)$ have the same value at the searched solution (convergence) point where $x = \psi(x)$.

In theory, practically instant convergence is reached with this new scheme if the slope of the curve of equation (B.14) is equal to zero at the solution point (see Fig. B.2.1). The main advantage of the method is that the slope of the latter curve (B.14) can be adjusted and forced to a near zero value by varying the parameter ξ, thus yielding extremely fast convergence.

The optimal value of ξ is given by

$$0 = \frac{d}{dx}\ (1-\xi)x + \xi\,\psi(x) = 1-\xi + \xi\,\frac{d\psi}{dx} \tag{B.15}$$

Thus

$$\xi_{opt.} = 1/(1-\frac{d\psi}{dx}) \tag{B.16}$$

Use of this method in the calculation of the ice-front temperature by iteration in the simulation permitted to reache convergence in 2 to 4 iterations on the average. The acceleration coefficient ξ was constantly updated during a given iteration. It should be noted that the iteration by the first scheme (direct feed back of the computed value) was highly divergent.

- APPENDIX C -

SAMPLE CALCULATIONS (RUN No. 15)

C.1 Calculation of h

For drying on both sides (symmetric slab), Eq. (9.5) gives

$$h = \Delta H_s \frac{1 + \beta}{T_R - T_{i,1}} \frac{\dot{m}_1}{2A_1} \qquad (C.1)$$

with

$$\beta = \frac{h\,\delta_1}{k_D} \qquad (C.2)$$

From Fig. 9.3 at $t = t_1$

$$\dot{m}_1 = 6.2 \text{ g/hr} = 1.7 \times 10^{-3} \text{ g/sec}$$

Approximate A_1 by A_o. Thus from Appendix E

$$A_o = 61.5 \text{ cm}^2$$

Assume a room (vacuum chamber) temperature of 20°C. Approximate $T_{i,1}$ by the frost temperature of the vacuum chamber at P_R^W = .3mmHg (cf. Table 9.1). Then, from the ice-water vapor equilibrium curve

$$T_{i,1} = -29.5°\text{C}$$

From m_1, m_o, m_f, and L_1 (cf. Appendix E) determine δ_1

$$\delta_1 = \left(1 - \frac{m_1 - m_f}{m_o - m_f}\right) L_1 = (1 - .936)(.78) = .05 \text{ cm}$$

where L_1 is approximated by L_o.

From Fig. 6.4, at P_R = .3mmHg one has

$$k_D = 10^{-4} \text{ cal/sec/cm/°C}$$

From Table 6.1

$$\Delta H_s = 675 \text{ cal/g}$$

Substitution of the numerical values in Eq. (C.1) gives

$$h = 2.1 \times 10^{-4} \text{ cal/sec/cm}^2/°\text{C}$$

C.2 Calculation of E

From Eqs. (9.1) and (9.2) one has

$$E^2 = \frac{\Delta H_s \dot{m}}{K_F(T_F)\ V_F + K_D(T_D)\ V_D} \tag{C.3}$$

From Table 6.1

$$\Delta H_s = 675 \text{ cal/g}$$

Assume an average $T_F = -5°C$. Then from Fig. 6.5

$$K_F = 4. \times 10^{-6} \text{ cal/sec/cm}^3/(\text{V/cm})^2$$

Assume an average $T_D = 10°C$. Then from Fig. 6.6

$$K_D = .9 \times 10^{-6} \text{ cal/sec/cm}^3/(\text{V/cm})^2$$

The volumes V_F and V_D are determined by (symmetric slab)

$$V_F = S\ V_F^o = 2\ S\ L_o\ A_o \tag{C.4}$$

$$V_D = (1-S)\ V_D^f = 2(1-S)\ L_f\ A_f \tag{C.5}$$

L, A are given in Appendix E. The overall drying rate $\dot{m}$ (drying) on both sides) is obtained from Fig. 9.3. The electric field is then calculated for two locations of the ice-front (interface).

At S = .5 :

$$m = 20.6 \text{ g/hr} = 5.7 \times 10^{-3} \text{ g/sec}$$

$$L_o = .78 \text{ cm}; \quad L_f = .7 \text{ cm}$$

$$A_o = 61.5 \text{ cm}^2; \quad A_f = 51.0 \text{ cm}^2$$

Thus

$$V_F^o = 2 \times .78 \times 61.5 = 95.7 \text{ cm}^3$$

$$V_D^f = 2 \times .70 \times 51.0 = 71.3 \text{ cm}^3$$

$$E^2 = \frac{675 \times 5.7 \times 10^{-3}}{4 \times 10^{-6} \times .5 \times 95.7 + .9 \times 10^{-6} \times .5 \times 71.3}$$

$$= 1.8 \times 10^4 \ (V/cm)^2$$

$$E = 134 \ V/cm$$

Similarly at S = .3 :

$$m = 11.8 \ g/hr = 3.28 \times 10^{-3} \ g/sec$$

and

$$E^2 = \frac{675 \times 3.28 \times 10^{-3}}{4 \times 10^{-6} \times .3 \times 96.7 + .9 \times 10^{-6} \times .7 \times 71.3}$$

$$= 1.38 \times 10^4 \ (V/cm)^2$$

$$E = 117 \ V/cm$$

Average field peak strength,

$$E = \tfrac{1}{2}(134 + 117) = 125 \ V/cm$$

- APPENDIX D -

COMPUTER OUTPUT

The computer output pertaining to this investigation are in the possession of Professor Yi Hua Ma of the Department of Chemical Engineering, Worcester Polytechnic Institute, Worcester, Mass. 01609. They are kept in Room 225.

- APPENDIX E -

EXPERIMENTAL RESULTS

The experimental results are known with the following accuracies (on an absolute basis):

$\Delta m = .2g$

$\Delta L = .2cm$

$\Delta A = .5cm^2$

$\Delta P_R = .03-.09mmHg$

$\Delta P_R^W = .01mmHg$

The power measurements, which could not provide quantitative information due to calibration problems, and the start-up portion of the drying curves are not reproduced here. They are in the possession of Professor Y.H. Ma of the Department of Chemical Engineering, Worcester Polytechnic Institute, Worcester MA 01609. Room 225.

RUN No 25

m_o = 73.0 g m_f = 26.2 g

L_o = .80 cm L_f = .70 cm

A_o = 49.0 cm^2 A_f = 45.3 cm^2

$t-t_1$ hr	P_R^w mmHg	P_R mmHg	m g
0	.24	1.0	70.3
.5	.45	1.0	63.7
1.0	.45	1.0	55.6
1.5	.41	1.0	47.3
2.0	.31	1.0	40.9
2.5	.24	1.0	36.3
3.0	.20	.9	33.2
3.5	.16	.9	30.9
4.0	.13	.9	29.0
4.5	.11	.9	27.7
5.0	.09	.9	26.8
5.5	.07	.9	26.2

RUN No 27

m_o = 78.0 g m_f = 25.4 g

L_o = .80 cm L_f = .75 cm

A_o = 48.7 cm^2 A_f = 45.0 cm^2

$t-t_1$ hr	P_R^w mmHg	P_R mmHg	m g
0	.21	.21	75.3
.5	.23	.23	68.7
1.0	.21	.21	60.5
1.5	.20	.20	51.6
2.0	.18	.18	43.9
2.5	.16	.16	38.3
3.0	.15	.15	34.9
3.5	.14	.14	32.3
4.0	.13	.17	30.2
4.5	.12	.16	28.7
5.0	.11	.12	27.3
5.5	.11	.12	26.4
6.0	--	--	25.7
6.5	--	--	25.4

RUN No 29

m_o = 74.2 g m_f = 26.3 g

L_o = .75 cm L_f = .70 cm

A_o = 49.6 cm^2 A_f = 39.1 cm^2

$t-t_1$ hr	P_R^w mmHg	P_R mmHg	m g
0	--	3.4	73.3
.5	.55	3.5	65.0
1.0	.52	3.7	52.4
1.5	.42	3.7	41.1
2.0	.39	3.7	31.3
2.5	--	--	27.6
3.0	--	--	26.6
3.5	--	--	26.3

RUN No 12

m_o = 74.5 g m_f = 22.1 g

L_o = .71 cm L_f = --

A_o = 58.6 cm^2 A_f = --

$t-t_1$ hr	P_R^w mmHg	P_R mmHg	m g
0	.23	.32	72.1
.5	.29	.29	66.7
1.0	.26	.26	60.4
1.5	.23	.23	54.9
2.0	.21	.22	50.3
2.5	.20	.22	46.5
3.0	.19	.20	43.0
3.5	.18	.20	39.8
4.0	.17	.20	36.9
4.5	.16	.19	34.1
5.0	.16	.18	31.7
5.5	.15	.18	29.3
6.0	.15	.17	27.2
6.5	.14	.17	25.3
7.0	.12	.17	23.9
7.5	.12	.17	22.9
8.0	.10	.17	22.3
8.5	--	--	22.1

RUN No 13

m_o = 88.0 g m_f = 26.2 g

L_o = .74 cm L_f = --

A_o = -- A_f = --

$t-t_1$ hr	P_R^w mmHg	P_R mmHg	m g
0	.27	.29	84.9
.5	.26	.26	77.2
1.0	.25	.21	69.3
1.5	.22	.21	61.1
2.0	.21	.20	54.3
2.5	.18	.20	49.4
3.0	.17	.18	45.2
3.5	.16	.17	41.7
4.0	.15	.17	38.4
4.5	.15	.17	35.3
5.0	.14	.16	32.7
5.5	.14	.16	30.3
6.0	--	--	28.5
6.5	--	--	27.1

RUN No 14

m_o = 85.6 g m_f = 26.0 g

L_o = .71 cm L_f = --

A_o = 60.5 cm^2 A_f = --

$t-t_1$ hr	P_R^W mmHg	P_R mmHg	m g
0	.23	.24	79.9
.5	.26	.26	65.5
1.0	.23	.23	48.5
1.5	.19	.19	39.3
2.0	.17	.17	34.2
2.5	.16	.16	30.9
3.0	.15	.15	28.3
3.5	.14	.14	26.6

RUN No 15

m_o = 87.5 g m_f = 25.3 g

L_o = .78 cm L_f = .70 cm

A_o = 61.5 cm^2 A_f = 51.0 cm^2

$t-t_1$	P_R^w	P_R	m
hr	mmHg	mmHg	g
0	.30	.30	83.2
.5	.30	.30	73.1
1.0	.28	.28	61.8
1.5	.24	.24	51.3
2.0	.21	.21	44.1
2.5	.19	.19	39.1
3.0	.18	.18	35.2
3.5	.16	.16	32.1
4.0	.15	.15	29.5
4.5	.14	.14	27.5
5.0	.13	.13	26.1
5.5	.12	.12	25.4

RUN No 16

m_o = 87.5 g m_f = 27.0 g

L_o = .76 cm L_f = --

A_o = 61.0 cm^2 A_f = --

$t-t_1$	P_R^w	P_R	m
hr	mmHg	mmHg	g
0	.30	.31	83.7
.5	.32	.32	72.4
1.0	.30	.30	58.5
1.5	.25	.25	46.8
2.0	.21	.21	40.5
2.5	.20	.20	35.9
3.0	.19	.19	32.5
3.5	.16	.16	30.0
4.0	.15	.15	28.0
4.5	.14	.14	27.1

RUN No 17

$m_o = 94.0$ g $\quad m_f = 28.3$ g

$L_o = .71$ cm $\quad L_f = .62$ cm

$A_o = 60.8$ cm^2 $\quad A_f = 56.5$ cm^2

$t-t_1$ hr	P_R^w mmHg	P_R mmHg	m g
0	.27	.26	86.3
.5	.22	.22	77.5
1.0	.20	.20	68.4
1.5	.19	.19	59.6
2.0	.18	.18	51.8
2.5	.17	.17	45.4
3.0	.16	.16	44.4
3.5	.16	.16	36.5
4.0	.15	.15	33.2
4.5	.14	.14	30.6
5.0	.13	.13	28.7

- APPENDIX F -

```
C
C
C
```

```
C
C
C
C
C
C
C
C                SUBROUTINE  MWFD
C
C
C       THIS SUBROUTINE SIMULATES THE FREEZE-DEHYDRATION
C       PROCESS USING MICROWAVE DIELECTRIC HEATING.  IT
C       IS DIRECTLY APPLICABLE TO THE FREEZE-DRYING OF
C       BEEF MEAT (A DIFFERENT TYPE OF MATERIAL TO BE DRIED
C       WILL NECESSITATE A  CHANGE OF THE PHYSICAL DATA
C       OF BEEF MEAT, ASSUMED HERE):
C           ENTER OPERATING CONDITIONS THROUGH ARGUMENTS OF SUB-
C       ROUTINE ACCORDING TO NOMENCLATURE AND UNITS BELOW.
C         FIELD: ELECTRIC FIELD PEAK STRENGTH IN VACUUM INSIDE
C                THE CAVITY, V/CM.
C         PR: TOTAL PRESSURE IN VACUUM CHAMBER, MM-HG.
C         PWR: PARTIAL PRESSURE OF WATER VAPOR IN VACUUM CHAMBER
C              MM-HG.
C         TR: AMBIANT TEMPERATURE IN CAVITY, DEG K.
C         TØ: INITIAL TEMPERATURE OF FROZEN PRODUCT, DEG K.
C         THICK: PRODUCT SLAB THICKNESS, CM.
C         WATER: INITIAL PRODUCT MOISTURE CONTENT-WET BASIS (NOT
C                IN %),-.
C         FAT: FAT CONTENT-WET BASIS, -.
C         MELT: RETURNS TO MAIN PROGRAM 1 IF MELTING OCCURS, OTHER-
C                WISE EQUAL TO ZERO.
C
C       GENERAL NOMENCLATURE:
C         DK(P): THERMAL CONDUCTIVITY-DRIED PRODUCT, CAL/CM/SEC/
C             DEG K; ARGUMENT: LOCAL PRESSURE, MM-HG.
C         FK(T): THERMAL CONDUCTIVITY-FROZEN PRODUCT, CAL/CM/SEC
C                /DEG K; ARGUMENT: LOCAL TEMPERATURE:DEG K.
C         D(P): EFFECTIVE DIFFUSIVITY, CM2/SEC.
C         DL(T): DISSIPATION COEFF.-DRIED PRODUCT, CAL/CM3/SEC/
C                (V/CM); ARGUMENT: LOCAL TEMPERATURE IN DEG K.
C         FL(T): DISSIPATION COEFF.-FROZEN PRODUCT, CAL/CM3/SEC/
C                (V/CM); ARGUMENT : TEMPERATURE, DEG K.
C         FE(T): ICE-VAPOR EQUILIBRIUM RELATIONSHIP; ENTER EQU.
C         TEMPERATURE IN DEG K, RETURNS EQU. CONCENTRATION OF
C         WATER VAPOR IN GR/CM3.
C         WCAP: SPECIFIC HEAT OF WATER VAPOR, CAL/GR/DEG K.
C         DCAP: SPECIFIC HEAT OF DRIED PRODUCT, CAL/GR/DEG K.
C         FCAP: SPECIFIC HEAT OF FROZEN PRODUCT, CAL/GR/DEG K.
C         DENS: DENSITY OF ICE, GR/CM3.
C         FDENS: BULK DENSITY OF FROZEN PRODUCT, GR/CM3.
C         DDENS: BULK DENSITY OF DRIED PRODUCT, GR/CM3.
C         HTC : HEAT TRANSFER COEFFICIENT AT EXT. SURFACE.
C               CAL/CM2/SEC/DEG K.
C         HS: HEAT OF SUBLIMATION OF ICE, CAL/GR.
C         CTP: WATER VAPOR CONCENTRATION AT TRIPLE POINT, GR/CM3
C         CR: AMBIANT WATER VAPOR CONCENTRATION, GR/CM3.
C         PGC: PERFECT GASES CONSTANT, MM-HG/DEG K/(GR/CM3).
C         MM: NUMBER OF SPACE INCREMENT-FROZEN CORE; MUST BE
C             LESS (OR EQUAL) THAN 200.

C         KK: NUMBER OF SPACE INCREMENTS-DRIED LAYER; MUST BE
```

```
C           LESS (OR EQUAL) THAN 200.
C         EUF: MICROWAVE ENERGY USAGE FACTOR; RATIO OF
C              TOTAL ENERGY NEED FOR SUBLIMATION /
C              TOTAL MICROWAVE ENERGY CONSUMED.
C
C
      SUBROUTINE MWFD(FIELD,PR,PWR,TR,T0,THICK,WATER,FAT,MELT)
      COMMON N,TIME,AL(199),BE(199),GA(199)
      DIMENSION CN1(21),TND1(21),TNF1(21)
      DIMENSION CN2(21),TND2(21),TNF2(21)
      DIMENSION FC(201),DC(201),DI1(201),DI2(201),FP1(201),FP2
     1(201),DP1(201),DP2(201),QF1(201),QF2(201),QD1(201),QD2(
     2201)
      INTEGER EPSI
      REAL LA1
C
C     FUNCTIONS BLOCK:
      DK(P)=1.E-4*(1.126+ALOG(P)*(0.1351+ALOG(P)*(0.01565+ALOG
     1(P)*(-3.187E-3+ALOG(P)*(-5.483E-4)))))
      FK(T)=AK+BK*SQRT(271.65-T)
      D(P)=28.1/(1.34+P)
      FL(T)=1.E-6*(294.7+T*(-3.628+T*(1.464E-2-1.922E-5*T)))
      DL(T)=1.E-6*(14.39+T*(-0.1577+T*(5.577E-4-5.924E-7*T)))
      FE(T)=EXP(-63.23+0.2969*T-4.038E-4*T*T)
C
C     ENTER CONSTANTS:
      CALL OFILE(20,'PRINT1')
      CALL OFILE(21,'HIST')
      CALL OFILE(22,'PROF')
      CALL OFILE(23,'PRINT2')
      CALL OFILE(19,'CHECK')
      DATA WCAP,FCAP,DCAP,DENS,FDENS,DDENS/.5,.43,.36,.92,.96,
     1.32/
      DATA HTC,HS,CTP,PGC/1.9E-4,675.,4.84E-6,3.46E3/
      DATA KK,MM/20,20/
      AK=1.E-3*(2.95-25.*FAT)
      BK=1.E-3*(0.02+1.8*(WATER-0.65))
      POR=WATER*FDENS/DENS
      CR=PWR/PGC/TR
      FC0=FK(T0)
      FD0=FC0/FDENS/FCAP
      FP0=FL(T0)*FIELD**2.
      DELZ=1./FLOAT(KK)
      DELY=1./FLOAT(MM)
      DELT=0.072
      DETAU=DELT*FD0/THICK**2.
      C=HTC*THICK/FC0
      M1=MM+1
      K1=KK+1
      A1=FDENS*FCAP*(TR-T0)/DENS/POR/HS
      A2=DDENS*DCAP/FDENS/FCAP
      A3=FP0*THICK**2./FC0/(TR-T0)
      A4=DENS*WCAP*POR/DDENS/DCAP/DELZ
      A5=0.5*WCAP*THICK*DELZ/FC0
      A6=HS*THICK/FC0/(TR-T0)
      A7=THICK/DENS/POR/FD0
      A8=FD0*(CTP-CR)/THICK
      A9=DENS*WCAP*POR/FDENS/FCAP+.9875*A2
C
C     PREPRINT ASSUMED EXP. CONDITIONS:
      WRITE(20,200) FIELD,PR,PWR,TR,T0,THICK,WATER,FAT
```

```
      WRITE(23,200) FIELD,PR,PWR,TR,T0,THICK,WATER,FAT
C
C     ENTER ALL INITIAL VALUES:
      TIME=0.
      N=0
      S0=1.
      S1=.999*S0
C     TEMPERATURE PROFILES:
      TNS=1./(1.+DK(PR)/HTC/THICK/(1.-S1))
      DO 1 M=1,M1
1     TNF1(M)=0.
      DO 2 K=1,K1
      TND1(K)=TNS*(1.-FLOAT(K-1)/FLOAT(KK))
2     TND2(K)=TND1(K)
      GRTD1=(TND1(KK+1)-TND1(KK))/DELZ
      GRTF1=(TNF1(MM+1)-TNF1(MM))/DELY
C     DRYING RATE FROM ENERGY BALANCE AT INTERFACE:
      COEF1=A6-A5*GRTD1-.25*A7*(A2*(2.-DELZ)*DELZ*GRTD1-(2.-DE
     1LY)*DELY*GRTF1)
      COND1=-DK(PR)/FC0/(1.-S1)*GRTD1
      DR1=COND1/COEF1
C     CONCENTRATION PROFILE:
      GRC1=DR1*(1.-S1)*THICK/(CTP-CR)/D(PR)
      DO 3 K=1,K1
      CN1(K)=GRC1*FLOAT(K-1)/FLOAT(KK)
3     CN2(K)=CN1(K)
C     HEAT CONSUMPTION AT INTERFACE:
      QI1=COND1-(COEF1-A6)*DR1
      DELQI=0.
C     MISCELLANUOUS:
      TI1=0.
      DELTI=0.
      X=0.75
      SF1=S1*S1
      SD1=(1.-S1)*(1.-S1)
      FIELD1=0.
      MELT=0
      TMWE=0.
C
C
C
C     SIMULATION LOOP-HEAD:
4     CONTINUE
      TIME=TIME+DELT/3600.
      N=N+1
C
C
C     UPDATE ALL PROPERTIES:
      NTC=1.E2*(T0+TNF1(1)*(TR-T0))
      IF(NTC.LE.27165)GO TO 40
      MELT=1
      WRITE(5,101)TIME,N
      RETURN
40    CONTINUE
      FIELD2=FIELD
      IF(N.LT.710)FIELD2=0.
      AF1=A3*DETAU/FP0*FIELD1*FIELD1
      AF2=A3*DETAU/FP0*FIELD2*FIELD2
      AD1=AF1/A2
      AD2=AF2/A2
      DO 6 M=1,M1

      TF=T0+TNF1(M)*(TR-T0)
```

```
      FC(M)=FK(TF)/FC0
      FLTF=FL(TF)
      FP1(M)=FLTF*FIELD1*FIELD1/FP0
      FP2(M)=FLTF*FIELD2*FIELD2/FP0
      QF1(M)=FLTF*AF1
6     QF2(M)=FLTF*AF2
      DO 7 K=1,K1
      TD=T0*TND1(K)*(TR-T0)
      PRE=PR-PWR+PGC*(CR+CN1(K)*(CTP-CR))*TD
      DC(K)=DK(PRE)/FC0
      DI1(K)=D(PRE)/FD0
      DLTD=DL(TD)
      DP1(K)=DLTD*FIELD1*FIELD1/FP0
      DP2(K)=DLTD*FIELD2*FIELD2/FP0
      QD1(K)=DLTD*AD1
7     QD2(K)=DLTD*AD2
C
C     INTERFACE POSITION:
      QIG=QI1+DELQI
      ITER=1
70    CONTINUE
      QI=0.5*(QI1+QIG)
      S2=S1-DETAU*A1*QI
C
C     EXT. SURFACE BOUNDARY CONDITION:
      CD1=(DC(1)+DC(2))/2./(1.-S1)/DELZ
      CD2=(DC(1)+DC(2))/2./(1.-S2)/DELZ
      CV=.5*A9*(S2-S1)/DETAU
      AC=.25*A2*DELZ/DETAU*(2.-S2-S1)
      PR1=.5*A3*DELZ*(1.-S1)*(.25*DP1(2)+.75*DP1(1))
      PR2=.5*A3*DELZ*(1.-S2)*(.25*DP2(2)+.75*DP2(1))
      DE1=(CD2-CV-.5*AC)/(-C-CD2+CV-1.5*AC)
      LA1=-(TND1(1)*(-C-CD1+CV+1.5*AC)+TND1(2)*(CD1-CV+.5*AC
     1)+PR2+PR1+2*C)/(-C-CD2+CV-1.5*AC)
C
C     ITERATION LOOP-HEAD:
      ICOUNT=1
      EPSI=10
      TIG=TI1+DELTI
5     CONTINUE
C
C     TEMPERATURE PROFILE-DRIED LAYER:
      RD1=.5*(1.-S1)*(S2-S1)
      RD2=.5*(1.-S2)*(S2-S1)
      SD2=(1.-S2)*(1.-S2)
      SD=SD1+SD2
      DO 8 K=2,KK
      PK=A4+FLOAT(K-1)
      RD=DC(K)/A2*DETAU/DELZ/DELZ
      DRD=.25*(DC(K+1)-DC(K-1))/A2*DETAU/DELZ/DELZ
      AL(K-1)=-(2.*RD+SD)/(RD-DRD+PK*RD2)
      BE(K-1)=(RD+DRD-PK*RD2)/(RD-DRD+PK*RD2)
8     GA(K-1)=-((RD-DRD+PK*RD1)*TND1(K-1)-(2.*RD-SD)*
     1TND1(K)+(RD+DRD-PK*RD1)*TND1(K+1)+QD1(K)*SD1+QD2(K)*
     2SD2)/(RD-DRD+PK*RD2)
      CALL EMMA(KK,DE1,LA1,0.,TIG,TND2)
C
C     TEMPERATURE PROFILE-FROZEN CORE:
      RF2=.5*S2*(S2-S1)
      RF1=.5*S1*(S2-S1)
      SF2=S2*S2
```

```
      SF=SF1+SF2
      DO 9 M=2,MM
      RF=FC(M)*DETAU/DELY/DELY
      DRF=.25*(FC(M+1)-FC(M-1))*DETAU/DELZ/DELZ
      AL(M-1)=-(2.*RF+SF)/(RF-DRF-FLOAT(M-1)*RF2)
      BE(M-1)=(RF+DRF+FLOAT(M-1)*RF2)/(RF-DRF-FLOAT(M-1)*RF2)
9     GA(M-1)=-((RF-DRF-FLOAT(M-1)*RF1)*TNF1(M-1)-(2.*RF-SF)
     1*TNF1(M)+(RF+DRF+FLOAT(M-1)*RF1)*TNF1(M+1)+QF1(M)*SF1+
     2QF2(M)*SF2)/(RF-DRF-FLOAT(M-1)*RF2)
      CALL EMMA(MM,-1.,0.,0.,TIG,TNF2)
C
C     THERMAL EQUILIBRIUM AT INTERFACE:
      TE=T0+TIG*(TR-T0)
      CE=FE(TE)
      CNI=(CE-CR)/(CTP-CR)
C
C     APPROXIMATE DIFFUSIVITY:
      DO 90 K=1,K1
      TD=T0+TND2(K)*(TR-T0)
      PRE=PR-PWR+PGC*(CR+CN2(K)*(CTP-CR))*TD
90    DI2(K)=D(PRE)/FD0
C
C     CONCENTRATION PROFILE
      SD=SD*POR
      DO 10 K=2,KK
      RC1=DI1(K)*DETAU/DELZ/DELZ
      RC2=DI2(K)*DETAU/DELZ/DELZ
      DRC1=.25*(DI1(K+1)-DI1(K-1))*DETAU/DELZ/DELZ
      DRC2=.25*(DI2(K+1)-DI2(K-1))*DETAU/DELZ/DELZ
      AL(K-1)=-(2.*RC2+SD)/(RC2-DRC2+FLOAT(K-1)*RD2)
      BE(K-1)=(RC2+DRC2-FLOAT(K-1)*RD2)/(RC2-DRC2+FLOAT(K-1)*RD2)
10    GA(K-1)=-((RC1-DRC1+FLOAT(K-1)*RD1)*CN1(K-1)-(2.*RC1-SD)*
     1CN1(K)+(RC1+DRC1-FLOAT(K-1)*RD1)*CN1(K+1))/(RC2-DRC2+FLOAT(
     2K-1)*RD2)
      CALL EMMA(KK,0.,0.,0.,CNI,CN2)
C
C     ENERGY BALANCE AT THE INTERFACE:
      GRTD2=(TND2(KK+1)-TND2(KK))/DELZ
      GRTF2=(TNF2(MM+1)-TNF2(MM))/DELY
      GRC2=(CN2(KK+1)-CN2(KK))/DELZ
      COEF2=-A5*GRTD2+A6-.25*A7*(A2*(2.-DELZ)*DELZ*GRTD2-(2.-
     1DELY)*DELY*GRTF2)
      COND1=-.5*((FC(MM+1)+FC(MM))/S1*GRTF1+(DC(KK+1)+DC(KK))/
     1(1.-S1)*GRTD1)
      COND2=-.5*((FC(MM+1)+FC(MM))/S2*GRTF2+(DC(KK+1)+DC(KK))/
     1(1.-S2)*GRTD2)
      PROD1=.5*A3*((.75*DP1(KK+1)+.25*DP1(KK))*(1.-S1)*DELZ+(.
     175*FP1(MM+1)+.25*FP1(MM))*S1*DELY)
      PROD2=.5*A3*((.75*DP2(KK+1)+.25*DP2(KK))*(1.-S2)*DELZ+(
     1.75*FP2(MM+1)+.25*FP2(MM))*S2*DELY)
      ANEAR=.0625*(A2*(2.-S1-S2)*DELZ*(TND2(KK)-TND1(KK))+(S2+
     1S1)*DELY*(TNF2(MM)-TNF1(MM)))/DETAU
      AINTER=.1875*(A2*(2.-S1-S2)*DELZ+(S2+S1)*DELY)/DETAU
      DR1=.5*A8*(DI1(KK+1)+DI1(KK))/(1.-S1)*GRC1
      DR2=.5*A8*(DI2(KK+1)+DI2(KK))/(1.-S2)*GRC2
      DELTIC=.5*(COND1+COND2-COEF1*DR1-COEF2*DR2+PROD1+PROD2-
     12.*ANEAR)/AINTER
      TI=TI1+DELTIC
C
C     ITERATION LOOP-TAIL:
      IF(ICOUNT.EQ.1)GO TO 12

      IF(ICOUNT.LT.3)GO TO 11
```

```
      TC1=TC2
      TG1=TG2
11    TC2=TI
      TG2=TIG
      IF(ICOUNT.LT.3)GO TO 12
      NY1=1.E7*ABS(TG2-TG1)
      IF(NY1.LT.15)GO TO 12
      SLO=(TC2-TC1)/(TG2-TG1)
      NR=1.E7*ABS(SLO-1)
      IF(NR.LT.10)GO TO 14
      X=1./(1.-SLO)
12    CONTINUE
      NY=1.E7*ABS(TIG-TI)
      IF(NY.LE.EPSI)GO TO 15
      TIG=(1.-X)*TIG+X*TI
      ICOUNT=ICOUNT+1
C     MONITOR AND CONTROL ITERATION CONVERGENCE:
      IF(ICOUNT.EQ.10)EPSI=50
      IF(ICOUNT.EQ.30)EPSI=100
      IF(ICOUNT.EQ.50)EPSI=500
      IF(ICOUNT.EQ.100)EPSI=1000
      IF(ICOUNT.NE.1000)GO TO 5
      WRITE(5,100) N
      RETURN
C     ITERATION LOOP-OUT:
14    TI2=(TIG+TI)/2.
      GO TO 16
15    TI2=(1.-X)*TIG+X*TI
16    DELTI=TI2-TI1
      AVER2=AVER2+FLOAT(ICOUNT)/FLOAT(N)/2.
C
C     HEAT CONSUMPTION AT THE INTERFACE:
      QS1=COND1-(COEF1-A6)*DR1+PROD1
      QS2=COND2-(COEF2-A6)*DR2+PROD2
      ACCUM=AINTER*DELTIC+ANEAR
      QI2=QS2+QS1-2.*ACCUM-QI1
      IF(ITER.GE.2)GO TO 150
      QIG=QI2
      ITER=ITER+1
      GO TO 70
150   CONTINUE
      DELQI=QI2-QI1
C
C     MICROWAVE POWER GENERATION/SUBLIMATION POWER CONSUMPTION
      N1=(N-509)/50
      IF(N.NE.1.AND.N.NE.509.AND.(N-509).NE.N1*50)GO TO 164
      DMWP=(DP2(1)+DP2(K1))/2.
      FMWP=(FP2(1)+FP2(M1))/2.
      DO 160 K=2,KK
      DMWP=DMWP+DP2(K)
160   FMWP=FMWP+FP2(K)
      DMWP=DMWP*FP0*THICK*(1.-S2)*DELZ*4.184
      FMWP=FMWP*FP0*THICK*S2*DELY*4.184
      TMWP=DMWP+FMWP
      TMWE=TMWE+TMWP*DELT*50.
      CONS=HS*DR2*4.184
C
C     FILE ON DISK CHARACTERISTIC VARIABLES HISTORY:
      IF(N.NE.1)GO TO 161
      WRITE(20,201)
161   K=1
```

```
162     K=K+1
        IF(K.GT.K1)GO TO 163
        IF(TND2(K).GT.TND2(K-1))GO TO 162
163     TDM=TND2(K-1)*(TR-TØ)+TØ-273.15
        ZM=(K-2)*DELZ
        TC=TNF2(1)*(TR-TØ)+TØ-273.15
        TT=TI2*(TR-TØ)+TØ-273.15
        WRITE(2Ø,2Ø2) N,TIME,AVER2,ZM,S2,TC,TT,TDM,FMWP,TMWP,CONS
        WRITE(21,2Ø3) TIME,ZM,S2,TC,TT,TDM,FMWP,TMWP,CONS
164     CONTINUE
C
C       FILE ON DISK TEMPERATURE AND VAPOR PRESSURE PROFILES:
        N2=(N-959)/5ØØ
        IF(N.NE.1.AND.N.NE.5Ø9.AND.N.NE.7Ø9.AND.N.NE.759.
        1AND.(N-959).NE.N2*5ØØ)GO TO 166
        IF(N.EQ.459)GO TO 166
        WRITE(23,2Ø4)TIME
        DO 165 L=1,K1
        Z=DELZ*(L-1)
        TF=TNF2(L)*(TR-TØ)+TØ-273.15
        TD=TND2(L)*(TR-TØ)+TØ-273.15
        PW=PGC*(CN2(L)*(CTP-CR)+CR)*(TD+273.15)
        CONC=CN2(L)*(CTP-CR)+CR
        WRITE(23,2Ø6) Z,TF,TD,PW,CONC
165     WRITE(22,2Ø5) Z,TF,TD,CONC
166     CONTINUE
C
C       CHECK:
        WRITE(19,4ØØ)AVER2,TNF2(1),TNF2(1Ø),TNF2(21),TND2(1Ø)
        1,TND2(1),CN2(1Ø),CN2(21),GRC2,GRTD2,GRTF2,X,DELS
4ØØ     FORMAT(F6.3,11F1Ø.5,E14.5)
C
C       UPDATE ALL PARAMETERS:
        DO 17 K=1,K1
        TND1(K)=TND2(K)
17      CN1(K)=CN2(K)
        DO 18 M=1,M1
18      TNF1(M)=TNF2(M)
        GRTD1=GRTD2
        GRTF1=GRTF2
        GRC1=GRC2
        COEF1=COEF2
        SD1=SD2
        SF1=SF2
        DELS=S2-S1
        S1=S2
        TI1=TI2
        QI1=QI2
        FIELD1=FIELD2
        AVER2=AVER2*FLOAT(N)/FLOAT(N+1)
C
C       SIMULATION LOOP-TAIL:
        IF(N.GT.1ØØØØ)RETURN
        IF(S1.GT.Ø.ØØ1)GO TO 19
        TEN=DENS*POR*THICK*HS
        EUF=TEN/TMWE/4.184
        WRITE(2Ø,2Ø7)TIME,EUF
        RETURN
19      CONTINUE
        IF(N.EQ.1ØØ)GO TO 21
        IF(N.EQ.5ØØ)GO TO 21

        GO TO 4
```

```
21      DETAU=DETAU*10.
        DELT=DELT*10.
        X=.2
        GO TO 4
C
C
100     FORMAT(' ITERATION STUCK AT TIME INCREMENT N= ',I5,'; CO
        1MMAND IS RETURNED TO THE MAIN PROGRAMM')
101     FORMAT(' MELTING OCCURS AT SLAB CENTER AT TIME=',F6.3,'
        1HRS, N= ',I7,/' COMMAND IS RETURNED TO MAIN PROGRAM')
200     FORMAT(' EXPERIMENTAL CONDITIONS:'/3X'FIELD= ',E11.4/3X'
        1PR= ',E11.4/3X'PWR= ',E11.4/3X'TR= ',E11.4/3X'TØ= '
        2,E11.4/3X'THICKNESS= ',E11.4/3X'WATER CONTENT= '
        3,E11.4/3X'FAT CONTENT= ',E11.4/)
201     FORMAT(//' TIME HISTORY:'/2X'N',4X'TIME',1X'AVER.',2X'ZM
        1AX',6X'S2',8X'TFMAX',9X'TI',8X'TDMAX',8X'FMWP',8X'TMWP'
        2,9X'QI')
202     FORMAT(I5,3F6.2,7(1XE11.4))
203     FORMAT(2F6.2,7E11.4)
204     FORMAT(//' TIME= ',F6.2,' HRS'/1X'Z,Y',7X'TF',10X'TD',10X'
        1PW',11X'C')
205     FORMAT(F5.2,3(1XE11.4))
206     FORMAT(F5.2,4(1XE11.4))
207     FORMAT(//' TOTAL DRYING TIME: ',F5.2,' HRS'/
        1' MICROWAVE ENERGY USAGE FACTOR: ',F5.3)
        END
```

- NOMENCLATURE -

Letters:

A	sample cross section area, cm^2
C	concentration of water vapor in the pores, g/cm^3
C_D	specific heat of the dried material, cal/g/°K
C_F	specific heat of the frozen material, cal/g/°K
C_{pw}	specific heat of the water vapor, cal/g/°K
D	effective diffusivity, cm^2/sec
D^o	effective diffusivity at 1 atm., cm^2/sec
D_K	effective Knudsen diffusivity, cm^2/sec
E	electric field peak strength in the vacuum, V/cm
E_B	electric field peak strength at breakdown, V/cm
E_d	electric field peak strength in the dielectric, V/cm
f	microwave frequency, Hz
f_E	ice-vapor equilibrium relationship. Relates the concentration to the temperature
f_1	ice-vapor equilibrium relationship. Relates the normalized concentration to the normalized temperature
h	heat transfer coefficient, $cal/sec/cm^2/°K$
ΔHs	enthalpy of sublimation, cal/g
k	effective thermal conductivity, cal/sec/cm/°K
K	dissipation coefficient defined by Eq. (3.6), $cal/sec/cm^3/(V/cm)^2$
m	weight of the sample, g
$\mathring{m}$	overall drying rate, g/sec
P	total pressure, mmHg
P^w	partial pressure of water vapor, mmHg
Q	heat flux, $cal/sec/cm^2$
S	normalized interface position
t	process time, sec
T	temperature, °K
V	volume, cm^3

W	effective mass flux of water vapor, $g/sec/cm^2$
x	space-coordinate, cm
X	interface position, cm
x_w	initial moisture content of beef sample (wet basis)
x_f	initial fat content of beef sample (wet basis)
y	normalized space-coordinate in the frozen region
z	normalized space-coordinate in the dried layer

Greek letters:

α	effective thermal diffusivity, cm^2/sec
β	Biot Number
δ	thickness of the dried layer, cm
ϵ_o	dielectric constant in vacuum (CGS)
ϵ'	relative dielectric constant
ϵ''	relative loss factor
θ	normalized temperature
μ	fraction of the initial moisture content
μ'	corrected fraction of the initial moisture content defined by Eq. (9.3)
ξ	acceleration factor in the iteration
π	number Pi
ρ	density of ice, g/cm^3
ρ_D	density of the dried material, g/cm^3
ρ_F	density of the frozen material, g/cm^3
σ	porosity (void fraction)
σ_e	electric conductivity, mho/cm
τ	normalized time
Φ	total microwave power absorbed, cal/sec
ω	density of microwave power absorbed, $cal/sec/cm^3$
Ω	microwave power absorbed per unit area, $cal/sec/cm^2$

Indices (superscripts or subscripts):

o	initial value; before the microwave power is turned on
1	starting value; <u>immediately</u> before the microwave power is turned on

2	final value; as the frozen core disappears
f	final value; as the material is fully dried
D	in the dried layer
F	in the frozen region
i	at the interface
R	in the vacuum (room)
S	at the outer surface
max.	maximum value
*	normalized value

- REFERENCES -

Awbery, J.H., and Griffiths, E., "Thermal Properties of Meat," J. Soc. Chem. Ind., 52, 326 (1933)

Bankoff, S.G., "Heat Conduction or Diffusion with Change of Phase," in Adv. in Ch. Eng., Ac. Press, N.Y., 5, 75 (1964)

Bengtsson, N.E., and Risman, P.O., "Dielectric Properties of Foods at 3 GHz as Determined by a Cavity Perturbation Technique, II. Measurements on Food Materials," J. Microwave Power, 6(2), 107 (1971)

Branjnikov, A.M., Vassiliev, A.I., Voskoboinikov, V.A., and Krautchechvili, E.I., "Transfert de Chaleur et de Masse dans les Matériaux Poreux Pendant la Lyophilisation sous vide," in Symposium on Thermodynamics Aspects of Freeze-Drying, International Institute of Refrigeration, Comission X, Lausanne, Switzerland, (1969)

Bralsford, R., "Freeze-Drying of Beef," J. Food Technol., 2, 339-363 (1967)

Clark, J.P., PhD Thesis, Univ. of Calif., Berkeley (1968)

Copson, D.A., "Microwave Sublimation of Foods," Food Technol., 12, 270 (1958)

Copson, D.A., Microwave Heating in Freeze-Drying, Electronic Ovens and other Applications, Avi Pub. Co., Westport, Ct. (1962)

Decareau, R.V., "Microwave Freeze-Drying," in Freeze-Drying of Foodstuffs, Cotson, S., and Smith, D.B., Columbine Press, Manchester, England (1962)

Dyer, D.F., Carpenter, D.K., and Sunderland, J.E., "Equilibrium Vapor Pressure of Frozen Bovine Muscle," J. Food Sci., 31, 196 (1966)

Dyer, D.F., and Sunderland, J.E., "Bulk and Diffusional Transport in the Region Between Molecular Flow and Viscous Flow," Int. J. Heat Mass Transfer, 9,(6), 519 (1966)

Dyer, D.F., and Sunderland, J.E., "The Role of Convection in Drying," Chem. Eng. Sci., 23, 965 (1968)

Fox, E.C., and Thompson, W.J., "Coupled Heat and Mass Transport in Unsteady Sublimation Drying," AIChE J., 18, 792 (1972)

Gould, J.W., and Kenyon, F.M., "Gas Discharge and Electric Field Strength in Microwave Freeze-Drying," J. Microwave Power, 6,(2), 151 (1971)

Hammond, L.H., "Economic Evaluation of UHF Dielectric vs Radiant Heating for Freeze-Drying." Food Technol., 21, 736 (1967)

Hardin, T.C., PhD Thesis, Georgia Inst. of Tech, Atlanta, Ga. (1965)

Harper, J.C., "Microwave Spectra and Physical Characteristics of Fruit and Animal Products Relative to Freeze-Dehydration," QM Contract Report, DA 19-129 -QM- 1349 (1961)

Harper, J.C., "Transport Properties of Gases in Porous Media at Reduced Pressures with Reference to Freeze-Drying," AIChE J., 8, 298 (1962)

Harper, J.C., Chichester, C.O., and Roberts, T.E., "Freeze-Drying of Foods," Agr. Eng., 43(2), 78 (1962)

Hatcher, J.D., M.S. Thesis, Georgia Inst. of Tech., Atlanta, Ga. (1964)

Hill, J.E., Leitman, J.D., and Sunderland, J.E., "Thermal Conductivity of Various Meats," Food Technol., 21, 1143 (1967)

Hill, J.E., and Sunderland, J.E., "Sublimation-Dehydration in the Continuum, Transition, and Free-Molecule Flow Regimes," Int. J. Heat Mass Transfer, 14, 625 (1971)

Hohner, G.A., PhD Thesis, Mich. St. University, East Lansing, Mich. (1970)

Hoover, M.W., Markantonatos, A., and Parker, W.N., "UHF Dielectric Heating in Experimental Acceleration of Freeze-Drying of Foods," Food Technol., 20, 103 (1966)

Hoover, M.W., Markantonatos, A., and Parker, W.N., "Engineering Aspects of Using UHF Dielectric Heating to Accelerate the Freeze-Drying of Foods," Food Technol., 20, 107 (1966)

Jackson, S., Rickter, S.L., and Chichester, C.O., "Freeze-Drying of Fruit," Food Technol., 11, 468 (1957)

Kan, B., and Yeaton, R.A., "Improving Freeze-Drying Process Efficiency through Improved Vapor Removal and In-Process Moisture Determination," QM Contract Report, DA 19-129 -QM- 1546 (1961)

King, C.J., Lam, W.K., and Sandall, O.C., Food Technol., 22, 1302 (1968)

King, C.J., Freeze-Drying of Foods, CRC Monoscience Series, (1971)

Kuprianoff, J., "Some Factors Influencing the Reversibility of Freeze-Drying of Foodstuff," in Freeze-Drying of Foods, Fisher, F.R/. Ed., Proceedings of a Conference, Chicago, (1961), Natl. Ac. Sci., Nat. Res. Counc., Washington, D.C., (1962)

Lentz, C.P., "Thermal Conductivity of Meats, Fats, Gelatin Gels, and Ice," Food Technol., 15, 243 (1961)

Ma, Y.H., and Peltre, P., "Mathematical Simulation of a Freeze-Drying Process Using Microwave Energy," AIChE Symposium Series, 69(132), 47 (1973)

MacDonald, A.D., Microwave Breakdown in Gases, John Wiley & Sons, N.Y., (1966)

Massey, W.M., and Sunderland, J.E., "Measurement of Thermal Conductivity During Freeze-Drying of Beef," Food Technol., 21, 408 (1967)

Meryman, H.T., "Induction and Dielectric Heating for Freeze-Drying," in Aspects Théoriques et Industriels de la Lyophilisation, Rey, L., Ed., Hermann, Paris (1964)

Miller, H.L., and Sunderland J.E., "Thermal Conductivity of Beef," Food Technol., 17, 124 (1963)

Nelson, S .O., "Electrical Properties of Agricultural Products - A Review," Paper presented at the 1971 Winter Meeting American Society of Agricultural Engineers, Chicago (1971)

Parker, W.N., "Freeze-Drying," in Microwave Power Engineering, Okress, E.C., Ed., Vol. 2, Ac. Press, N.Y. (1968)

Rey, L., Aspects Théoriques et Industriels de la Lyophilisation, Herman, Paris (1964)

Sandall, O.C., PhD Thesis, Univ. of Calif., Berkeley (1966)

Sandall, O.C., King, C.J., and Wilke, C.R., "The Relationship Between Transport Properties and Rates of Freeze-Drying of Poultry Meat," AIChE J., 13, 428 (1967)

Saravacos, G.D., and Stinchfield, R.M., "Effect of Temperature and Pressure on the Sorption of Water Vapor by Freeze-Dried Food Materials," J. Food Sci., 30(5), 779 (1965)

Smith, G.D., Numerical Solution of Partial Differential Equations, Oxford Univ. Press, N.Y. & London (1965)

Therlkeld, J.L., Thermal Environmental Engineering, Prentice Hall, Inc., Englewood Cliffs, N.J. (1962)

Wakao, N., Otani, S., and Smith, J.M., "Significance of Pressure Gradients in Porous Materials: Part 1., Diffusion and Flow in Fine Capillaries: Part 2., Diffusion and Flow in Porous Catalysts," AIChE J., 11, 435 (1965)

FOOD ENGINEERING LABORATORY DISTRIBUTION LIST

Process Development Branch

Copies

1 - Commander
U.S. Army Materiel Command
ATTN: AMCRD-TI
5001 Eisenhower Avenue
Alexandria, VA 22333

1 - Commanding Officer
Navy Food Service Systems Office
ATTN: Mrs. Marjorie Kehoe
Building 166
Washington Navy Yard
Washington, D.C. 20374

2 - Commandant of the Marine Corps
Headquarters U.S. Marine Corps
ATTN: Code RD-44
Washington, D.C. 20380

1 - Commander
U.S. Army Foreign Science & Technical Center
ATTN: AMXST-GE (Victoria Dibbern)
220 7th Street, N.E.
Charlottesville, VA 22901

2 - Mr. Roland Finch, Chief
Fishery Products, Research & Inspection Division
National Marine Fisheries Service,NOAA
U.S. Department of Commerce
3300 Whitehaven Street, N.W., Room 300
Washington, D.C. 20035

1 - Commander
U.S. Army Medical Research & Development Command
ATTN: SGRD-MDI-N
Washington, D.C. 20314

2 - Commander
LAIR
PSF, CA 94129

Copies

1 - Commanding Officer
U.S. Air Force Service Office (AFLC)
ATTN: Mrs. Germaine Gotshall
2800 South 20th Street
Philadelphia, Pa. 19101

1 - Director
Division of Biology & Medicine
U.S. Atomic Energy Commission
Washington, D.C. 20545

2 - Commandant of the Marine Corps
Headquarters U.S. Marine Corps
ATTN: Code LFS-4
Washington, D.C. 20380

1 - Director AF Hospital Food Service
Headquarters USAF/SGB-1
6B153 James Forrestal Bldg.
Washington, D.C. 20314

4 - Commander
U.S. Army Troop Support Agency
ATTN: DALO-TA-D
Fort Lee, VA 23801

1 - Library
USDA, Southern Regional Research Center
P.O. Box 19687
New Orleans, Louisiana 70179

5 - U.S. Department of Agriculture
Animal & Plant Health & Inspection Service
ATTN: Director, Standards & Services Division
Washington, D.C. 20250

1 - USDA, National Agricultural Library
Current Serial Record
Beltsville, Maryland 20705

FOOD ENGINEERING LABORATORY DISTRIBUTION LIST

Process Development Branch

Copies

1 - Administrator
Agricultural Research Service
U.S. Department of Agriculture
ATTN: Dr. Fred Senti
Washington, D.C. 20250

1 - Mary E. Carter, Director
Southern Regional Research Center
Agricultural Research Service
U.S. Department of Agriculture
P.O. Box 19687
New Orleans, Louisiana 70179

1 - Dr. C.H. Harry Neufeld, Director
Southeastern Marketing & Nutrition Research Division
Agricultural Research Service
U.S. Department of Agriculture
P.O. Box 5677
Athens, Georgia 30604

1 - D F Davis
USDA ARS
P.O. Box 14565
Gainesville, Florida 32601

2 - Headquarters 12th Support Brigade
ACofS Services
ATTN: Food Advisor
Fort Bragg, North Carolina 28307

1 - Dr. K.C. Emerson
Assistant for Research
Office of Assistant Secretary of the Army (R&D)
Department of the Army
Washington, D.C. 20310

2 - Dr. Frank R. Fisher
Executive Director, ABMPS
National Academy of Sciences
National Research Council
2101 Constitution Avenue
Washington, D.C. 20418

Copies

1 - CDR Harold J. Janson, MSC, USN
Head, Food Service Branch
Bureau of Medicine & Surgery
Navy Department
Washington, D.C. 20390

1 - Dr. Louis J. Ronsivalli
Fishery Products Technology Lab.
U.S. Department of Commerce
National Oceanic & Atmospheric Administration
National Marine Fisheries Service
Northern Region
Emerson Avenue
Gloucester, MA 01930

1 - HQDA (DARD-ARL)
WASH DC 20310

1 - Subsistence Management Policy Director
ATTN: OASD(I&L)
Pentagon 2B323
Washington, D.C. 20301

3 - Office of the Coordinator of Research
University of Rhode Island
Kingston, Rhode Island 02881

3 - Exchange & Gift Division
Library of Congress
Washington, D.C. 20540

1 - Headquarters, USAF (AF/RDPS)
DCS/Research & Development
Washington, D.C. 20330

1 - Subsistence & Culinary Arts Department
U.S. Army QM School
Fort Lee, VA 23801

1 - Logistics Library
Bunker Hall
Fort Lee, VA 23801

FOOD ENGINEERING LABORATORY DISTRIBUTION LIST

Process Development Branch

Copies

2 - HQDA (DALO-SMT-F)
WASH DC 20310

1 - Professor Walter M. Urbain
Dept. of Food Science &
Human Nutrition
Michigan State University
East Lansing, MI 48823

1 - Commander
U.S. Army Test & Evaluation
Command
ATTN: AMSTE-BC
Aberdeen Proving Ground, MD 21005

1 - Technical Service Branch
Technical Operation Division
Directorate Subsistence
Defense Personnel Support Center
ATTN: Director of Subsistence
DPSC-STS
2800 South 20th Street
Philadelphia, PA 19101

1 - Stimson Library
ATTN: Documents Librarian
U.S. Army Medical Field Service
School
Brooke Army Medical Center
Fort Sam Houston, TX 78234

1 - U.S. Army Advanced Materiel
Concepts Agency
ATTN: AMXAM-AC (J.H. Berardelli,
Plans & Operations Officer)
Washington, D.C. 20315

1 - Headquarters, Defense Supply Agency
ATTN: Mr. Jobe, DSAH-OP
Cameron Station
Alexandria, VA 22314

2 - Director
Development Center (ATTN: M&S Div)
Marine Corps Development &
Education Command
Quantico, VA 22134

Copies

1 - Assistant Director for
Isotopes Development
Division of Applied Technology

U.S. Atomic Energy Commission
Washington, D.C. 20545

1 - Commander
LAIR
ATTN: Col. James L. Fowler, VC
PSF, CA 94129

1 - Consumer Products Division, 730
Bureau of Domestic Commerce
U.S. Department of Commerce
Washington, D.C. 20230

1 - Chief, U.S. Army Food
Service Center
ATTN: DALO-TAD-D
Fort Lee, VA 23801

2 - Executive Secretary
Interdepartmental Committee on
Radiation Preservation of Food
ATTN: Mr. Jerome Deitch
Bureau of Domestic Commerce
U.S. Department of Commerce
Washington, D.C. 20230

5 - Chief, Food Service Division
Walter Reed General Hospital
Washington, D.C. 20012

11 - NRC Committee Members

1 - Headquarters
Air Force Systems Command (DLH)
Andrews Air Force Base, MD 20331

1 - Air Force Services Office
DPKF
2800 South 20th Street
Philadelphia, PA 19101

1 - USAFSAM
SME: ATTN: Dr. Vanderveen
Brooks Air Force Base, TX 78235

FOOD ENGINEERING LABORATORY DISTRIBUTION LIST

Process Development Branch

Copies

1 - Government Documents Department
University of California Library
Davis, California 95616

1 - Food Service School
Service Support Schools
Marine Corps Base
Camp Lejeune, NC 28542

1 - Manager, Analytical and
Technical Services
RJR Foods, Inc.
Department of Food Science
and Technology
P.O. Box 3037
Winston-Salem, NC 27102

1 - Dr. Jack E. Roberts
Manager, Research & Development
Ore-Ida Foods, Inc.
Technical Center
P.O. Box 10
Ontario, Oregon 97914

1 - NASA Johnson Space Center
ATTN: DB-3
Houston, TX 77058

3 - Eastern Regional Research Center
ARS, USDA
600 E. Mermaid Lane
Philadelphia, PA 19118

FOOD ENGINEERING LABORATORY INTERNAL DISTRIBUTION LIST

Copies

24 - Military Requirements & Development Programs Office, Food Engineering Laboratory, NLABS (12 for transmittal to Defense Documentation Center)

2 - Technical Library, NLABS

20 - Division and Branch Chiefs, Food Engineering Laboratory, NLABS

2 - Marine Liaison Officer, NLABS

3 - Air Force Liaison Officer, NLABS

1 - Special Assistant for DOD Food Program, NLABS

1 - US Army Representative for DOD Food Program, NLABS

1 - US Air Force Representative for DOD Food Program, NLABS

1 - US Navy Representative for DOD Food Program, NLABS

2 - Chief, Engineering Programs Management Office, ATTN: Standardization Management Section (Mr. Richman), NLABS

6 - Director, Food Sciences Laboratory, NLABS

30 - Project Officer, Food Engineering Laboratory, NLABS

25 - Alternate Project Officer, Food Engineering Laboratory, NLABS